Ultrasound-Assisted Cell Eradication

MSc Thesis **2019/10/02**

University of the Witwatersrand

Supervisors: Prof. Michiel Postema and Prof. David Rubin
Co-supervision: Dr Marietha Nel

Charl Smalberger

A dissertation submitted to the Faculty of Engineering and the Built Environment, University of the Witwatersrand, Johannesburg, in fulfilment of the requirements for the degree of Master of Science in Engineering.

Johannesburg, July 2019

Declaration

I declare that this dissertation is my own, unaided work, except where otherwise acknowledged. It is being submitted for the degree of Master of Science in Engineering to the University of the Witwatersrand, Johannesburg. It has not been submitted before for any degree or examination to any other university.

Signed this ____ day of _____ 20__

_____

Charl Smalberger

Abstract

Ultrasound-based cell separation and eradication methods are advantageous because of cost-effectiveness, efficiency and its non-invasive nature.

The purpose of the research was to manipulate white and red blood cells with ultrasound and force these cells to translate. This research will contribute towards an ultrasound-based method to differentiate between malaria-infected cells and healthy cells.

An experimental setup was built to accommodate optical microscopy and ultrasound transducers. The ultrasound transducers located at a variable distance and angle with respect to the optical region of interest to create different ultrasound characteristics. Findings were captured with a high-speed camera.

This research illustrated that when sonicated, white and red blood cells translate to the pressure nodes and pressure anti-nodes of an ultrasound field.

Acknowledgements

I would like to thank the department of electrical and information engineering for funding this research.

Mr. Jere Claase form Wirsam Scientific (Johannesburg, South-Africa) for lending our research team a CKX31 inverted microscope with a Olympus C-Plan N 20× objective lens and advising on microscope optics.

The South African National Blood Service for providing blood samples under clearance number: 2019/0468. (*cf.* appendix C).

The DFG Emmy Noether Programme (grant no. 38355133) and Engineering and Physical Sciences Research Council (EPSRC) (grant no. EP/F037025/1). For providing funds to acquire a high-speed camera.

Dr. Tanya Augustine and Ms. Khutlwano Xulu for kindly providing a recipe for Tyrode's solution.

Contents

List of Figures

Nomenclature

WBC White blood cell

RBC Red blood cell

Pf-IRBCs Red blood cells infected with *Plasmodium falciparum*

Pv-IRBCs Red blood cells infected with *P. vivax*

SWR Standing wave ratio

Chapter 1

Introduction

Living cells can be manipulated in sound-fields [3]. The ultimate purpose of ultrasonic cell manipulation is the detection, quantification, manipulation, and eradication of individual cells [1]. The use of ultrasound technology is popular in medicine because of it's availability, affordability and non-invasive nature [4]. Current therapeutic uses for ultrasound include extracorporeal shockwave lithotrypsy [5], high-intensity focussed ultrasound [6], ultrasound contrast agent-assisted drug delivery [7], and combinations thereof [8]. The mentioned studies [5, 6, 7, 8] focused on the macro-structural manipulation of tissue. Some studies have claimed that ultrasound can be used for pain relief [9, 10], whilst others suggest that ultrasound exposure increases tissue repair [11, 12]. However, thermal effects could not be excluded in the acoustic experimental setups of [11, 12]. The motivation for this research comes from the developments in the field of ultrasonic manipulation at micro-structural level, *i.e.*, individual cellular level. The types of behaviour experienced by cells when subjected to ultrasound include proliferation, translation, apoptosis, lysis, transient membrane permeation, and oscillation [1].

The aim of this research is to manipulate cells in an affordable, efficient and non-invasive manner with the use of ultrasound. This research intends to explore the effects of acoustics on cells and how the cells will behave under different acoustic conditions. The primary goal is to subject cells to ultrasound and determine under which conditions cell translation is expected to occur. Translations of cells subject to different ultrasound-fields and the direction of these translations compared to cells not subject to ultrasound are of particular interest. This research contributes to an ultrasound-based cell separation and eradication method. This is significant because removal of damaged cells, *i.e.*, cells containing parasites or cancerous cells, from human and animal bodies could contribute towards a non-invasive cure for certain life threatening diseases, malaria in particular.

1.1 Problem Statement

Cells or blood cells containing parasites or cancer, cause life-threatening diseases such as malaria, and need to be removed from human and animal bodies. Existing cell separation and eradication methods are expensive and inefficient.

1.2 Research Question

In which manner and under what ultrasound characteristics are blood cells forced to translate?

The research objectives are to:

I. Determine what ultrasound characteristics will yield significant blood cell translation.

II. Determine to which locations do blood cells translate to in the ultrasound-field.

III. Determine how ultrasound-forced translations differ from translations of blood cells not under the influence of ultrasound.

Chapter 2

Background

2.1 Cells

Cells are complex structures that make up living organisms. There are about 10^{14} cells present in the adult body [13]. Knowledge on the mechanical properties of cells is necessary to form an understanding on how the cells will behave in an ultrasound field. The average mammal cell size ranges from 6 μm to 40 μm [13]. A cell's complex structure can be simplified for the purpose of understanding cellular acoustics as shown in figure 2.1.

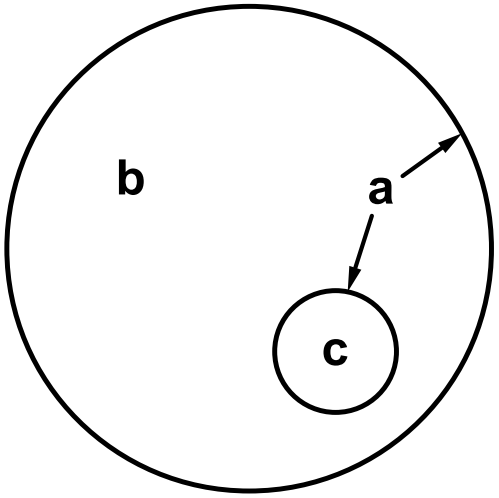

Figure 2.1: Simplified model of a standard mammalian cell, with nucleus (c), cytoplasma (b) and bilayer membranes (a) enclosing the cell and the nucleus. Reprinted from [1] with permission.

Most cells are comprised of three parts, a plasma membrane, cytoplasm and nucleus. The plasma membrane is the cell's semi-permeable elastic outer surface. This lipid-based membrane separates the cell's cytoplasm from its external surroundings [13]. The fluidity of the plasma membrane is dictated by the amount of double bonds in the organic compound of the plasma membrane. With fluidity being directly proportional to the amount of double bonds. Membrane fluidity also aids various cellular processes such as growth, movement, division, and secretion [13]

The cytoplasm is a gel-like fluid. It makes up all the material inside the cell, excluding the nucleus [13]. The cytoplasm is incompressible and this causes cells to have no ability to compress, forces exerted on cells can only cause the cells to elongate and not shrink [14].

The nucleus is the centre of the cell, it is an organelle structured with genetic material that preforms explicit cell functions. The nucleus is not present in all cell types with red blood cells being an example [13].

Damaged cells often cause life-threatening diseases, making it important to remove these cells from human and animal bodies [15]. Living organisms can naturally separate damaged cells from healthy cells. After separation the body's internal mechanisms such as apoptosis will destroy damaged cells. Techniques have been developed to separate cells; these techniques are mostly based on adherence, density, and antibody binding [15]. The most used in-vitro density-based method is centrifugation, which is inefficient and costly. There is a need for a cost-effective, efficient method to remove damaged cells, not only in vitro, but also in vivo—from the human body.

White and red blood cells were used for the experiments, to furfill this research.

2.1.1 Red Blood Cells Affected by the Malaria Parasite

Red blood cells are required to deform substantially as they pass through the microvasculature and the sinusoids of the spleen [16]. There are five parasite species that cause malaria. The most common species are *Plasmodium falciparum* and *Plasmodium vivax*. These parasites change the mechanical properties of red blood cells. Red blood cells infected with *Plasmodium falciparum* (Pf-IRBCs) loose flexibility as they mature. Splenetic clearance, which is essential to break down damaged red blood cells, is avoided by sequestering in veins and capillaries [16].

In contrast, red blood cells infected with *P. vivax* (Pv-IRBCs) increase in flexibility

as they mature. Coincidentally, the Pv-IRBCs' surface area increased from 56.7 ± 1.3 $(\text{mm})^2$ to 74.7 ± 0.6 $(\text{mm})^2$ to 90.9 ± 1.1 $(\text{mm})^2$ in ring-, trophozoite-, and schizont-stage respectively [16]. Thus, Pv-IRBCs are able to pass through the spleen. The changes in mechanical properties are key to the development of an ultrasound-based cure for malaria.

2.2 Ultrasound

Ultrasound fields are generated by transducers. A transducer refers to a device with both transmitting and receiving capability, whereas a hydrophone is a device intended to receive and quantify an ultrasound field [4]. An ultrasound field at a certain location is described by its dominant period, centre frequency, pulse length, peak-negative pressure, peak-positive pressure, peak-to-peak pressure, pulse-repetition time, pulse-repetition frequency, and duty cycle [17]. A representation of these parameters is seen in Figure 2.2. The dominant period is the time duration to complete a sonic cycle. The centre frequency is the inverse of the dominant period. The pulse length is the time period of a transmitted pulse. The pressure amplitude p_{A} can change in a pulse. Therefore, the pulse pressure is usually described by its peak-positive, peak-negative, and peak-to-peak pressures. The pulse-repetition period is the duration from the start of a pulse to the start of the following pulse. The pulse-repetition frequency is the inverse of the pulse-repetition period. The duty cycle is the fraction of a pulse sequence where the output waveform is considered to be active, usually expressed as a percentage.

The transmitted energy per unit time is termed the power W. Each point in a sound field lies on a surface S on which the intensity $I = W\,S^{-1}$ is the same. The average intensity is given by [17]:

$$< I >= \frac{{p_{\text{A}}}^2}{2\rho c}, \tag{2.1}$$

where p_{A} is the acoustic pressure amplitude, c is the speed of sound of the medium and ρ is the density of the medium.

By definition ultrasound is all sound with frequencies exceeding 20 kHz. However, in most medical applications frequencies exceeding 500 kHz are used [4]. In medical ultrasonics most acoustic waves propagate through the human body with ease. Only a small amount are scattered on micro-structures and tissue transitions [17]. One risk with ultrasound-based therapeutic treatments is inertial cavitation. This occurs when the peak-negative acoustic amplitude surpasses the cavitation threshold which

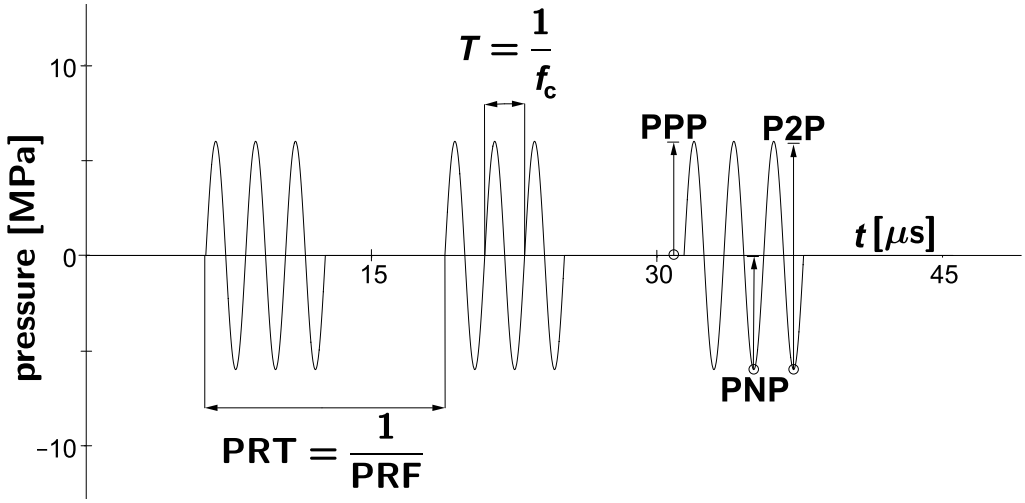

Figure 2.2: Representation of an ultrasound pulse sequence with dominant period T, centre frequency f_c, peak-positive pressure PPP, peak-negative pressure PNP, peak-to-peak pressure P2P, pulse-repetition period PRT, and pulse-repetition frequency PRF. Reprinted from [1] with permission.

can lead to bubble formation in a liquid [4]. Free radicals can form due to inertial cavitation [18, 19] which could have undesirable biological effects [20, 21].

Mechanical index is an indication of the potential mechanical damage of the ultrasound field due to internal cavitation and is calculated as follows:

$$\mathrm{MI} = \frac{\mathrm{PNP}}{\sqrt{f_c}}\,, \tag{2.2}$$

Where PNP is the maximum value of the peak negative pressure at any point in the ultrasound field, measured in water but reduced by an attenuation factor equal to that which would be produced by a medium having an attenuation coefficient of $0.3\,\mathrm{dB\,cm^{-1}\,MHz^{-1}}$, normalised by 1 MPa, and f_c is the centre frequency of the ultrasound normalised by 1 MHz [4].

A mechanical index of less than 0.3 is recommended for medical applications since cells will not be damaged and acoustic amplitude is considered to be low [4]. For mechanical index values between 0.3 and 0.7 slight damage to the neonatal lung or intestine is a possibility whereas, ultrasound with mechanical index values greater than 0.7 are unsafe as cavitation can occur [22].

2.3 Mechanical Bubble Response to Ultrasound

To gain a better understanding of how a cell will react when in an ultrasound field a background on how microbubbles behave when subjected to ultrasound is required, since this topic has been studied extensively in the past. A cell membrane is expected to behave like a microbubble when under the influence of an ultrasound field for reasons explained in section 2.4. Microbubble behaviour in an acoustic field includes oscillation, translation, ripening, coalesce, jetting, and clustering [23]. Oscillation and translation are of importance to this research.

2.4 Mechanical Cell Response to Ultrasound

To explain how cells will respond to ultrasound a, model of a cell is shown in figure 2.3. This cell model has a bilayer membrane with an inner radius R_1 and outer radius R_4, both membranes have a finite thickness and are separated by a gaseous void. The outer membrane is of thickness $(R_4 - R_3)$, the inner membrane is of thickness $(R_2 - R_1)$ and the gaseous void is of thickness $(R_3 - R_2)$ [24, 25].

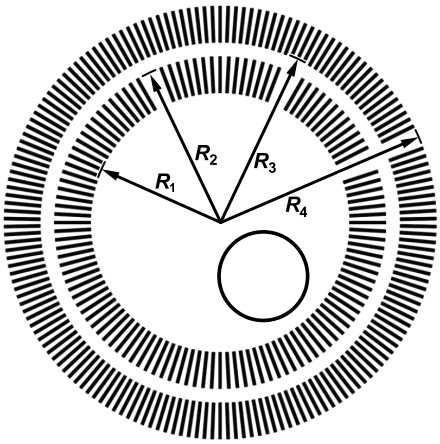

Figure 2.3: Highly simplified schematic of a cell with an outer monolayer membrane of thickness $(R_4 - R_3)$ and an inner monolayer membrane of thickness $(R_2 - R_1)$, separated by a gaseous void of thickness $(R_3 - R_2)$. Reprinted from [1] with permission.

2.4.1 Oscillation

Oscillation of cells in an ultrasound field can be explained by the bilayer sonophore model. The bilayer sonophore model states that ultrasound creates an oscillating structure in the intra-membrane hydrophobic space or gaseous void amongst two lipid monolayer leaflets of the cell membrane [3]. In other words, small "bubbles" or "gas pockets" form inside the cell membrane. These sonophores which form inside the bilayer of space of the cell membrane causes the cell's outer membrane to oscillate when subject to ultrasound. Thus, the membrane behaves similarly to a bubble in an ultrasound field. It is important to note these induced oscillations can not cause permanent damage to a human cell [25]. However, they apply enough force to the cell to induce translations. Inertial cavitation of bilayer membranes should not occur while the ultrasound field's amplitude is lower than the inertial cavitation threshold [25].

2.4.2 Translation

Translation is the critical phenomena to this research. Translation of microbubbles or cells in an ultrasound field is caused by two radiation forces, a primary Bjerknes radiation force and secondary Bjerknes radiation force [26]. The primary radiation force is caused by attraction or repulsion of a single cell from the pressure of a stationary acoustic field [27]. The movement is caused by the primary radiation force which induces a pressure difference across the surface of the cell [23]. The translation is at a maximum during the contraction phase of the cell oscillation [28]. The average velocity v of a bubble submerged in a steady fluid in the presence of an ultrasound field can be obtained from the following equation [29]:

$$v = \frac{4{p_a}^2}{\rho c f \eta C_{\mathrm{d}} \mathrm{Re}} \frac{\delta\left(\frac{f_0}{f}\right)}{\left[\left(\frac{f_0}{f}\right)^2 - 1\right]^2 + \left[\delta\left(\frac{f_0}{f}\right)\right]^2} \left[1 - e^{\left(\frac{3\eta C_{\mathrm{d}} \mathrm{Re}}{8\rho {R_0}^2} t\right)}\right], \tag{2.3}$$

where ρ is the fluid density, R_0 the equilibrium cell radius, p_a is the peak rarefactional acoustic pressure, c the speed of sound, δ a dimensionless damping constant, f the driving frequency, f_0 the cell reference frequency, η is denoted as the dynamic shear viscosity of the fluid, Re is Reynolds number and C_{d} the drag coefficient. It is assumed that equation 2.3 holds for a cell.

Secondary radiation forces cause cells to repel or attract each other [26]. These forces are proportional to cell size to the power of 5 and inversely proportional to

the squared distance between cells [23]. Cells that oscillate in phase attract each other and cells that oscillate out of phase repel each other [30, 31]. Cell resonant size serves as a threshold. If two cells are both above the resonant size, they attract each other. The same holds if both cells were to be below the resonant size [31]. If two cells are on opposite sides of the resonant phase threshold; they will oscillate out of phase and repel each other [31].

Cell Locations

The location of the microbubbles or cells are determined from the primary radiation force [2]. From equation 2.3 it can be stated that cells will move towards and then be trapped at either a node or anti-node of the standing wave ultrasound field [2]. Figure 2.4 shows node and anti-node locations assuming the pressure wave is of a sinusoidal nature.

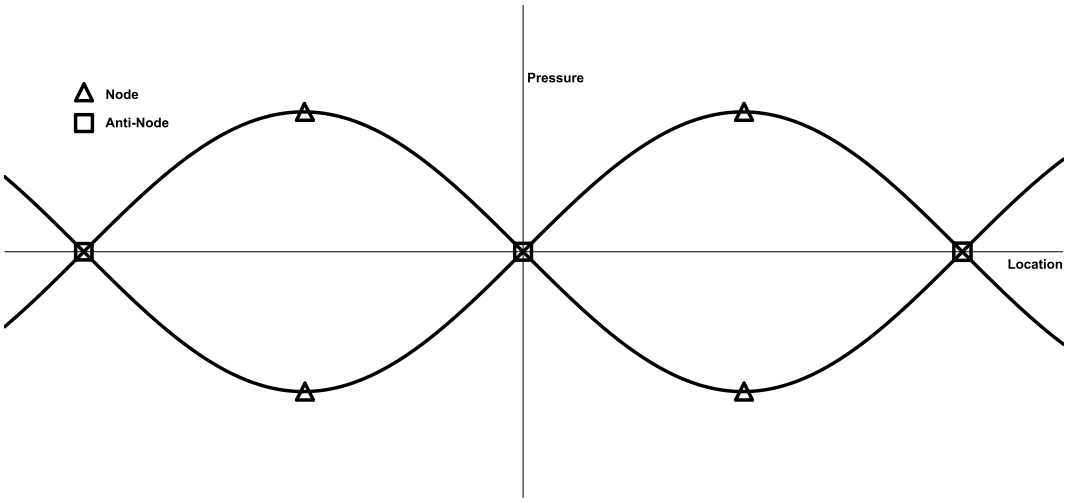

Figure 2.4: Sinusoidal pressure wave indicating the nodes and anti-nodes of the sound field. Adapted from [2].

There are three possibilities of where a cell will be trapped, depending on the transmitted ultrasound centre frequency f_C and the cell's resonance frequency f_0. The first scenario is if the cell's resonance frequency is higher than the ultrasound wave frequency. In this scenario, the primary radiation force is positive and works along a single wavelength where two locations are seen as stable where cells will be trapped at [2]. Referring to Figure 2.5 it can be seen how cells are trapped at stable locations. The arrows in Figure 2.5 indicate corrective forces which keep cells

at stable locations. It can be concluded from the aforementioned and Figure 2.4 that the stable locations are in fact anti-nodes of the ultrasound wave, which is half a wavelength apart.

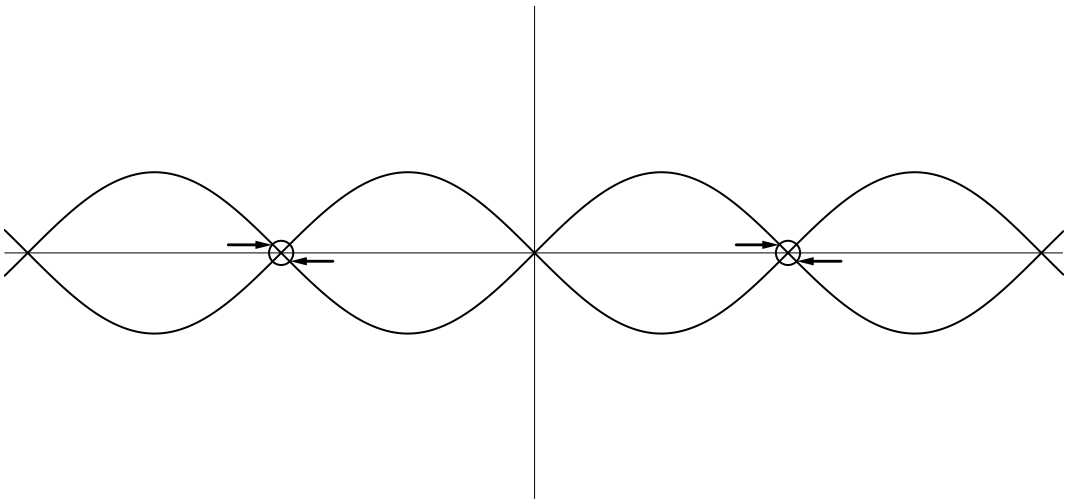

Figure 2.5: Radiation force wave with $f_0 > f$, adapted from [2].

The second scenario is where the frequency of the ultrasound wave is larger than the cell's resonance frequency. The primary radiation force is now inverted to the first scenario. In this case, the force works along a single wavelength, but three locations are considered to be stable [2]. The cells will now be trapped at these locations which are again half a wavelength apart as shown in Figure 2.6.

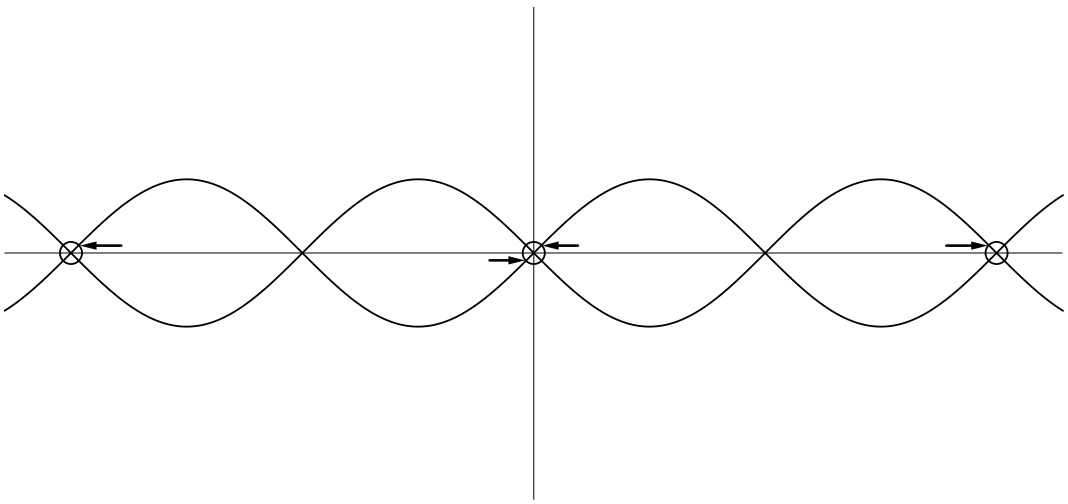

Figure 2.6: Radiation force wave with $f_0 < f$, adapted from [2].

The final scenario arises when the cell's resonance frequency equals the centre frequency of the ultrasound wave. When referring to equation 2.3, it can be noted that the primary radiation force will become zero. The cells will thus remain in their original locations and while oscillating at their maximum values [2].

Ultrasound-forced Cell Translations

Cells are expected to move towards the nodes and anti-nodes of a standing wave ultrasound field. Cells with resonance frequencies higher than the ultrasound centre frequency are expected to move towards the pressure anti-nodes and cells with resonance frequencies lower than the ultrasound centre are expected to move towards pressure nodes of the standing wave ultrasound field.

Chapter 3

Methodology

Section 3.1 is based on a paper submitted for publication in the 2019 SAIP conference proceedings [C. Smalberger, C. Carlson and M. Postema, "Experimental setup for optical observation of ultrasound-assisted cell manipulation "]. The experimental setup described in section 3.1 was the same setup used to conduct this research. For the engineering drawings see appendix A.

3.1 Experimental setup for optical observation of ultrasound-assisted cell manipulation

Living cells can be manipulated in sound fields [3]. The ultimate purpose of ultrasonic cell manipulation is the detection, quantification, manipulation and eradication of individual cells [1].

To observe the interaction of micromaterials with ultrasound, experimental setups are used to accommodate optical microscopy and ultrasound transducers. In these setups, the acoustic focus of an ultrasound transducer needs to line up with the optical region of interest during experimentation. For different sonication conditions, the transducer needs to be positioned at a variable angle and distance with respect to the optical region of interest.

Some experimental setups can only accommodate a transducer at a fixed distance and angle with respect to the optical region of interest [32, 23, 33], whereas other setups accommodate clamped transducers that are not integrated in the microscopy part of the setup [26, 34, 35]. The setup presented in this paper overcomes these shortcomings.

Potential applications of this experimental setup include cell separation, cell eradication, and parasite detection.

3.1.1 Experimental Setup

An experimental setup schematic is shown in Figure 3.1 with a line drawing and photograph of the experimental environment in Figure 3.2.

An AFG 3021B arbitrary function generator (Tektronix Incorporated, Beaverton, Oregon, United States) is used to generate a pulse sequence at a centre frequency and amplitude specific to the transducer. An A-150 55-dB linear power amplifier (ENI Technology, Inc., Rochester, NY) amplifies the signal. The power amplifier is connected to an ultrasound transducer. The transducer is placed in a bracket that can be positioned at a variable distance to the optical region of interest. The bracket is attached to a plate, which is manually tilted to set the angle of incidence. This plate is positioned in a perspex container with internal dimensions $580 \times 235 \times 65\,(\mathrm{mm})^3$. The container is filled with degassed water which serves as the medium of

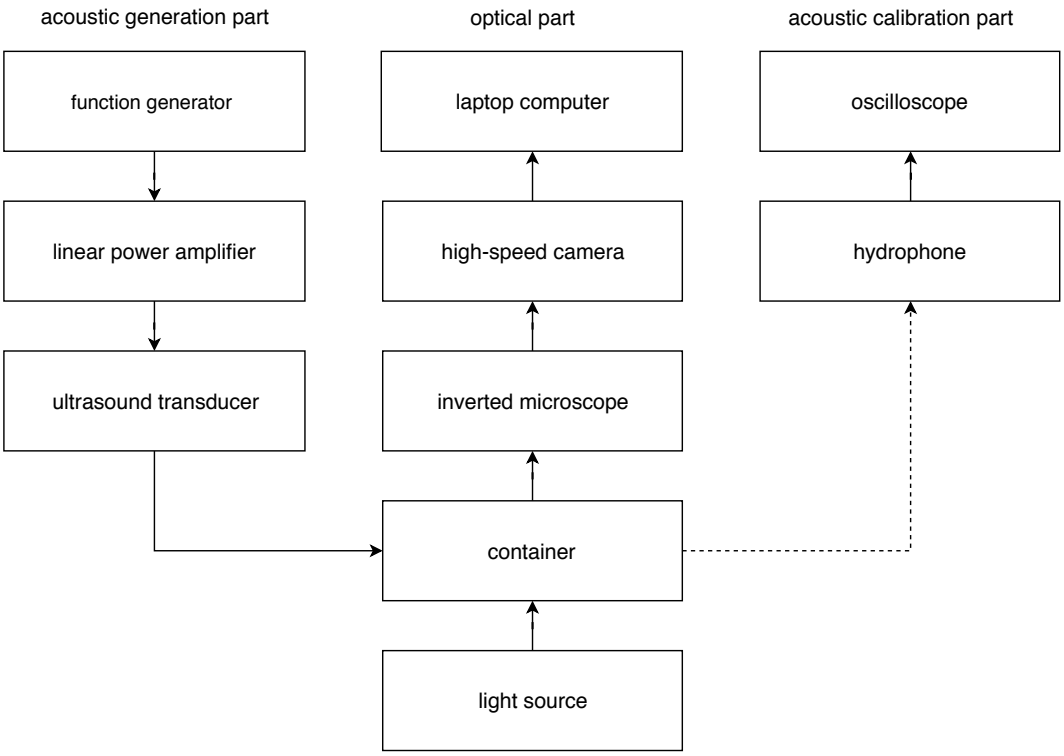

Figure 3.1: Schematic of experimental setup. The calibration part is removed after calibration (dashed).

propagation. The container is placed on the stage of a CKX31 inverted microscope (Olympus Corporation, Shinjuku, Tokyo, Japan) with a C-Plan N 20× objective lens (Olympus) that has a numerical aperture of 0.4 and a working distance of 1.2 mm. The microscope has a built-in 6-V, 30-W halogen lamp light source.

Micromaterial samples are in a CUPROPHAN® RC55 cellulose capillary (Membrana GmbH, Wuppertal, Germany) with a 200-μm inner diameter and an 8-μm wall thickness. The capillary is transparent to the ultrasound. Capillary action ensures the filling up of the capillary. The capillary is held in place on top of a microscope slide, fixed inside the bottom of the container (*cf.* Figure 3.3) by a LEGO® Part 3004 brick (The LEGO Group, Billund, Denmark) at each end. The middle of the

(a)

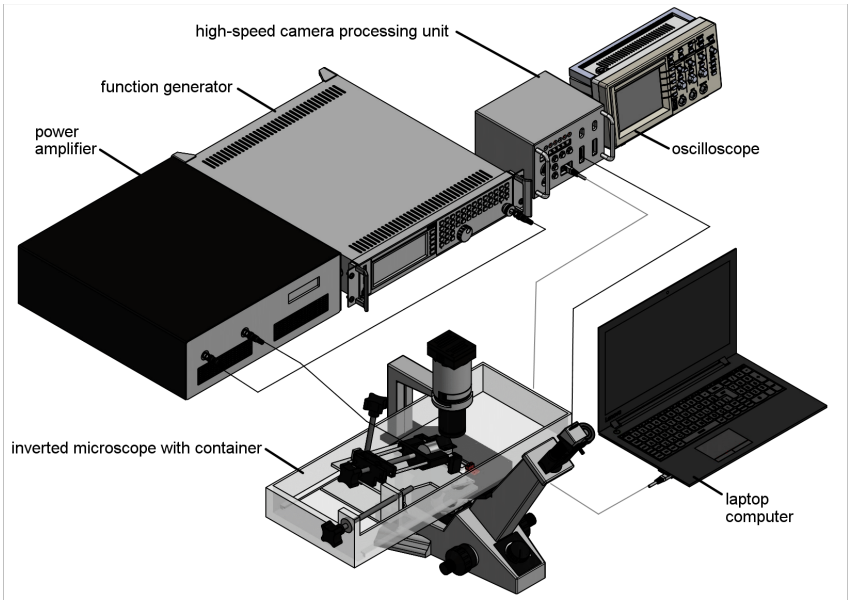

(b)

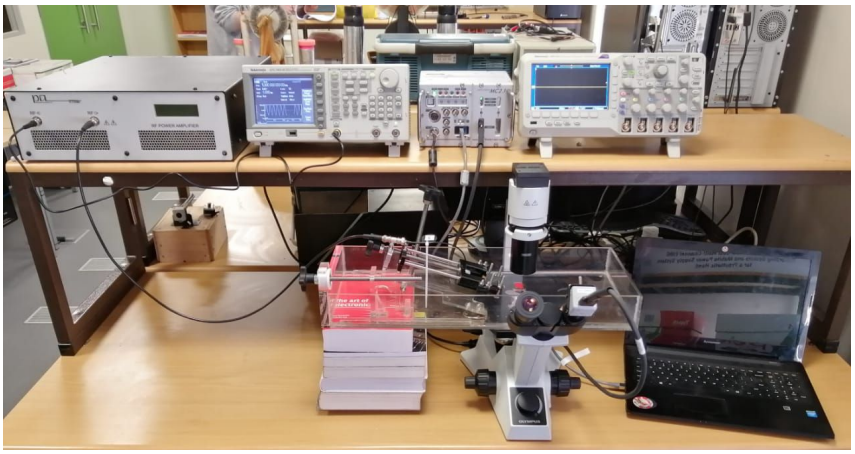

Figure 3.2: A line drawing (a) and photograph (b) of the experimental setup.

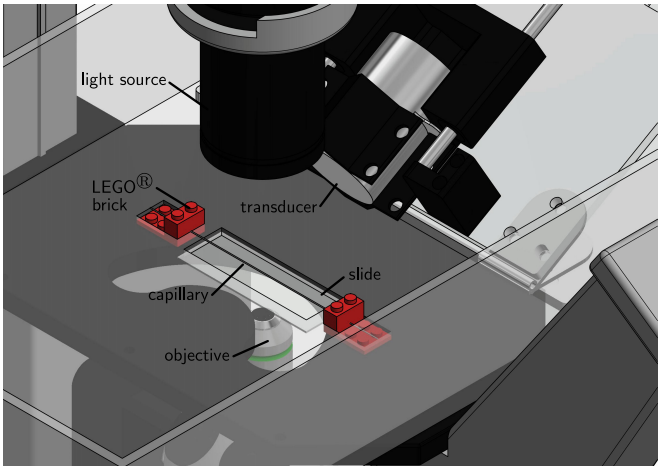

Figure 3.3: Close-up of the container with coinciding sound, light beam, and objective lens. The capillary can also be seen with the LEGO® bricks that hold it in place.

capillary coincides with the optical focus of the objective lens and with the positioned acoustic focus of the ultrasound transducer.

To calibrate the ultrasound field after positioning, an HGL-0200 bullet hydrophone (Onda Corporation, Sunnyvale California, USA) is used. The hydrophone is connected to an AH-2010 pre-amplifier (Onda) which is connected to a DPO 2014 digital phosphor oscilloscope (Tektronix). The hydrophone is removed from setup after calibration of the acoustic field.

The charge couple device (CCD) of a FASTCAM MC1 high-speed camera (Photron (Europe) Limited, West Wycombe, Bucks, United Kingdom) is mounted to the microscope eyepiece through a custom 3D-printed C-mount adaptor and connected to its processing unit. The high-speed camera can record up to 10 000 frames per second. The camera is controlled by a laptop computer. Image sequences are stored in the tagged image, *.tiff*, file format.

All image processing is done in MATLAB® (The Mathworks, Natick, Massachusetts, United States).

3.1.2 Field of view calibration

The 200-μm inner diameter of an ink-filled capillary was used to calibrate the frame size for the 20× objective lens.

The frames were found to correspond to a $211 \times 211\,(\mu\text{m})^2$ area, yielding a pixel size of $0.4 \times 0.4\,(\mu\text{m})^2$.

Quantison$^{\text{TM}}$ microbubbles (Upperton Ltd, Nottingham, UK) with 5-μm diameters were used to confirm this frame size (*cf.* Figure 3.4).

3.1.3 First Result

Antibubbles are gas bubbles containing a liquid droplet core and, typically, a stabilising outer shell. In a standing wave ultrasound field of sinusoidal nature, antibubbles were observed during pulsed 5.9-MHz, 0.3-MPa ultrasound with a 8.5% duty-cycle. Figure 3.5 demonstrates antibubble translation and accumulation.

Thus, this preliminary result shows that our experimental setup can record micromaterial dynamics under sonication.

3.2 Ultrasound

3.2.1 Transducer Classification

Transducer classification was done to find each transducer's resonance frequency. A transducer will deliver maximum power at its resonance frequency. Current through the transducer is dependent on the impedance, which in turn is dependent

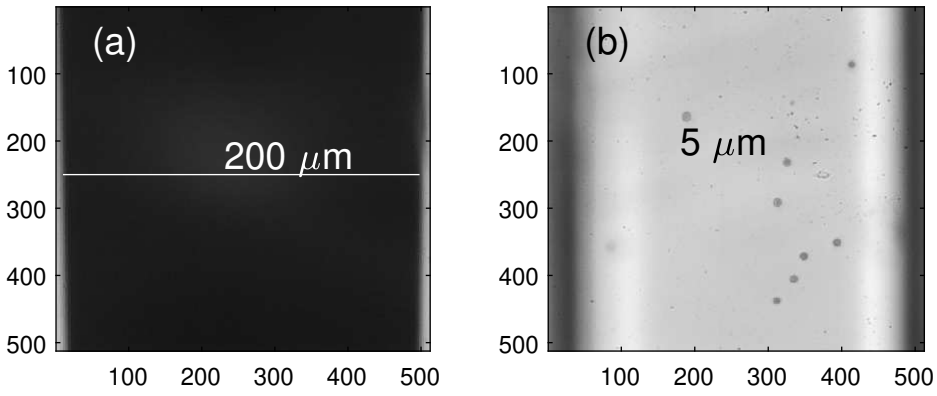

Figure 3.4: Capillary filled with ink (a) and with Quantison$^{\text{TM}}$ (b). Each frame corresponds to a $211 \times 211\,(\mu\text{m})^2$ area.

on frequency. At resonance, the impedance of the transducer is minimal and thud, maximum current flows through the transducer.

Transducer classification was started by connecting each transducer to a ZND vector network analyser (Rhode and Schwarz, Munich, Germany) and running an SWR (Standing Wave Ratio) plot over a range of frequencies. The maximum power is absorbed by a load when the SWR is equal to one. Hence, the maximum power delivered by the transducer. Figure 3.6 shows the SWR plot of a transducer with a 14.2 MHz resonance frequency.

3.2.2 Sound Field Calibration

The ultrasound field is calibrated using the HGL-0200 bullet hydrophone (Onda). For the documentation referred to in this section seen appendix B. The hydrophone is connected to a AH-2010 pre-amplifier (Onda) which is connected to a DPO 2014 digital phosphor oscilloscope (Tektronix).

The hydrophone is placed into the water-filled container where the optical focus of the objective lens and the acoustic focus of the transducer coincide. The ultrasound is switched on and the sound field is recorded by the hydrophone and displayed on the oscilloscope. The output waveform is then saved on a flash disk. Figure 3.7 shows the output of a measured sound field.

The measured hydrophone voltage was used to approximate the acoustic pressure

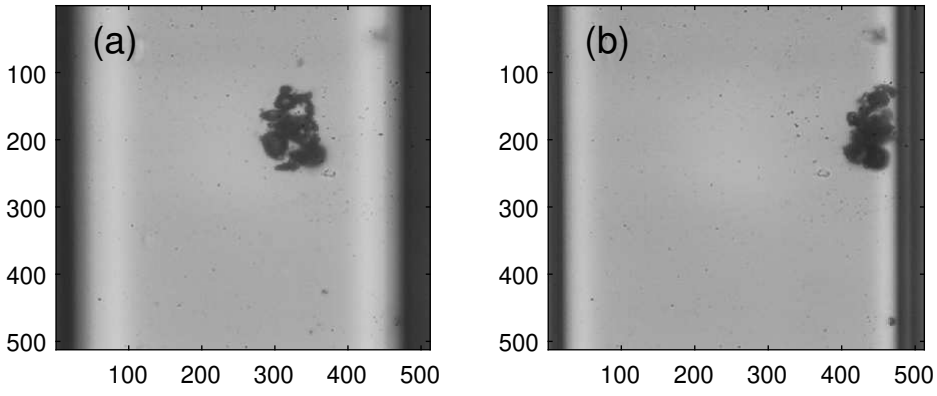

Figure 3.5: Cluster of antibubbles before (a) and after (b) ultrasound. The transducer is positioned towards the right of the frames. Each frame corresponds to a 211 × 211 $(\mu\text{m})^2$ area.

waveform using the following equation [36]:

$$p(t) = \frac{V(t)}{M(f_L)}, \tag{3.1}$$

where $p(t)$ is the acoustic pressure waveform, $V(t)$ the measured hydrophone voltage and $M(f_L)$ the sensitivity of the hydrophone, pre-amplifier combination.

With the hydrophone and amplifier impedances being primarily capacitive, the sensitivity of the hydrophone, pre-amplifier combination $M(f_L)$ can approximated as follows:

$$M(f_L) = G(f)M_c(f)\frac{C_H}{C_H + C_A}, \tag{3.2}$$

where $G(f)$ is the amplifier gain as a function of frequency and is obtained from the pre-amplifier calibration certificate in appendix E. $M_c(f)$ is the End-of-cable open circuit sensitivity obtained from the HGL hydrophones data sheet in appendix E. C_H and C_A are the capacitance of the hydrophone and amplifier respectively and are obtained fom the HGL hydrophones data sheet and the pre-amplifier calibration certificate respectively.

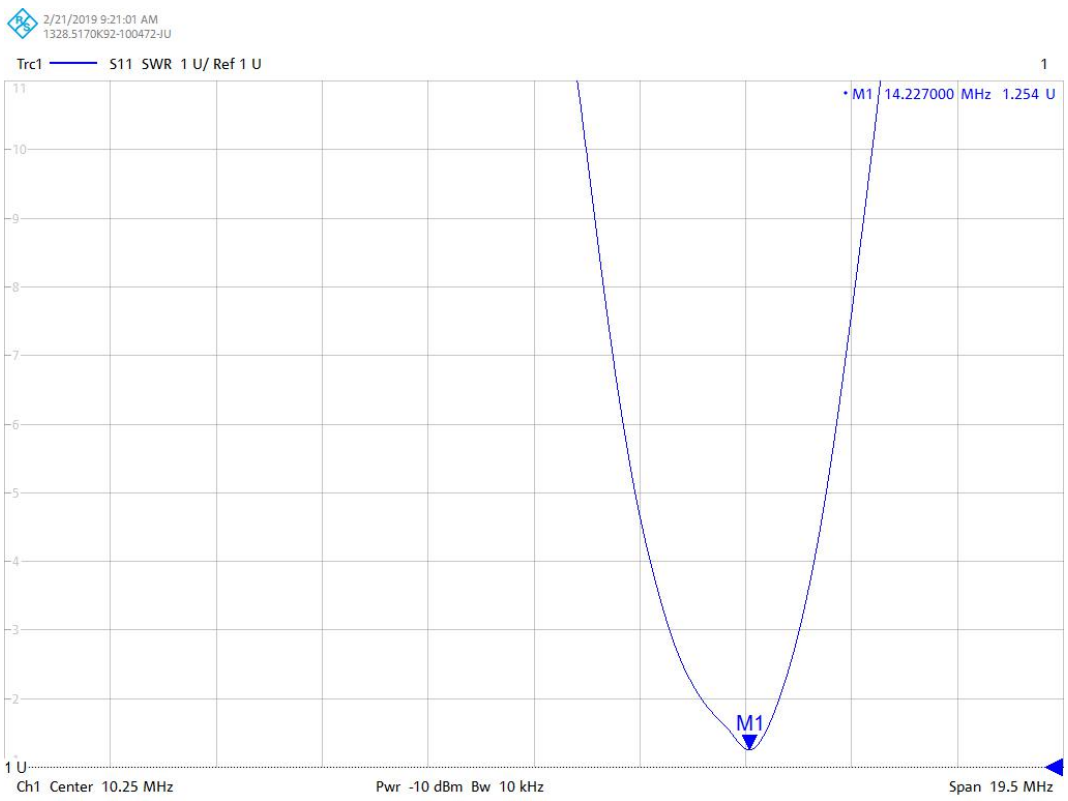

Figure 3.6: SWR-plot of a transducer with a 14.2-MHz resonance frequency.

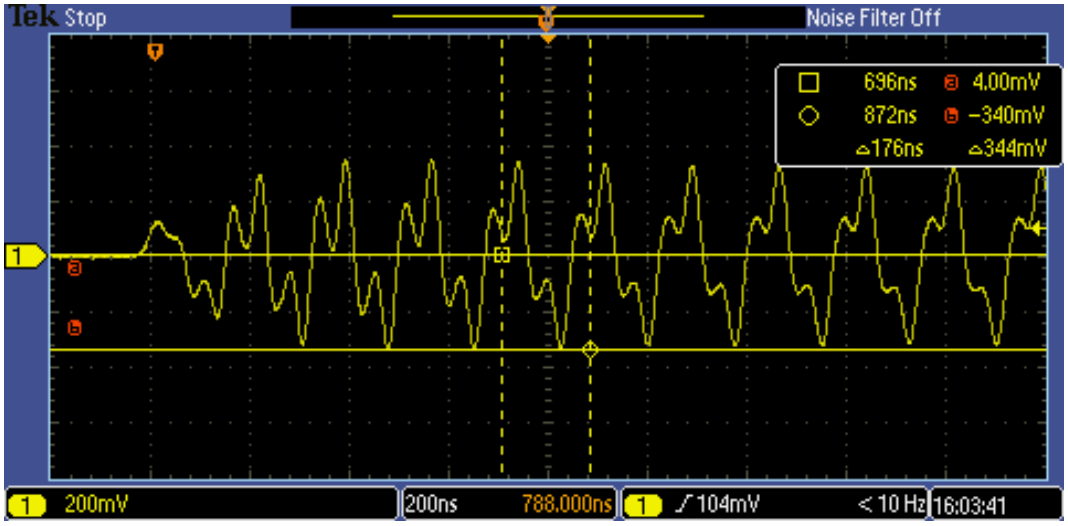

Figure 3.7: A hydrophone measured output waveform.

Equation 3.2 is substituted into equation 3.1 which yields:

$$p(t) = \frac{V(t)}{G(f)M_c(f)\frac{C_H}{C_H+C_A}}, \tag{3.3}$$

the voltage $V(t)$ is multiplied by the relative directivity factor R_{Amp} which changes with the variable angle of the transducer with respect to the hydrophone. R_{Amp} is obtained from the HGL-0200 bullet hydrophone (Onda) directivity plot in appendix E. The acoustic pressure is calculated as follows:

$$p(t) = \frac{V(t)R_{Amp}}{G(f)M_c(f)\frac{C_H}{C_H+C_A}}. \tag{3.4}$$

3.3 Samples

The samples used for this research were whole blood samples obtained from the South African National Blood Service (SANBS).

Blood samples used in this research did not conform to medical standards and was deemed unfit for patient use. The reason for non conformance is a short bleed. A short bleed is when a donor fails to donate the minimum of 525 ml required to fill a unit of blood. These samples are tested and safe. Figure 3.8 shows a category C whole blood unit which is tested blood from a regular donor and the safest available from the SANBS.

For the required ethics to use these samples see appendix C.

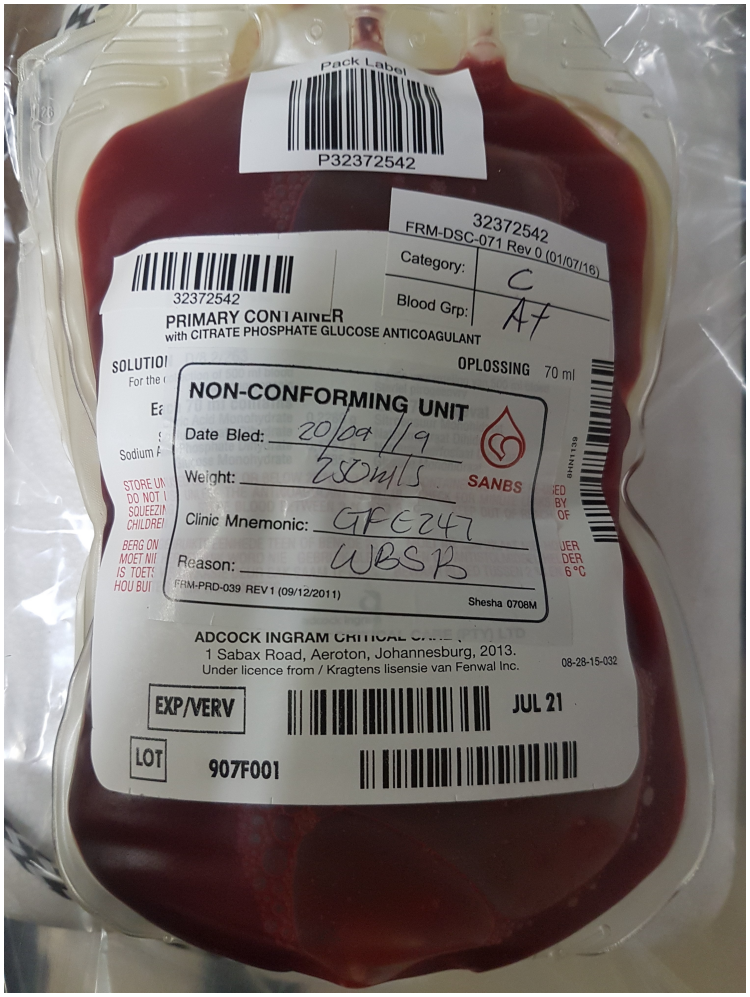

Figure 3.8: An SANBS blood unit.

Anticoagulants

Anticoagulants are used to prevent the blood from clotting. The SANBS unit bag contains the anti-coagulants citrate phosphate glucose (CPG) and ADSOL.

During experimentation blood samples are transferred from the unit to blue-top vacutainer (BIOCOM biotech, Centurion, South Africa) blood collection tubes. These plastic tubes have a plastic cap with a rubber stopper. Vacutainers contain 2.7 ml of sodium citrate. Sodium citrate an effective anticoagulant due to its mild calcium-chelating properties. The blood is transferred to a vacutainer by sticking a needle through the rubber stopper. The tube then automatically fills to the correct level to achieve the desired concentration as predetermined by the manufacturer.

3.3.1 Tyrode's Buffer

Tyrode's solution was used as a buffer to dilute the blood samples. The dilution was done to be able to see individual white and red blood cells as the effects of ultrasound could not be observed when the blood was too dense.

A litre of Tyrode's solution is mixed using the following: 7.83 g 6398 NaCl (EMSURE Merck, Darmsradt, West Germany), 0.1 g NaHCO3 (EMSURE Merck), 0.22 g KCl (EMSURE Merck), 0.05 g Na2HPO4 (EMSURE Merck), 0.1 g MgCl2 (EMSURE Merck) and 2.38 g HEPES 2-[4-(2-hydroxyethyl)piperazin-1-yl] ethanesulfonic (Sigma-Aldrich, St. Louis, MO, USA).

To mix Tyrode's solution the salts are dissolved in 800 ml of distilled water using a magnetic mixer. The pH of the solution is then measured and verified to be 7.4, after which another 200 ml of distilled water is added. The solution is stored at 4° C.

3.4 Experimental Procedure

An experimental procedure schematic is shown in Figure 3.9.

Initially, all experiments follow the same procedure. A unit of blood is stored at 4° C, 60 ml of blood is drawn from a blood unit using a syringe. The time at which this is done is recorded. The blood is then transferred to vacutainers, each vacutainer is agitated from side to side five times to mix the anticoagulant with the blood. A vacutainer is then transferred from the fridge to the experimental bench.

The vacutainer is opened and a timer is started. Blood is drawn from the vacutainer using a Nichipet EX pipette (Nichiryo, Saitama, Japan) and mixed with Tyrode's buffer in a tube. The tube is agitated from side to side four time. A capillary is placed in the tube and left to fill. Once the capillary is filled, the first split time is taken and the capillary is clamped at both ends and secured into position by two LEGO® bricks in the container, (*cf.* Figure 3.3). Once the capillary is secured, the second split time is taken.

The there are two types of experiments, experiments where no ultrasound field is applied to the sample and experiments where an ultrasound field is applied to the sample.

3.4.1 Null-Experiments

Recording commences after ensuring that the capillary is in the correct position with respect to the objective lens. The third split time is taken as recording commences. Once recording is finished, the timer is stopped and the video result is saved. The capillary is removed from the container and the contaminated syringes, tubes and capillaries are disposed in a sharps container.

3.4.2 Ultrasound-Experiments

With the capillary in position, the recording is stared with the ultrasound switched on immediately after recording commenced. The third split time is taken as recording commences. Once recording is finished the timer is stopped, the ultrasound is switched off and the video result is saved. The capillary is removed from the container and the contaminated syringes, tubes and capillaries are disposed in a sharps container.

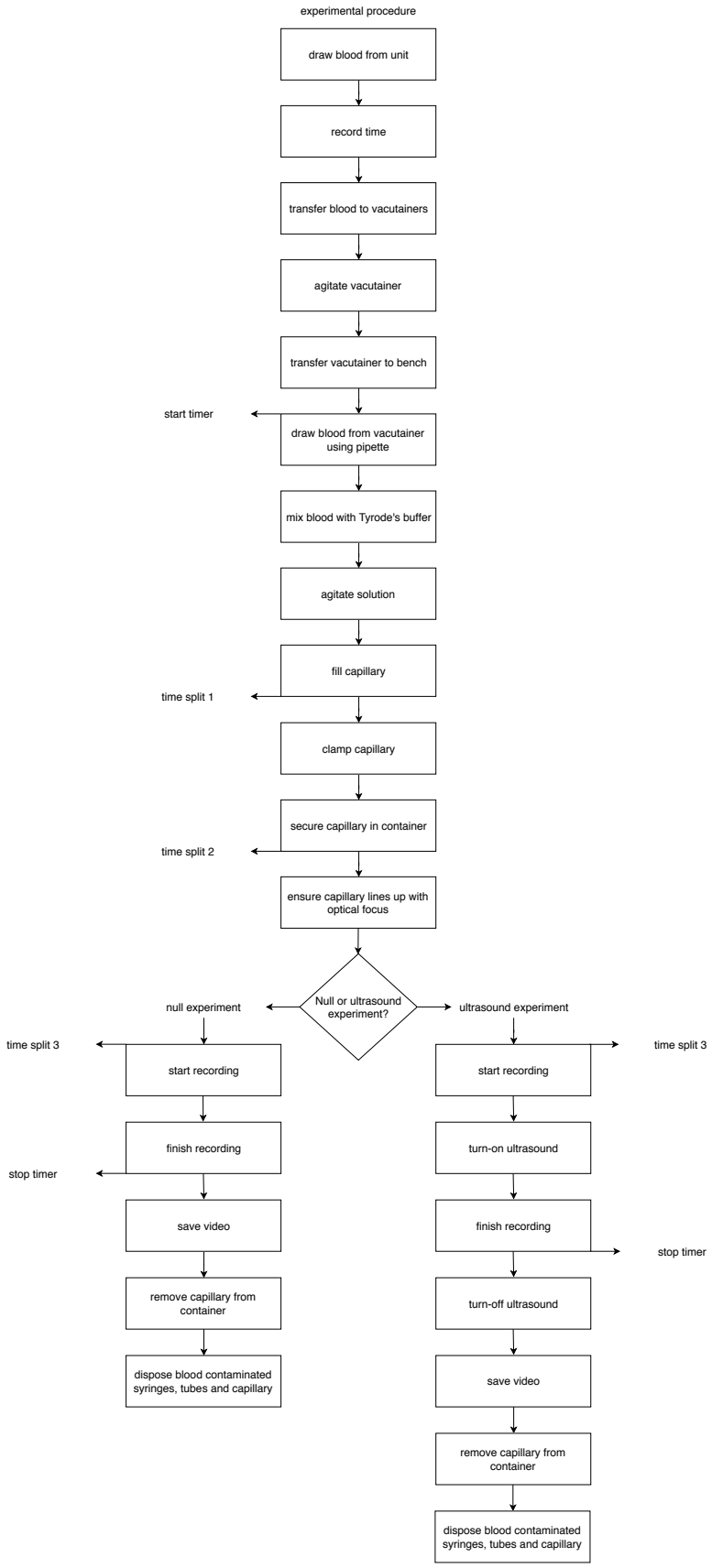

Figure 3.9: Schematic of experimental procedure. Showing two types of experiments, a null experiment and an experiment where ultrasound is applied to the sample.

Chapter 4

Results and Discussion

4.1 Data Acquisition

The centre of white and red blood cells were tracked in each video recorded. Tracking yielded the x and y-coordinates as pixel values of the centre of each tracked cell per frame as it moved throughout the video. Tracking of a cell continued until recording concluded or until the cell moved out of the field of view.

Each frame corresponds to a $211 \times 211\,(\mu\text{m})^2$ area, yielding a pixel size of $0.4 \times 0.4\,(\mu\text{m})^2$ (*cf.* Section 3.1.2).

4.2 Data Processing

Cell displacements were calculated from one frame to the next using equation 4.1:

$$d = 0.4\sqrt{(x_1 - x_0)^2}, \tag{4.1}$$

where x_1 is the x-coordinate of the centre of a cell in the current frame and x_0 is the x-coordinate of the centre of the same cell in the previous frame. Positive displacements were assumed to be away from the ultrasound transducer. All data processing was done in MATLAB® (The Mathworks). (*cf.* Appendix D).

4.3 Representation of Processed Data

The results are presented graphically. Displacement in the x-direction was plotted as a function of time. Cell initial and final position in the capillary was plotted, and cell x-displacement was plotted at various mechanical indices. All plotting scripts were done in MATLAB® (The Mathworks). (*cf.* Appendix D).

4.4 Results

Selected results are displayed throughout this section. For the complete results set see appendix E.

4.4.1 Null-Experiments

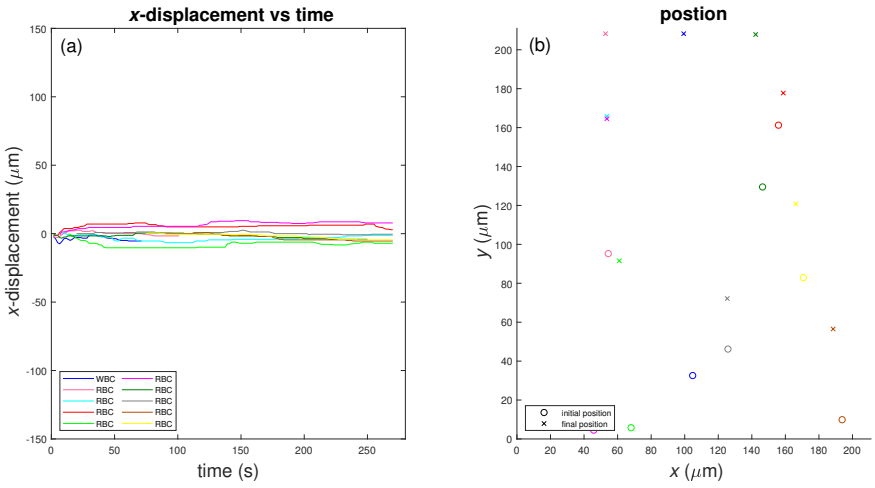

Figure 4.1: White and red blood cells x-displacement (a) and position (b) during a null-experiment.

From figure 4.1-4.5 it was observed that white and red blood cells all stream in the same vertical direction. There was minimal movement in the x-direction. The cells in figures 4.1 and 4.2 stream from the bottom of the capillary to the top and the cells in figures 4.3-4.5 stream from the top of the capillary to the bottom.

The total x-displacement of all null-experiments is illustrated in figures 4.18 and 4.19.

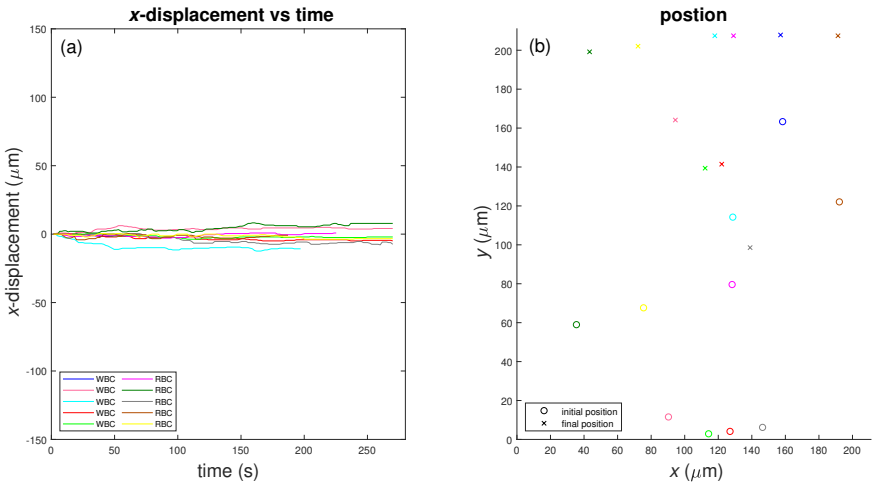

Figure 4.2: White and red blood cells x-displacement (a) and position (b) during a null-experiment.

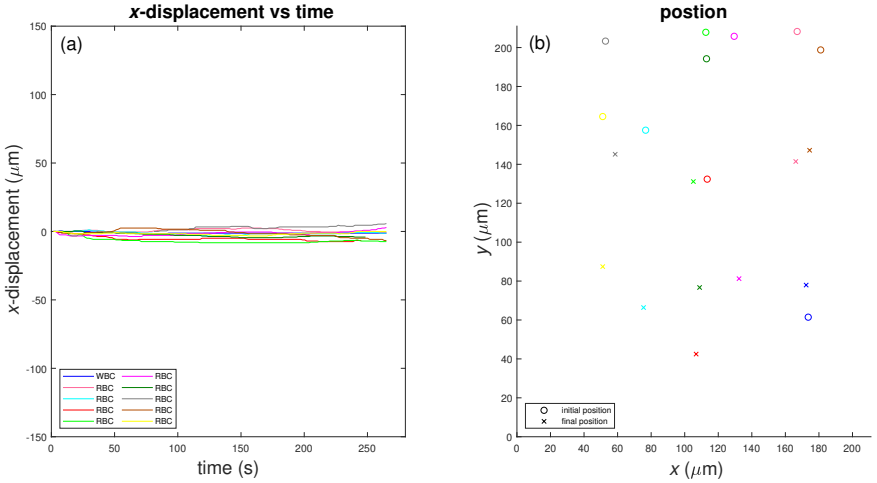

Figure 4.3: White and red blood cells x-displacement (a) and position (b) during a null-experiment.

4.4.2 Ultrasound-experiments

Figures 4.6-4.7 illustrated that the red blood cells all moved towards a region to the left of the capillary against the direction of the sound-field. The white blood cells remained to the right of the capillary near their initial position.

Figures 4.8-4.11 illustrated red blood cells move to a region on the left of the capillary, against the direction of the sound field. Where white blood cells move towards a

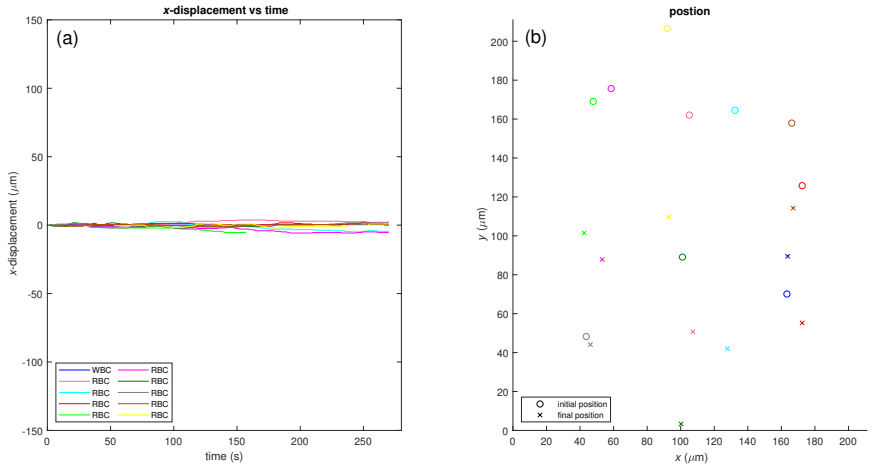

Figure 4.4: White and red blood cells x-displacement (a) and position (b) during a null-experiment.

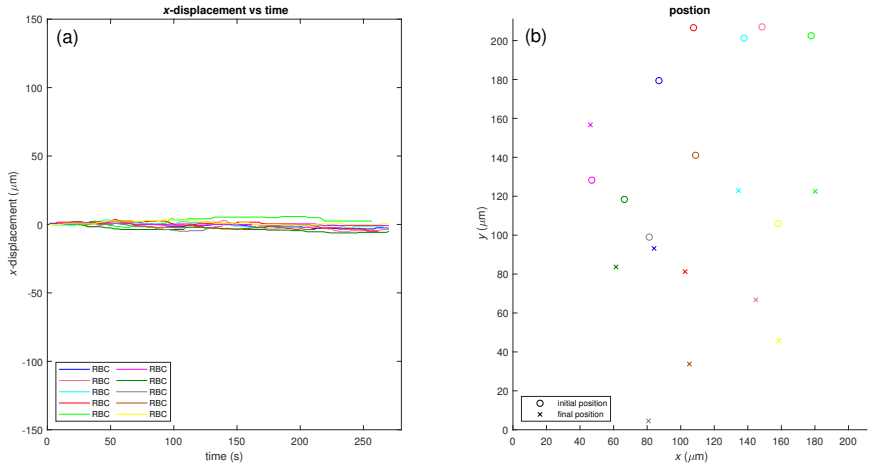

Figure 4.5: Red blood cells x-displacement (a) and position (b) during a null-experiment.

region to the right of the capillary in the direction of the sound field. In some cases a few red blood cells remained close to their initial horizontal positions.

Figures 4.12-4.14 illustrated all cells move in the same horizontal direction. In figures 4.12 and 4.13, against the direction of the sound-field and in figure 4.14, in the direction of the sound-field.

Figures 4.15-4.16 illustrated all cells move in a direction towards the sound-field except a for a few cells. The initial position of these exceptions are near the right

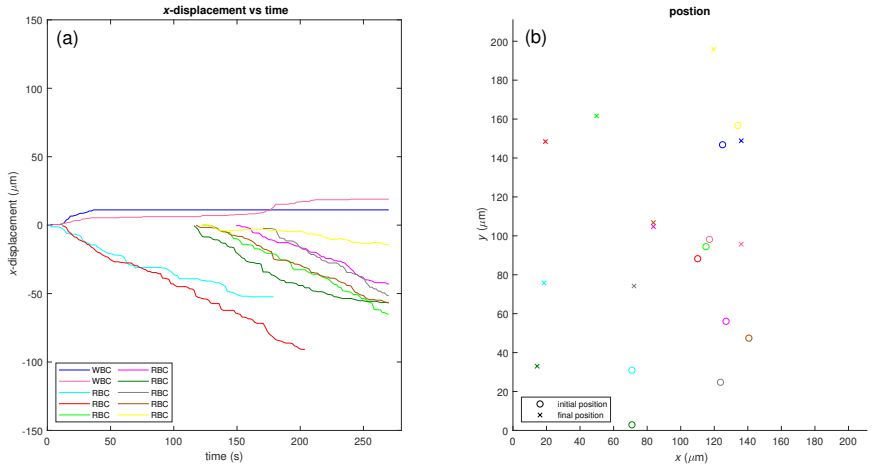

Figure 4.6: White and red blood cell x-displacement (a) and position (b) during a pulsed 5.8-MHz, 0.5-MPa ultrasound with a 10% duty-cycle.

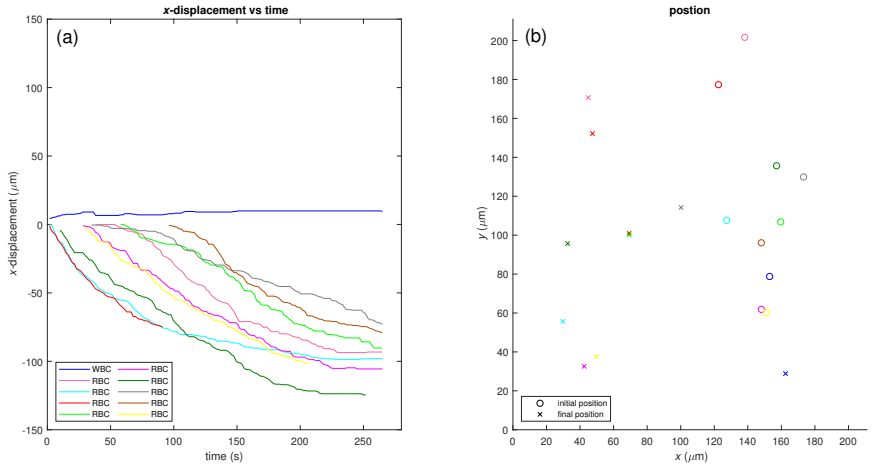

Figure 4.7: Red blood cell x-displacement (a) and position (b) during a pulsed 5.8-MHz, 0.8-MPa ultrasound with a 35% duty-cycle.

edge of the capillary.

Figure 4.17 illustrated how all cells move to one horizontal position in the capillary.

The total x-displacement at various mechanical indices of all ultrasound-experiments is illustrated in figures 4.18 and 4.19.

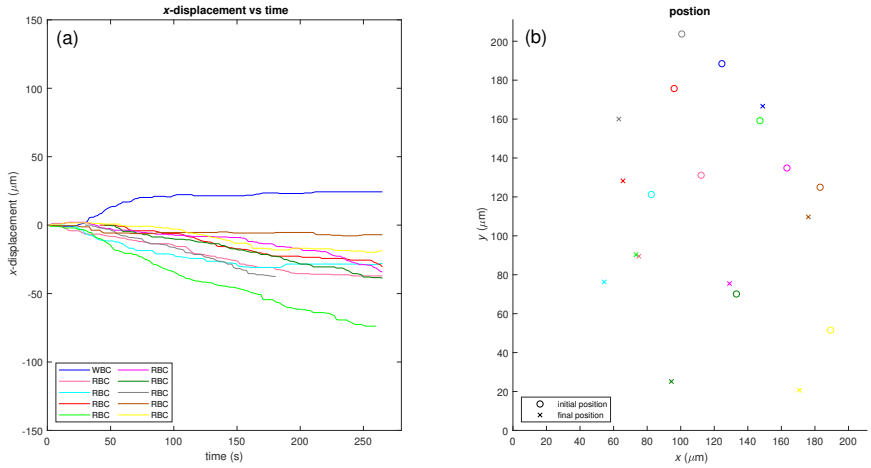

Figure 4.8: White and red blood cell x-displacement (a) and position (b) during a pulsed 5.8-MHz, 0.6-MPa ultrasound with a 35% duty-cycle.

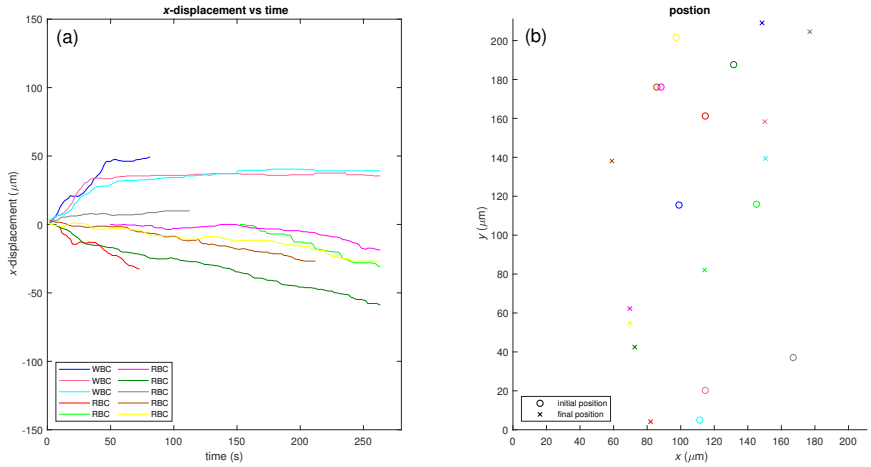

Figure 4.9: White and red blood cell x-displacement (a) and position (b) during a pulsed 5.8-MHz, 0.85-MPa ultrasound with a 35% duty-cycle.

4.5 Discussion

4.5.1 Null-Experiments

White and red blood cells moved from top to bottom or vice-versa in the y-direction of the capillary with minimal movement in the x-direction. The lack of movement in the x-direction illustrated that the blood is flowing through the capillary in a

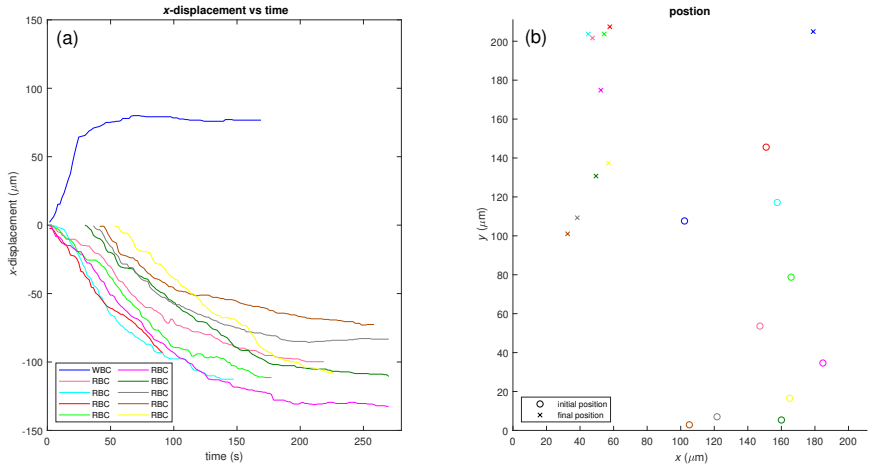

Figure 4.10: White and red blood cell x-displacement (a) and position (b) during a pulsed 5.8-MHz, 0.85-MPa ultrasound with a 35% duty-cycle.

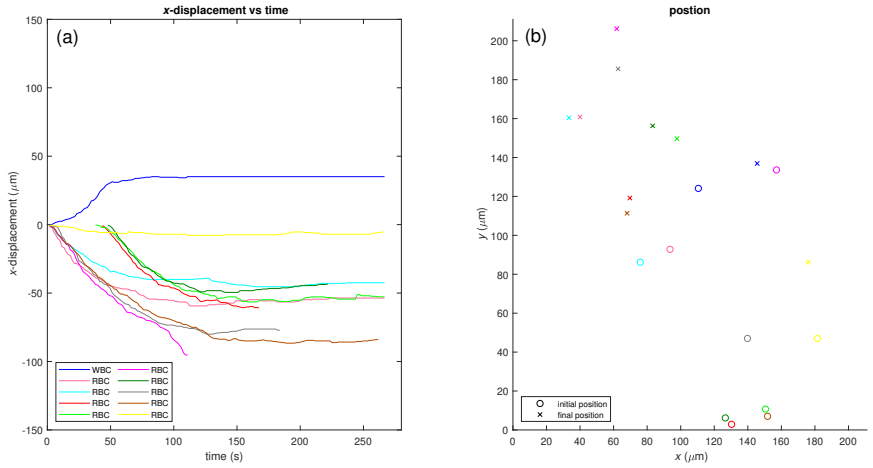

Figure 4.11: White and red blood cell x-displacement (a) and position (b) during a pulsed 5.8-MHz, 0.85-MPa ultrasound with a 35% duty-cycle.

laminar fashion. The flow can be described using Poiseuille's law:

$$\frac{v}{t} = \frac{\Delta p \pi R^4}{8\eta \mathrm{L}}. \tag{4.2}$$

The flow rate is proportional to the pressure difference between the ends of the capillary and the radius of the capillary. The flow rate is inversely proportional to the viscosity of the fluid, coefficient η, and the length of the capillary L. The change in the direction of the flow seen between figures 4.1, 4.2 and figures 4.3-4.5 could be attributed to the pressure difference across the ends of the capillary. The change in

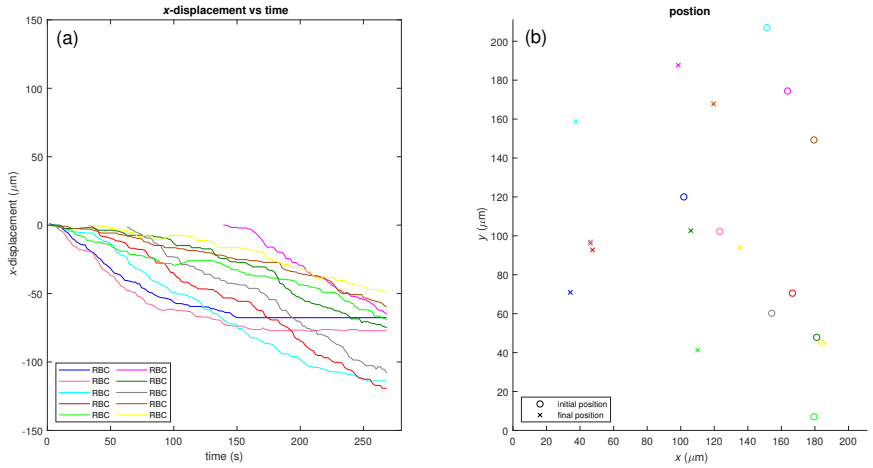

Figure 4.12: Red blood cell x-displacement (a) and position (b) during a pulsed 5.8-MHz, 0.8-MPa ultrasound with a 35% duty-cycle.

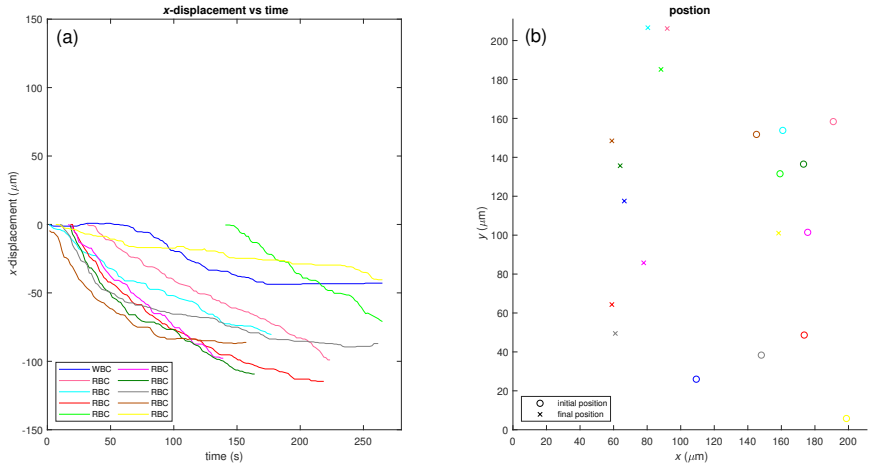

Figure 4.13: White and red blood cell x-displacement (a) and position (b) during a pulsed 5.8-MHz, 0.6-MPa ultrasound with a 35% duty-cycle.

pressure difference is due to capillaries not filled with the same amount of blood and not cut the same length for each experiment.

The displacement of cells in a laminar fashion was confirmed by the observation that cells in the middle of the capillary had greater velocity than cells close to the edges.

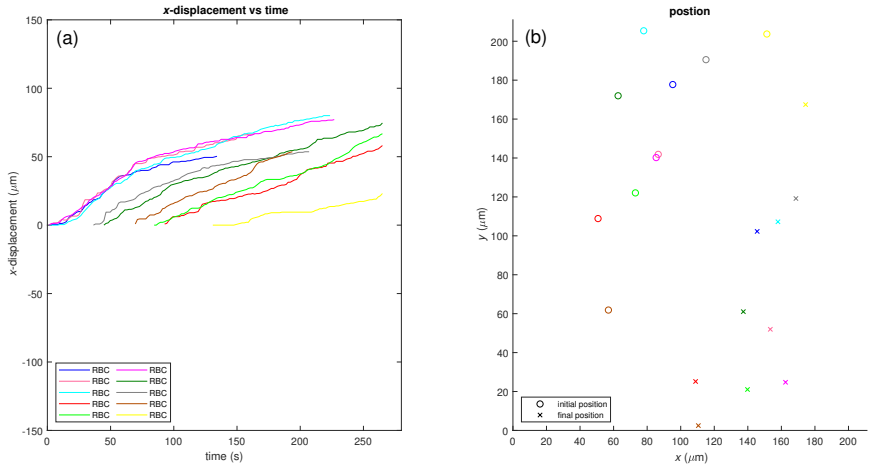

Figure 4.14: Red blood cell x-displacement (a) and position (b) during a pulsed 5.8-MHz, 0.6-MPa ultrasound with a 35% duty-cycle.

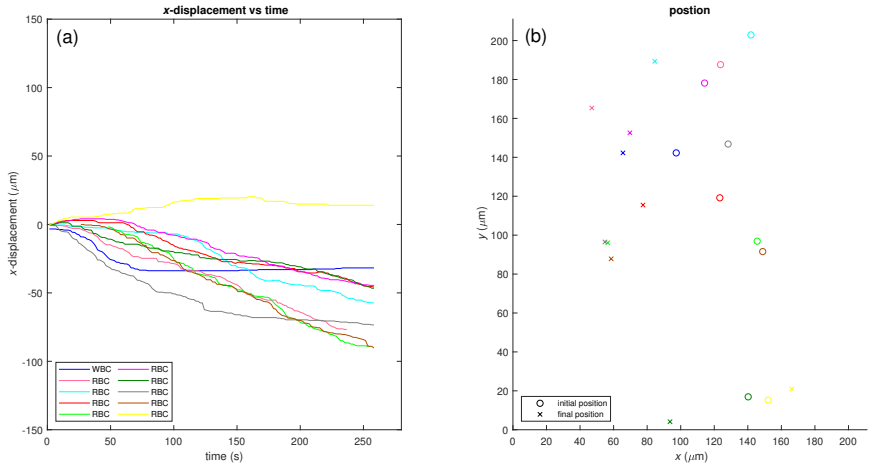

Figure 4.15: White and red blood cell x-displacement (a) and position (b) during a pulsed 5.8-MHz, 0.8-MPa ultrasound with a 35% duty-cycle.

4.5.2 Ultrasound-Experiments

Applying ultrasound to white and red blood cells results in movement in the x-direction. Most cells were seen to migrate towards certain vertical regions in the capillary and remained there. Often white blood cells migrated towards a different vertical region than red blood cells.

Movement in the x-direction could be attributed to the primary Bjerknes force

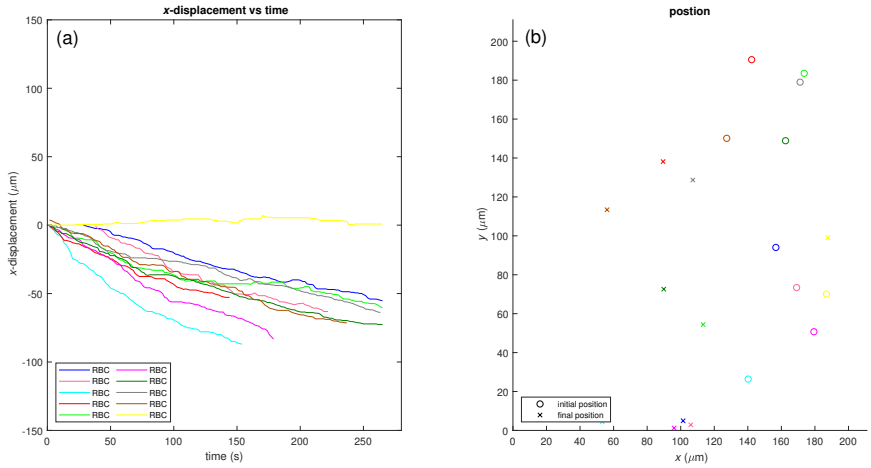

Figure 4.16: Red blood cell x-displacement (a) and position (b) during a pulsed 5.8-MHz, 0.85-MPa ultrasound with a 35% duty-cycle.

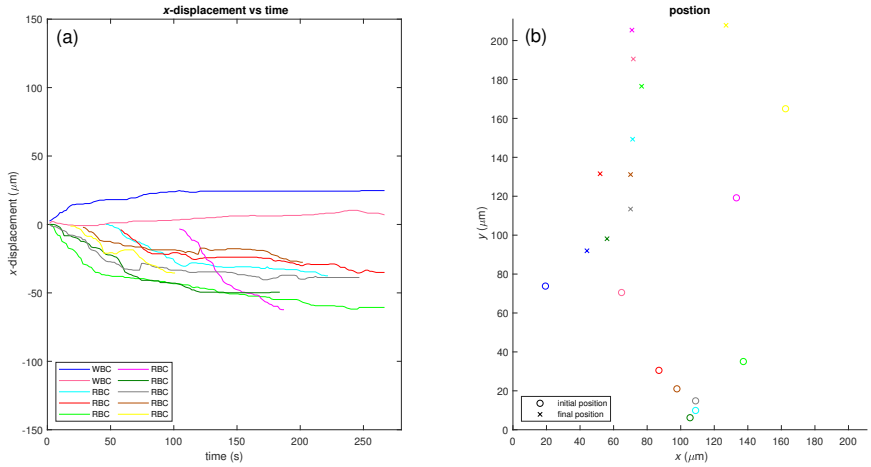

Figure 4.17: White and red blood cell x-displacement (a) and position (b) during a pulsed 5.8-MHz, 0.85-MPa ultrasound with a 35% duty-cycle.

experienced by white and red blood cells when subject to ultrasound. As discussed in section 2.4.2 a pressure difference is induced across the surface of a cell which causes the cell to move either in the direction of the sound-field away from the transducer or against the direction of the sound-field towards the transducer.

The vertical regions towards which cells migrated and remained are the pressure nodes and the pressure anti-nodes of the sound-field. The speed of sound in the Tyrode's buffer diluted blood sample is assumed to be $1540\,m/s$ The wavelength

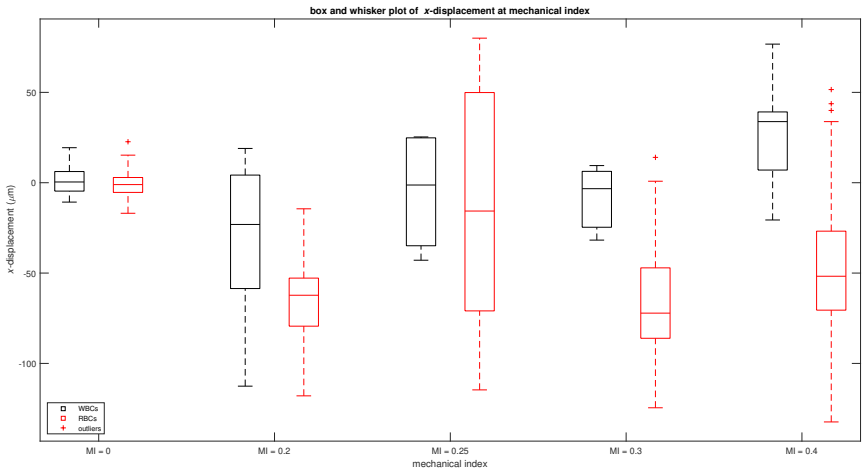

Figure 4.18: X-displacement at different mechanical indices. The direction of the sound field is assumed to be positive

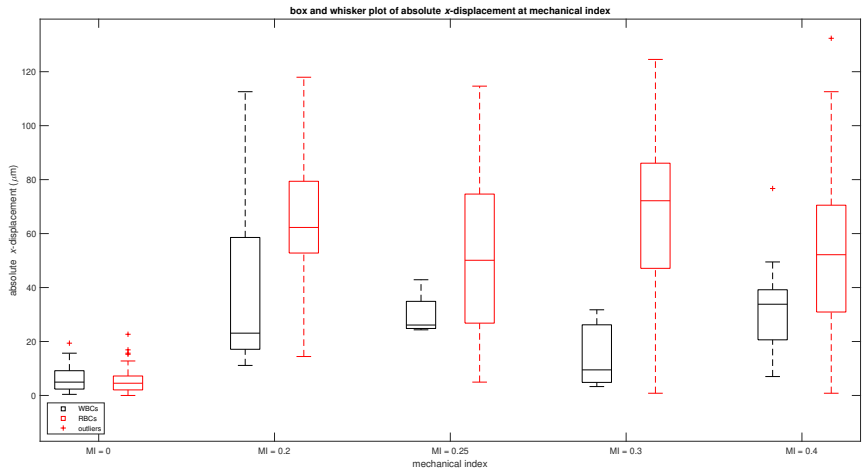

Figure 4.19: Absolute x-displacement at different mechanical indices. The direction of the sound field is assumed to be positive

of the 5.7-MHz ultrasound was calculated to be 270 μm. Nodes and anti-nodes are a quarter of a wavelength apart (*cf.* Figure 2.4). A capillary diameter of 200 μm guaranteed the presence of either two nodes and one anti-node or two anti-nodes and one node.

As discussed in section 2.4.2 the primary Bjerknes force will not only cause a cell to move in the x-direction but also cause cells to move towards nodes and anti-nodes and remain trapped there. Whether a cell moves to a node or anti-node depends on

the centre frequency of the ultrasound-field and the resonance frequency of the cell is related to the cell's initial size.

Some cells did not experience as much horizontal movement as others. This could be attributed to these cells' initial locations being close to a node or anti-nodes in the sound-field, as seen in figures 4.6 and 4.7. Often white blood cells moved to one region and red blood cells to the another as seen in figures 4.9, 4.10, and 4.11. This suggests that white blood cells are repelled by the ultrasound-field and red blood cells are attracted to the ultrasound-field or vice-versa. This can be attributed to the difference in initial size of the cells (*cf.* Equation 2.3), one cell type oscillates in phase with the sound fiend and the other not. . However, this was not always the case as illustrated in figures 4.13, 4.15 and 4.17. In some cases cells were attracted to the wall of a capillary as illustrated by the yellow marked red blood cells in figures 4.15 and 4.16. Note that these red blood cells start close to the wall of the capillary which could indicate a node or anti-node beyond the wall or the cell could get stuck to the wall of the capillary. It is concluded from the aforementioned that white and red blood cells move to either a node or anti-node in an ultrasound-field.

The behaviour of white and red blood cells under the influence of ultrasound confirms that cells oscillate in an ultrasound-field. This suggests that the bilayer sonophore model discussed in section 2.4 and 2.4.1 model holds for white and red blood cells. This means an oscillating structure is created in the gaseous void between the bilayers of a cell which causes the outer membrane of the cell to oscillate.

4.5.3 Answer of Research Questions

In which manner and under what ultrasound characteristics are blood cells forced to translate?

Blood cells are forced to translate to the pressure nodes and pressure anti-nodes of a standing wave ultrasound-field. These forced translations occurred in an ultrasound field with a frequency of 5.7-MHz and any mechanical index equal to or exceeding 0.2. The amount displacement of a cell depends on whether it is attracted to a pressure node or pressure anti-node and the initial distance from the node or anti-node.

The research objectives:

I. Determine what ultrasound characteristics will yield significant blood cell translation.

Significant blood cell translation was observed at all mechanical indices greater than zero, as illustrated in figures 4.18 and 4.19.

II. Determine to which locations do blood cells translate to in the ultrasound-field.

Blood cells translate to the pressure nodes and pressure anti-nodes of the ultrasound-field.

III. Determine how ultrasound-forced translations differ from translations of blood cells not under the influence of ultrasound.

Ultrasound-forced translations result in blood cells translating in the x-direction.

4.5.4 Limitations

Only one frequency was used. For ultrasound-assisted cell separation white blood cell are required to oscillate at a frequency higher than the ultrasound-field's centre frequency and red blood cells are required to oscillate at a frequency lower than the ultrasound-field's centre frequency, or vice-versa. This would ensure that white blood cells and red blood cells do not both move to the nodes or anti-nodes of the sound field but rather to opposite pressure points and be separated. To achieve this a centre frequency needs to be found where one cell type oscillates at a frequency below the centre frequency and the other cell type oscillates at a frequency above the centre frequency.

It was not possible to keep the position of the capillary constant from one experiment to the next. This lead to the locations of nodes and anti-nodes not remaining constant with respect to the objective lens as the experimental setup had to be moved by hand to line the capillary up with the optical focus of the objective lens.

The blood supplied from the SANBS was expired and differed from one experimental session to the next. The age of the blood and the donor could not be selected. The blood was also diluted with Tyrode's solution to be able to see individual white and red blood cells. The study was conducted at room temperature. However, blood in the human body flows at a higher temperature.

4.5.5 Recommendations

Recommendations include using various ultrasound centre frequencies during experimentation to find a suitable centre frequency to exhibit ultrasound-assisted cell

separation. Improving the experimental setup to be able to record at any frame rate desired and using an adjustable microscope stage to avoid having to move the setup by hand. Obtain ethics to draw fresh blood from the same donor for all experiments. Conduct experiments at the same temperature as what blood flows in the human body.

Chapter 5

Conclusion

This research illustrated that blood cells are forced to translate to the pressure nodes and pressure anti-nodes of an ultrasound-field. The motivation to achieve this came from the need to develop a safe, efficient and cost-effective ultrasound-based cell removal technique. Damaged cells cause life-threatening diseases such as malaria and cancer. It would be advantageous if we could remove these cells from our bodies.

An experimental setup was built to accommodate optical microscopy and ultrasound transducers. The ultrasound transducers located at a variable distance and angle with respect to the optical region of interest to create different ultrasound conditions.

White and red blood cells subject to ultrasound exhibited significant horizontal translation compared to cell not under the influence of ultrasound. This was attributed to the primary Bjerknes forces experienced by cells. These forces caused cells to either be attracted to or repelled by the ultrasound-field. Cells moved to locations seen as stable and migrated towards the pressure nodes and pressure anti-nodes of the sound-field.

This behaviour confirms the hypothesis that cells oscillate in an ultrasound-field. As suggested by the bilayer sonophore model, ultrasound creates an oscillating structure in the gaseous void between the bilayers of the cell. These oscillations can apply enough force to a cell and cause it to translate.

If more ultrasound centre frequencies were used, a frequency could have been found to ensure that white blood cells move to the nodes of a sound-field and red blood cells move to the anti-nodes of a sound field, or vice-versa. This was not always the case. Future studies can incorporate more frequencies.

This research was the first step towards an ultrasound-based cell eradication technique.

It was illustrated that it is possible to manipulate blood cells with ultrasound. Future research could lead to ultrasound-based treatments where mechanical differences between cells are could be exploited. This is useful when damaged cells have mechanical differences to their heath equivalents. These differences are present in parasitic diseases such as Malaria, and Cancer.

Bibliography

[1] D. M. Rubin, N. Anderton, C. Smalberger, J. Polliack, M. Nathan, and M. Postema, "On the behaviour of living cells under the influence of ultrasound," *Fluids*, vol. 3, no. 4, p. 82, 2018.

[2] N. Mazzawi, "Bubble-like response of living cells in an ultrasound field," Master's thesis, Technion-Israel Institute of Technology, 2013.

[3] N. Mazzawi, M. Postema, and E. Kimmel, "Bubble-like response of living blood cells and microparticles in an ultrasound field," *Acta Phys. Pol. A*, vol. 127, no. 1, pp. 103–105, 2015.

[4] M. Postema, *Fundamentals of Medical Ultrasonics*. London: Spon, 2011.

[5] W. Eisenmenger, "The mechanisms of stone fragmentation in ESWL," *Ultrasound Med. Biol.*, vol. 27, no. 5, pp. 683–693, 2001.

[6] G. R. ter Haar, "HIFU tissue ablation: concept and devices," in *Therapeutic Ultrasound*, ser. Adv. Exp. Med. Biol., J.-M. Escoffre and A. Bouakaz, Eds. Berlin: Springer, 2016, vol. 880, pp. 3–20.

[7] G. Dimcevski, S. Kotopoulis, T. Bjånes, D. Hoem, J. Schjøtt, B. T. Gjertsen, M. Biermann, A. Molven, H. Sorbye, E. McCormack, M. Postema, and O. H. Gilja, "A human clinical trial using ultrasound and microbubbles to enhance gemcitabine treatment of inoperable pancreatic cancer," *J. Control. Release*, vol. 243, pp. 172–181, 2016.

[8] Y. Kaneko, T. Maruyama, K. Takegami, T. Watanabe, H. Mitsui, K. Hanajiri, H. Nagawa, and Y. Matsumoto, "Use of a microbubble agent to increase the effects of high intensity focused ultrasound on liver tissue," *Eur. Radiol.*, vol. 15, no. 7, pp. 1415–1420, 2005.

[9] D. A. van der Windt, G. J. van der Heijden, S. G. van den Berg, G. ter Riet, A. F. de Winter, and L. M. Bouter, "Ultrasound therapy for musculoskeletal disorders: A systematic review," *Pain*, vol. 81, no. 3, pp. 257–271, 1999.

[10] F. Desmeules, J. Boudreault, J.-S. Roy, C. Dionne, P. Frémont, and J. C. MacDermid, "The efficacy of therapeutic ultrasound for rotator cuff tendinopathy: A systematic review and meta-analysis," *Phys. Ther. Sport*, vol. 16, no. 3, pp. 276–284, 2015.

[11] K. Lim, J. Kim, H. Seonwoo, S. H. Park, P.-H. Choung, and J. H. Chung, "In vitro effects of low-intensity pulsed ultrasound stimulation on the osteogenic differentiation of human alveolar bone-derived mesenchymal stem cells for tooth tissue engineering," *BioMed Res. Int.*, vol. 2013, p. 269724, 2013.

[12] J. Harle, V. Salih, F. Mayia, J. C. Knowles, and I. Olsen, "Effects of ultrasound on the growth and function of bone and periodontal ligament cells in vitro," *Ultrasound Med. Biol.*, vol. 27, no. 4, pp. 579–586, 2001.

[13] G. J. Tortora and B. H. Derrickson, *Principles of Anatomy and Physiology*, 13th ed. Philadelphia: Wiley, 2008.

[14] T. Yang, F. Bragheri, and P. Minzioni, "A comprehensive review of optical stretcher for cell mechanical characterization at single-cell level," *Micromachines*, vol. 7, no. 5, p. 90, 2016.

[15] M. J. Tomlinson, S. Tomlinson, X. B. Yang, and J. Kirkham, "Cell separation: terminology and practical considerations," *J. Tissue Eng.*, vol. 4, pp. 2041–7314, 2013.

[16] R. Suwanarusk, B. M. Cooke, A. M. Dondorp, K. Silamut, J. Sattabongkot, N. J. White, and R. Udomsangpetch, "The deformability of red blood cells parasitized by plasmodium falciparum and p. vivax," *J. Infect. Dis.*, vol. 189, no. 2, pp. 190–194, 2004.

[17] M. Postema, S. Kotopoulis, and K. Jenderka, "Basic Physical Principles of Medical Ultrasound," in *EFSUMB Course Book on Ultrasound*, C. Dietrich, Ed. London: EFSUMB, 2012, pp. 9–37.

[18] T. Kondo, Y. Fukushima, H. Kon, and P. Riesz, "Effect of shear stress and free radicals induced by ultrasound on erythrocytes," *Arch. Biochem. Biophys.*, vol. 269, no. 2, pp. 381–389, 1989.

[19] P. Riesz and T. Kondo, "Free radical formation induced by ultrasound and its biological implications," *Free Radic. Biol. Med.*, vol. 13, no. 3, pp. 247–270, 1992.

[20] D. Dalecki, "Mechanical bioeffects of ultrasound," *Annu. Rev. Biomed. Eng.*, vol. 6, pp. 229–248, 2004.

[21] E. Carstensen, P. Kelly, C. Church, A. Brayman, S. Child, C. Raeman, and L. Schery, "Lysis of erythrocytes by exposure to CW ultrasound," *Ultrasound Med. Biol.*, vol. 19, no. 2, pp. 147–165, 1993.

[22] M. Postema and O. H. Gilja, "Contrast-enhanced and targeted ultrasound," *World J. Gastroenterol.*, vol. 17, no. 1, pp. 28–41, 2011.

[23] M. Postema, A. Van Wamel, C. T. Lancée, and N. de Jong, "Ultrasound-induced encapsulated microbubble phenomena," *Ultrasound Med. Biol.*, vol. 30, no. 6, pp. 827–840, 2004.

[24] B. Krasovitski, V. Frenkel, S. Shoham, and E. Kimmel, "Intramembrane cavitation as a unifying mechanism for ultrasound-induced bioeffects," *Proc. Natl. Acad. Sci. U.S.A.*, vol. 108, no. 8, pp. 3258–3263, 2011.

[25] K. Johansen, E. Kimmel, and M. Postema, "Theory of red blood cell oscillations in an ultrasound field," *Arch. Acoust.*, vol. 42, no. 1, pp. 121–126, 2017.

[26] S. Kotopoulis and M. Postema, "Microfoam formation in a capillary," *Ultrasonics*, vol. 50, no. 2, pp. 260–268, 2010.

[27] C. Lee and T. Wang, "Acoustic radiation force on a bubble," *J. Acoust. Soc. Am.*, vol. 93, no. 3, pp. 1637–1640, 1993.

[28] A. J. Reddy and A. J. Szeri, "Coupled dynamics of translation and collapse of acoustically driven microbubbles," *J. Acoust. Soc. Am.*, vol. 112, no. 4, pp. 1346–1352, 2002.

[29] P. A. Dayton, K. E. Morgan, A. L. Klibanov, G. Brandenburger, K. R. Nightingale, and K. W. Ferrara, "A preliminary evaluation of the effects of primary and secondary radiation forces on acoustic contrast agents," *IEEE Trans. Ultrason. Ferroelectr. Freq. Control*, vol. 44, no. 6, pp. 1264–1277, 1997.

[30] M. Postema and G. Schmitz, "Ultrasonic bubbles in medicine: influence of the shell," *Ultrason. Sonochem.*, vol. 14, no. 4, pp. 438–444, 2007.

[31] T. G. Leighton, *The Acoustic Bubble*. London: Academic, 2012.

[32] P. Dayton, A. Goode, K. Morgan, S. Klibanov, G. Brandenburger, and K. Ferrara, "Action of microbubbles when insonified: experimental evidence," *Proc. IEEE Int. Ultras. Symp.*, vol. 2, pp. 1131–1134, 1996.

[33] M. Postema, M. Mleczko, and G. Schmitz, "Experimental setup for synchronous optical and acoustical observation of contrast microbubbles," *Biomed. Tech.*, vol. 51, pp. V75–V76, 2006.

[34] A. Delalande, S. Kotopoulis, T. Rovers, C. Pichon, and M. Postema, "Sonoporation at a low mechanical index," *Bub. Sci. Eng. Technol.*, vol. 3, no. 1, pp. 3–12, 2011.

[35] N. Kudo, "High-speed in situ observation system for sonoporation of cells with size-and position-controlled microbubbles," *IEEE Trans. Ultrason. Ferroelectr. Freq. Control*, vol. 64, no. 1, pp. 273–280, 2017.

[36] A. Hurrell, "Voltage to pressure conversion: are you getting "phased" by the problem?" vol. 1, no. 1, pp. 57–62, 2004.

.1 Appendix A-Engineering Drawings

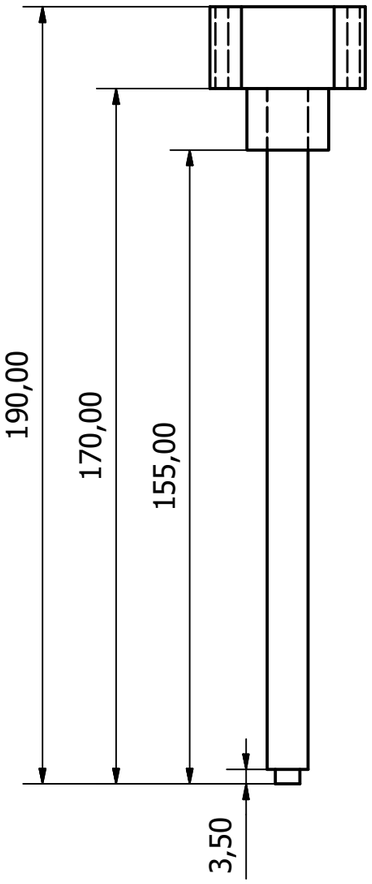

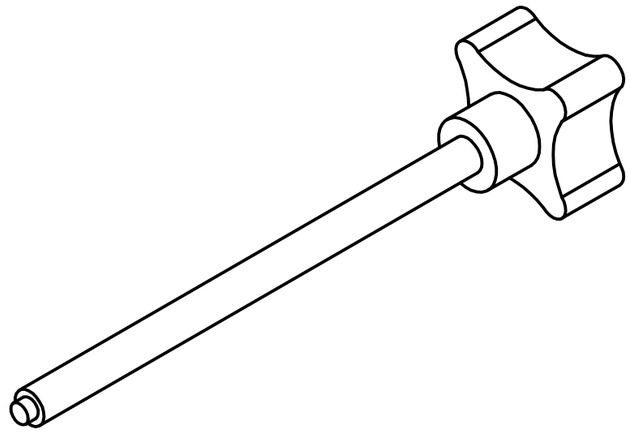

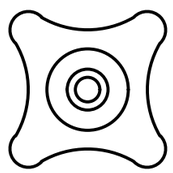

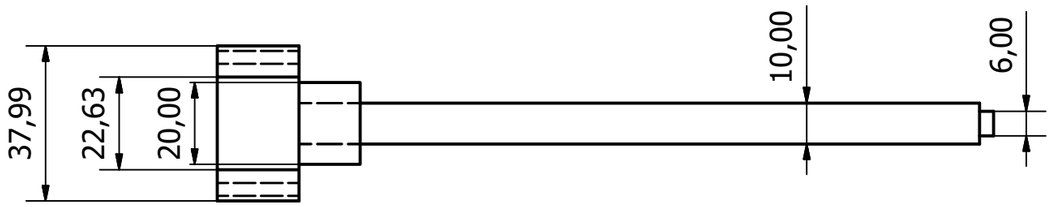

Designed by	Checked by	Approved by	Date		Date	
Charl Smalberger					2019/12/11	

University of the Witwatersrand	Adjuster Knob		
		Edition	Sheet 1 / 1

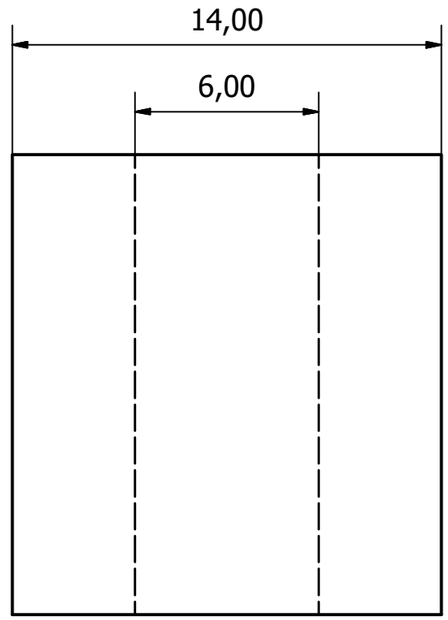

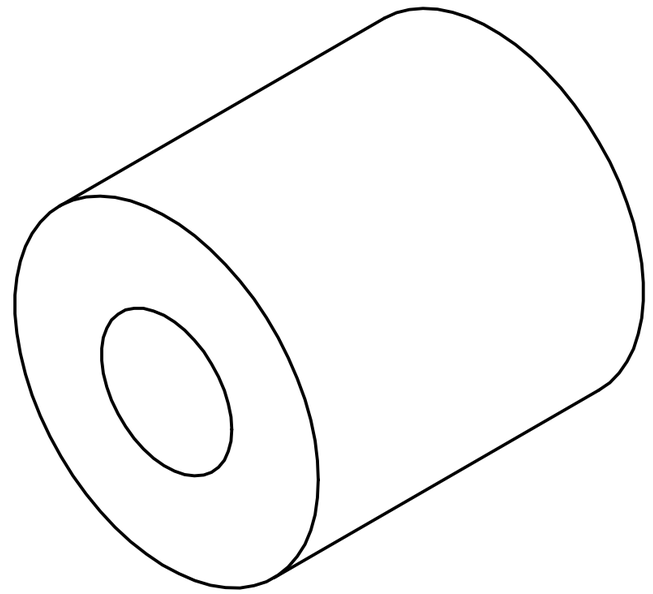

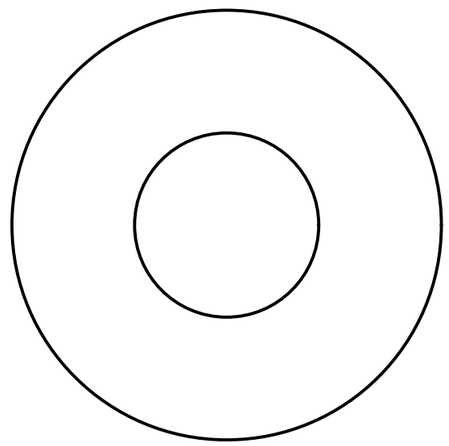

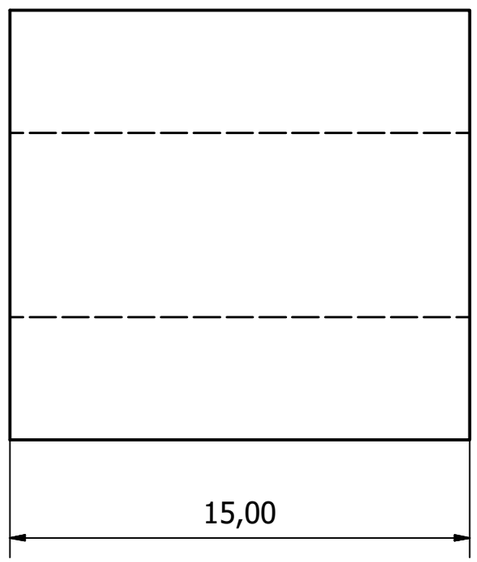

Designed by	Checked by	Approved by	Date		Date	
Charl Smalberger					2019/12/11	

University of the Witwatersrand	Rail Bearing		
		Edition	Sheet 1 / 1

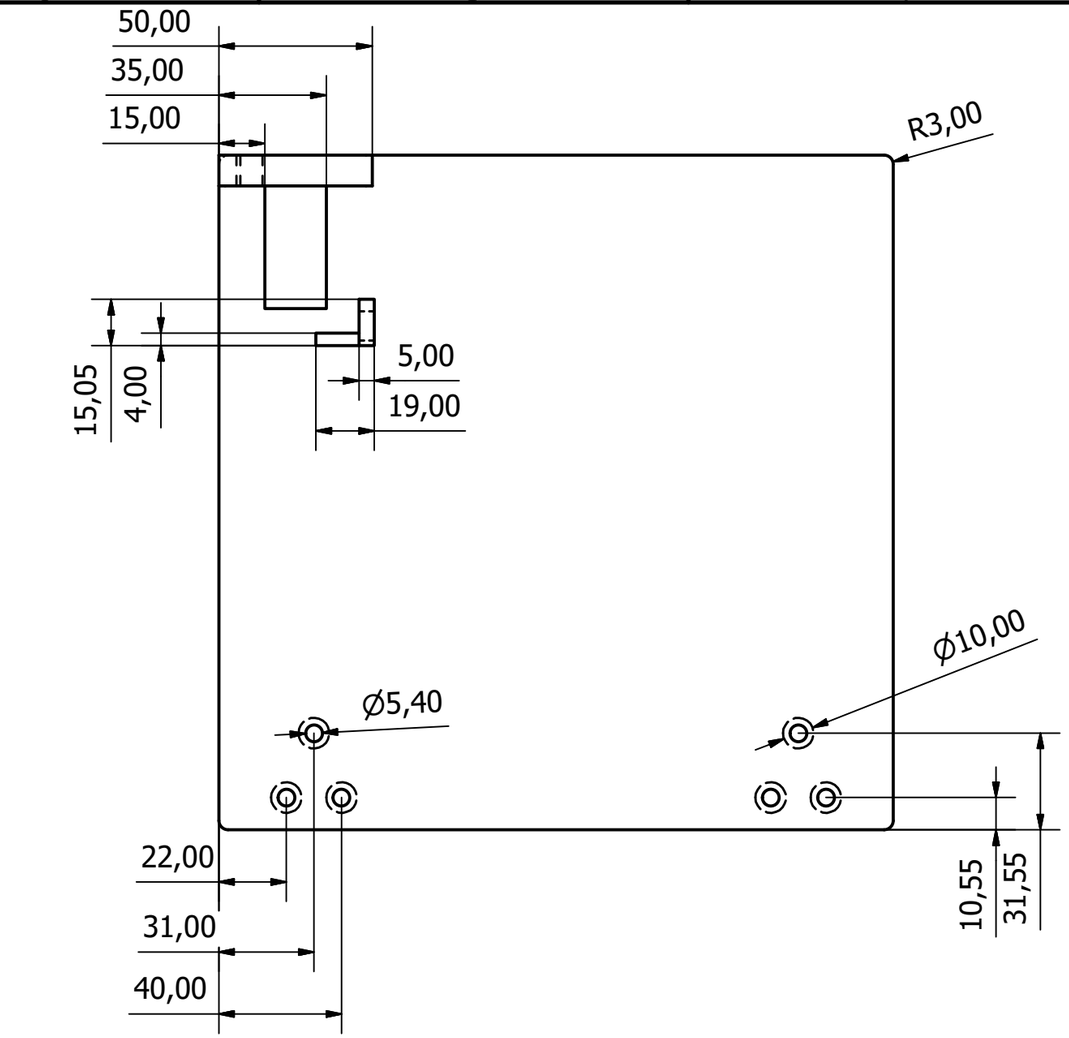

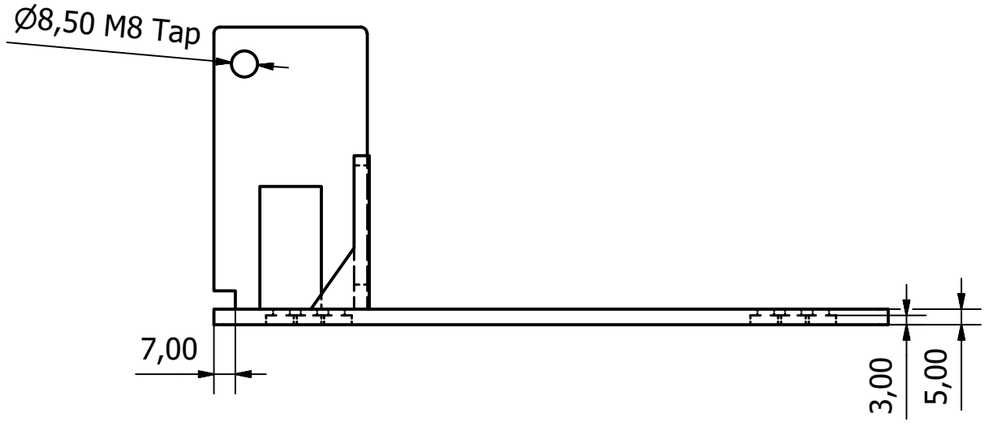

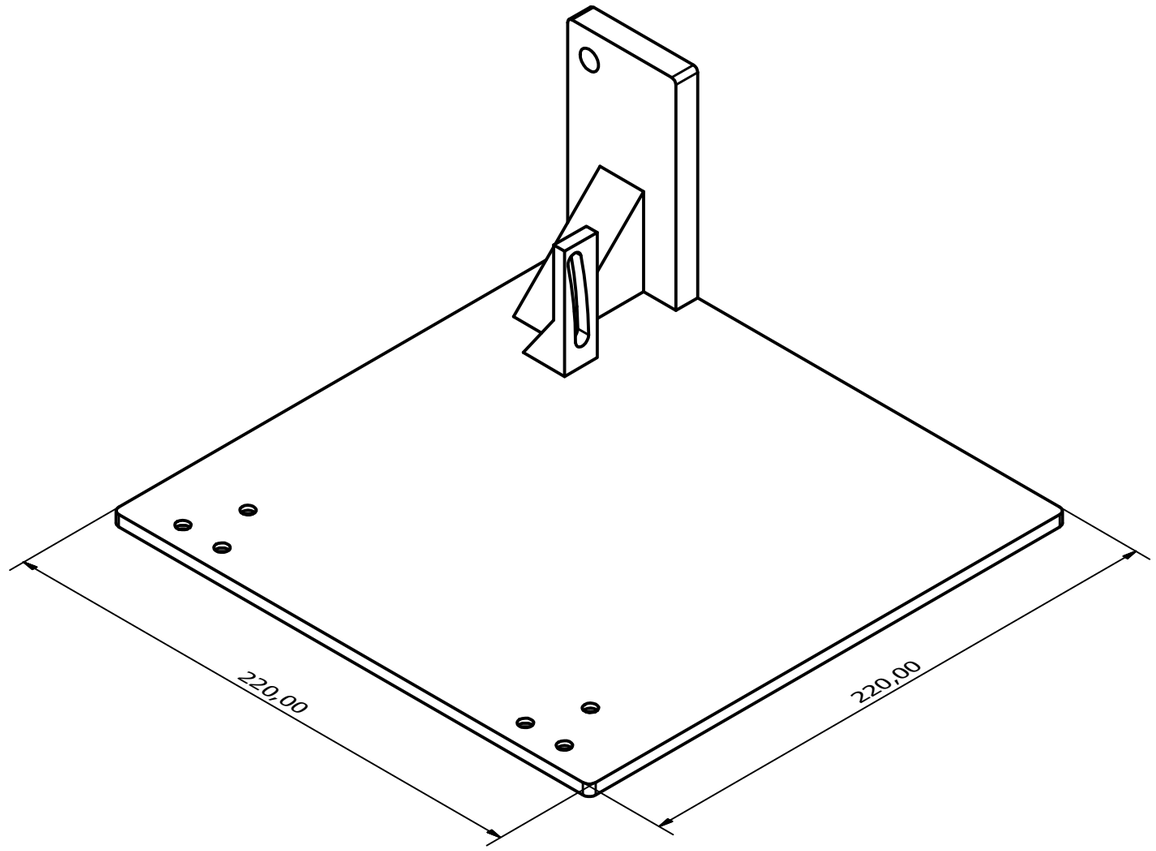

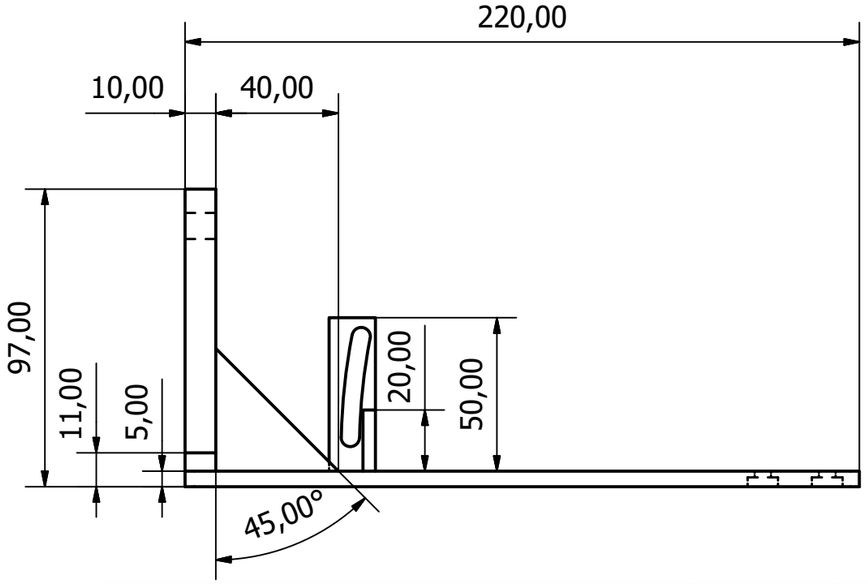

Designed by	Checked by	Approved by	Date		Date	
Charl Smalberger					2018/10/23	

University of the Witwatersrand	Bottom Plate		
		Edition	Sheet 1 / 1

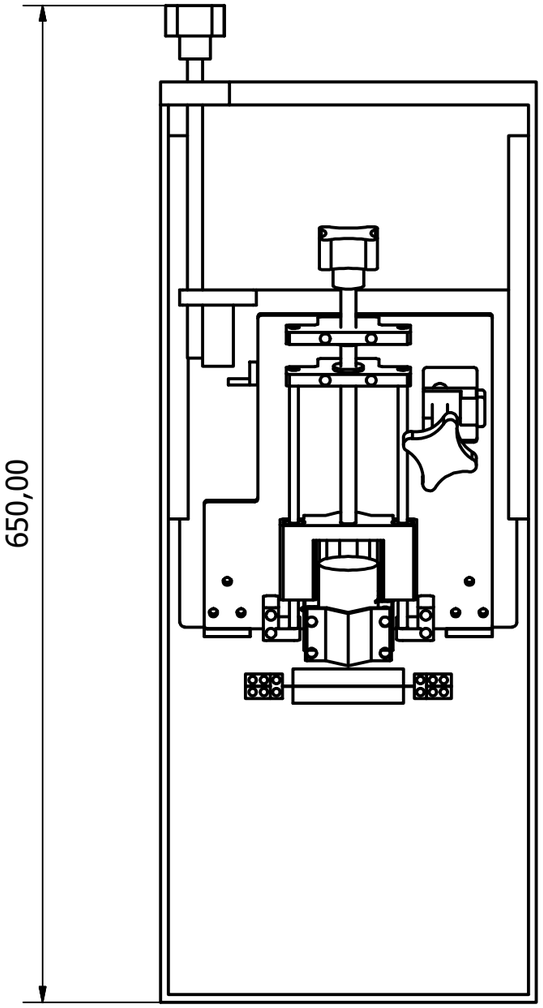

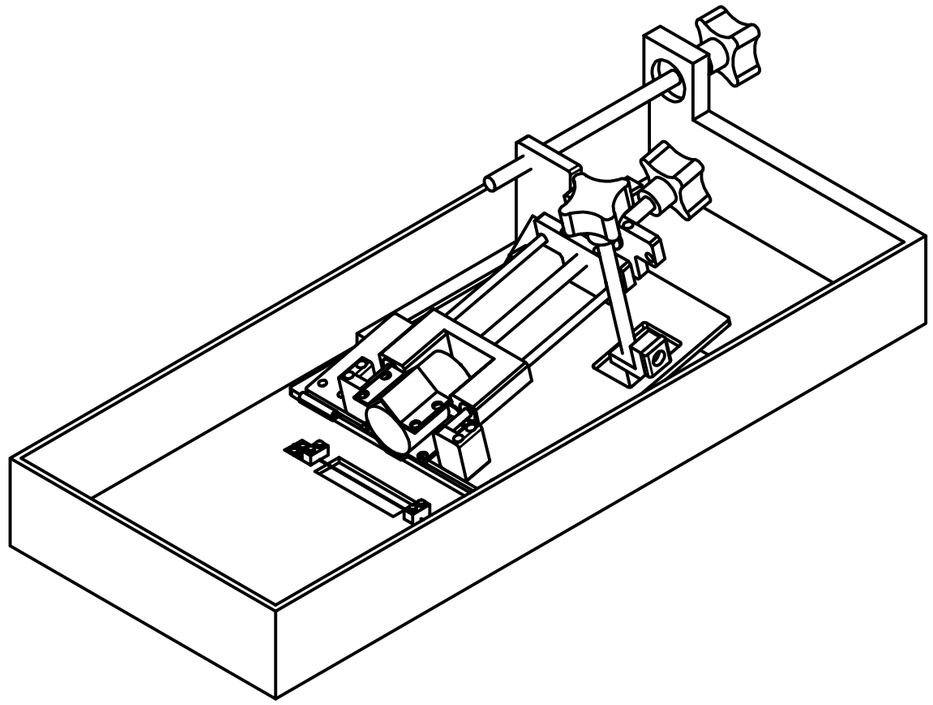

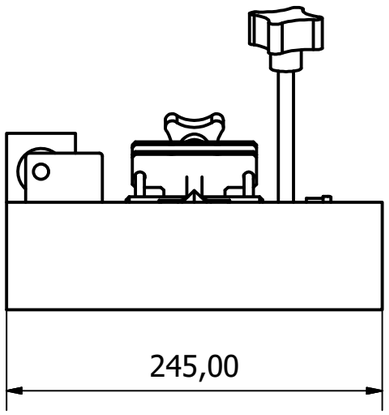

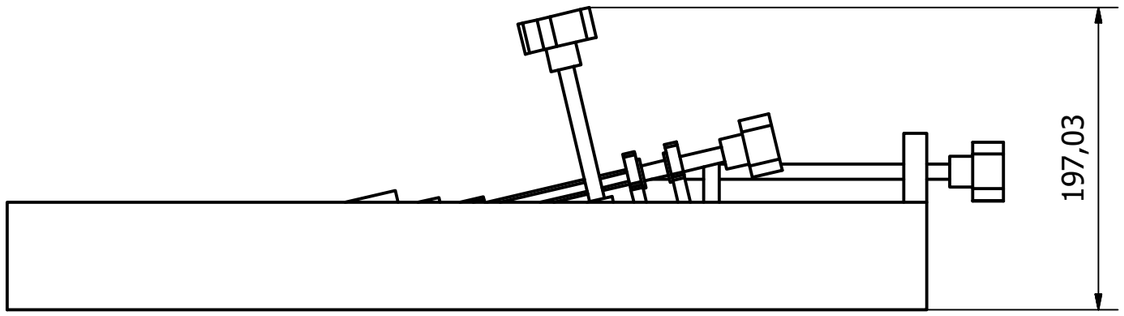

Designed by	Checked by	Approved by	Date		Date	
Charl Smalberger					2019/12/11	

University of the Witwatersrand	Experimental Setup		
		Edition	Sheet 1 / 1

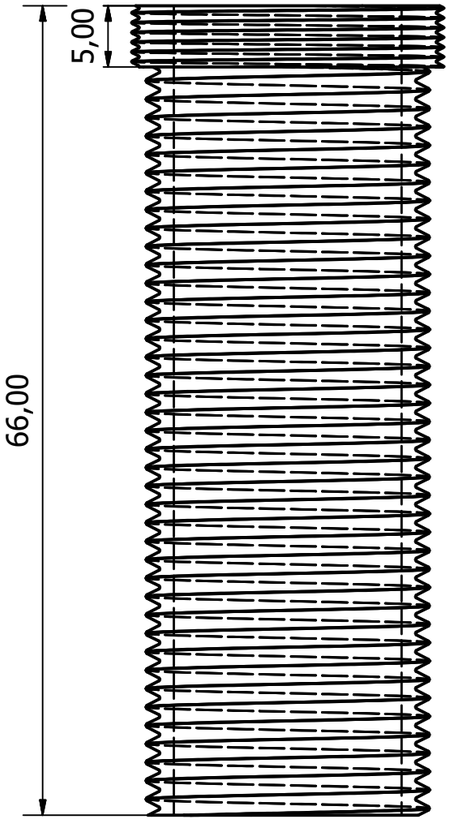

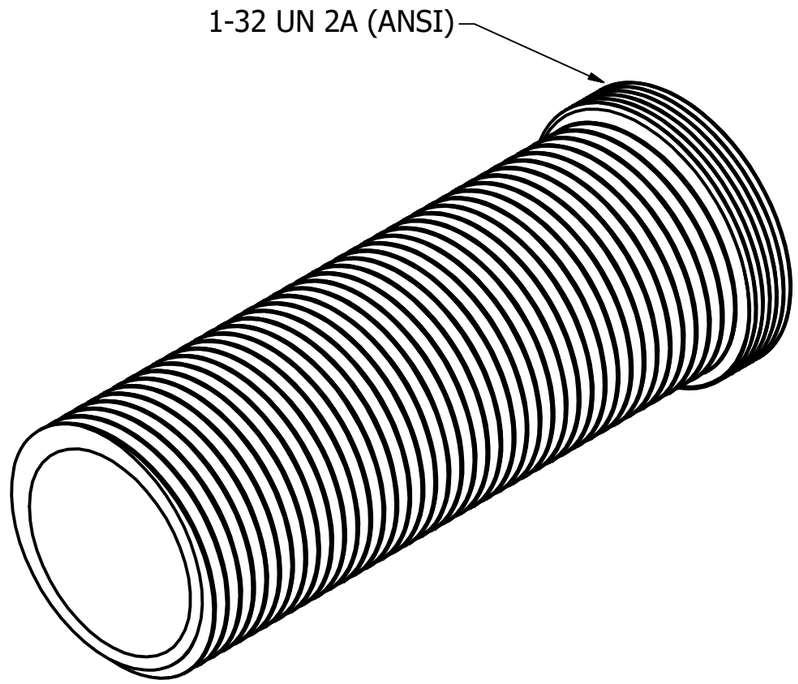

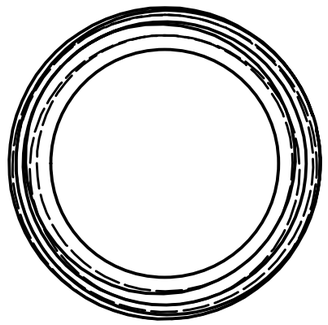

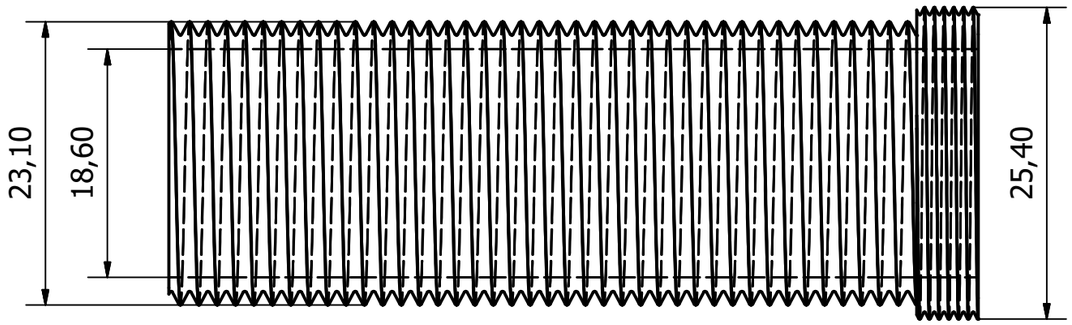

Designed by	Checked by	Approved by	Date		Date	
Charl Smalberger					2019/12/11	

University of the Witwatersrand	Eyepiece to C-mount Adapter		
		Edition	Sheet 1 / 1

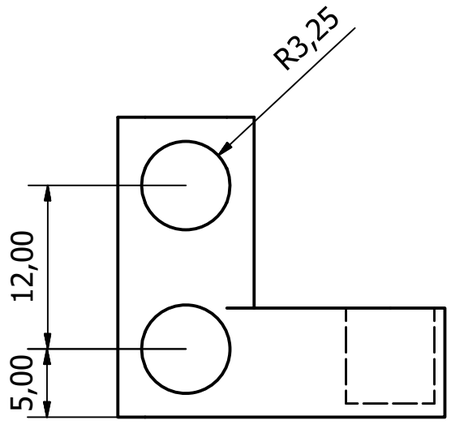

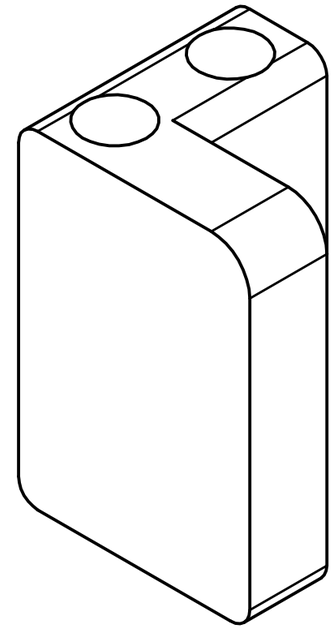

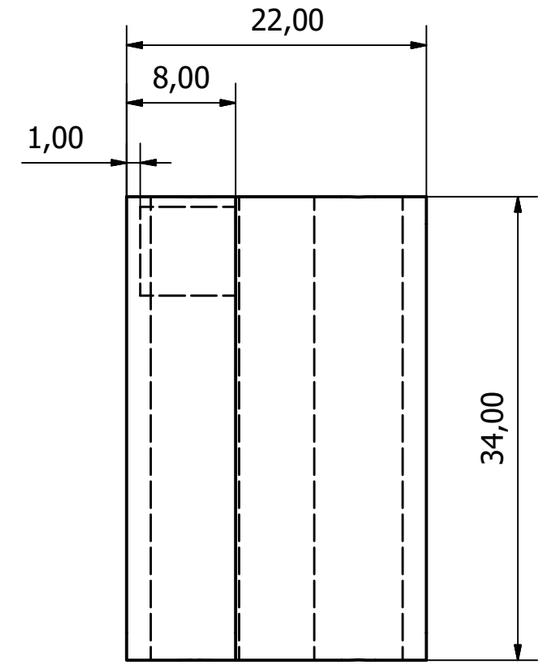

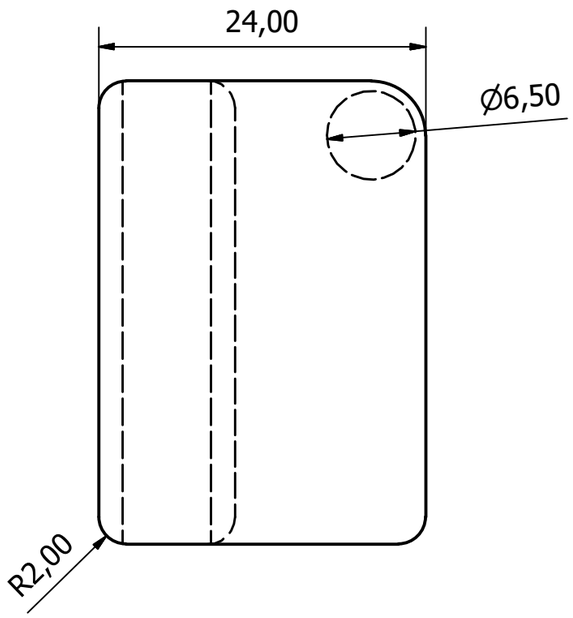

Designed by Charl Smalberger	Checked by	Approved by	Date	Date 2019/12/11	
University of the Witwatersrand		Rail Alignment Bracket Front			
			Edition	Sheet 1 / 1	

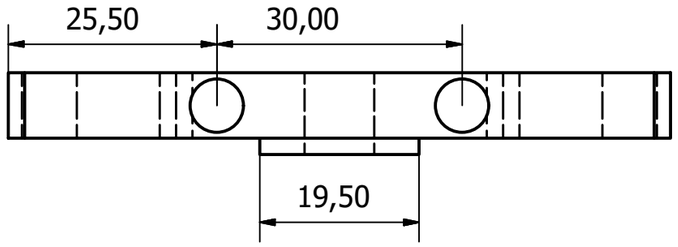

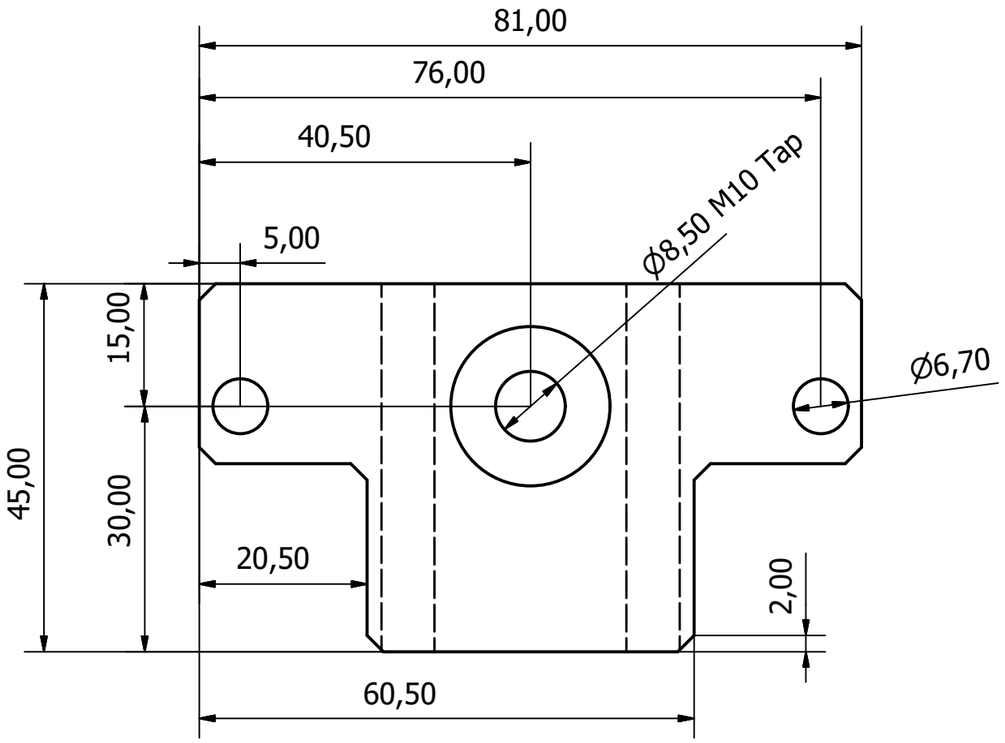

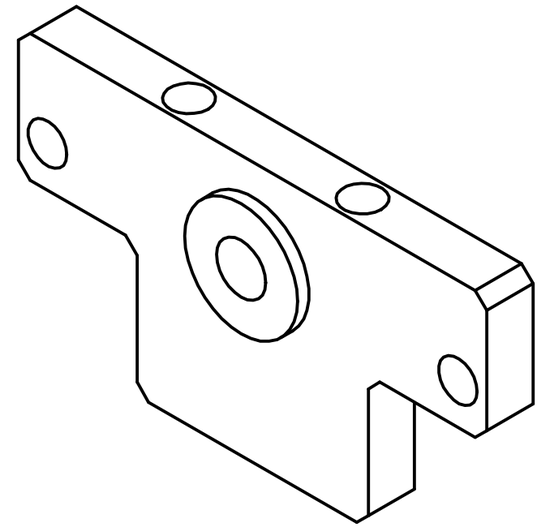

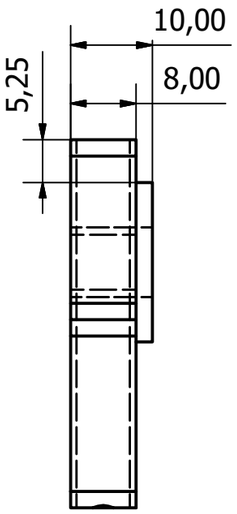

Designed by	Checked by	Approved by	Date		Date	
Charl Smalberger					2018/10/09	

Unversity of the Witwatersrand	Rail Alignment Bracket		
		Edition	Sheet 1 / 1

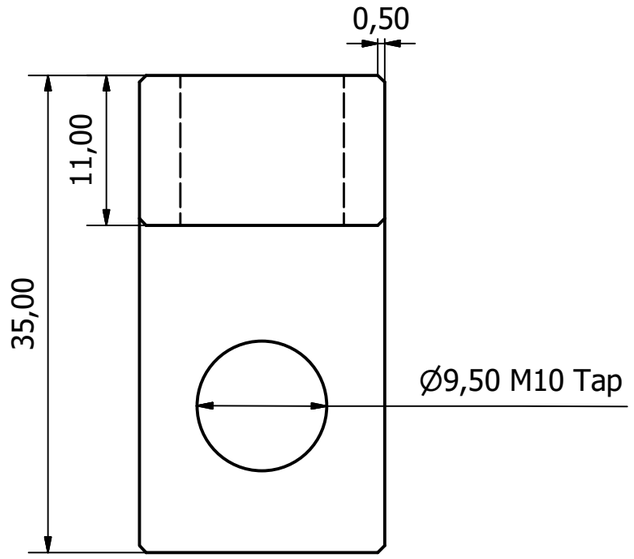

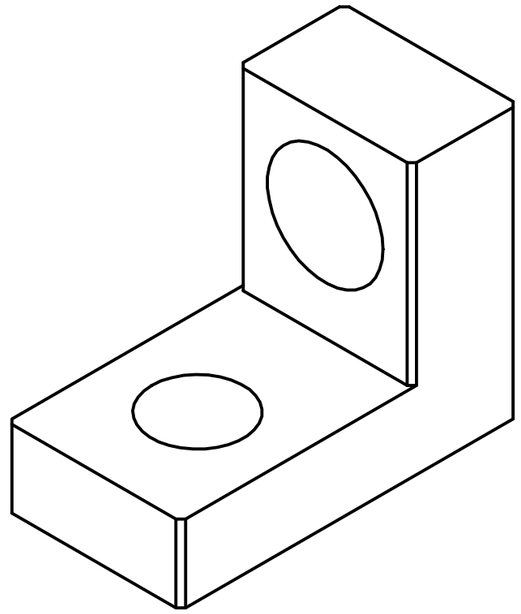

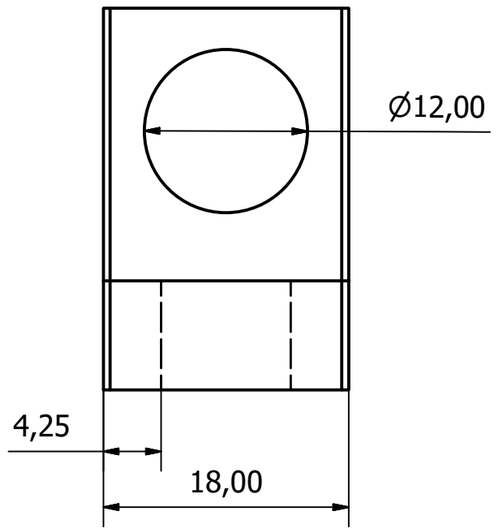

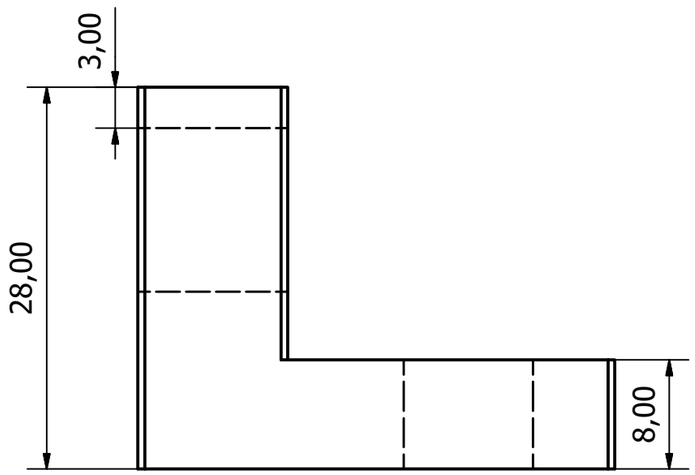

Designed by	Checked by	Approved by	Date		Date	
Charl Smalberger					2019/12/11	

University of the Witwatersrand	Rod Support		
		Edition	Sheet 1 / 1

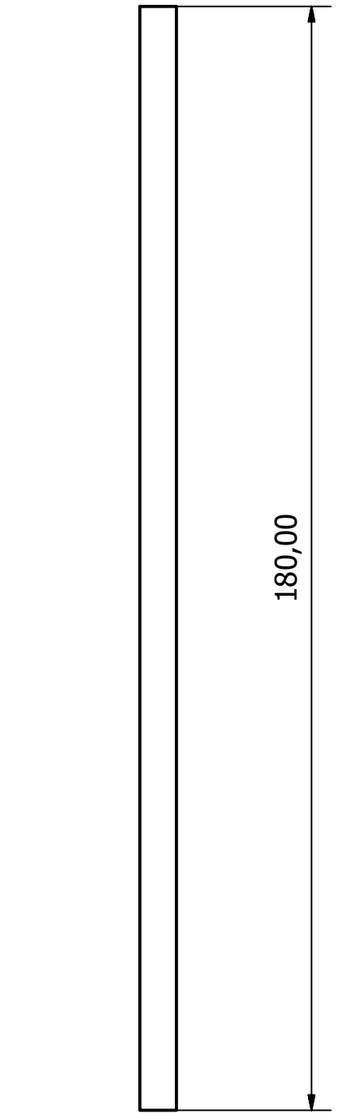

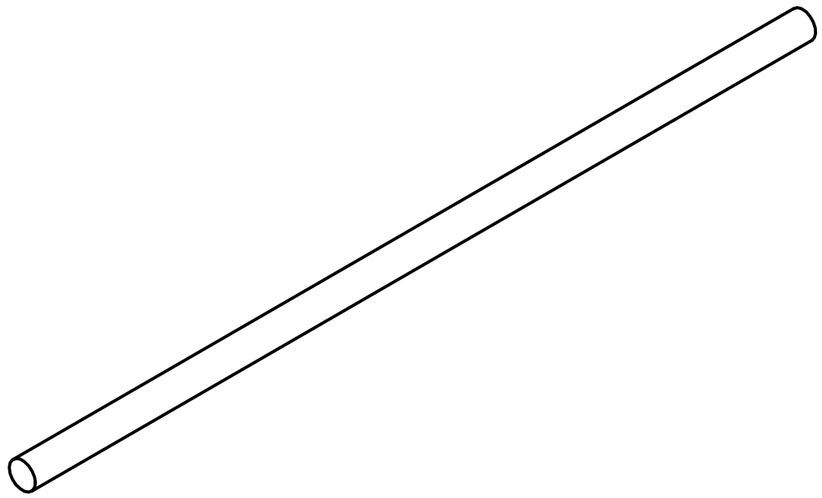

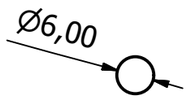

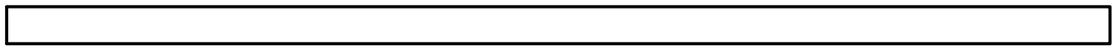

Designed by	Checked by	Approved by	Date		Date	
Charl Smalberger					2019/12/11	

University of the Witwatersrand	Rail Rod		
		Edition	Sheet 1 / 1

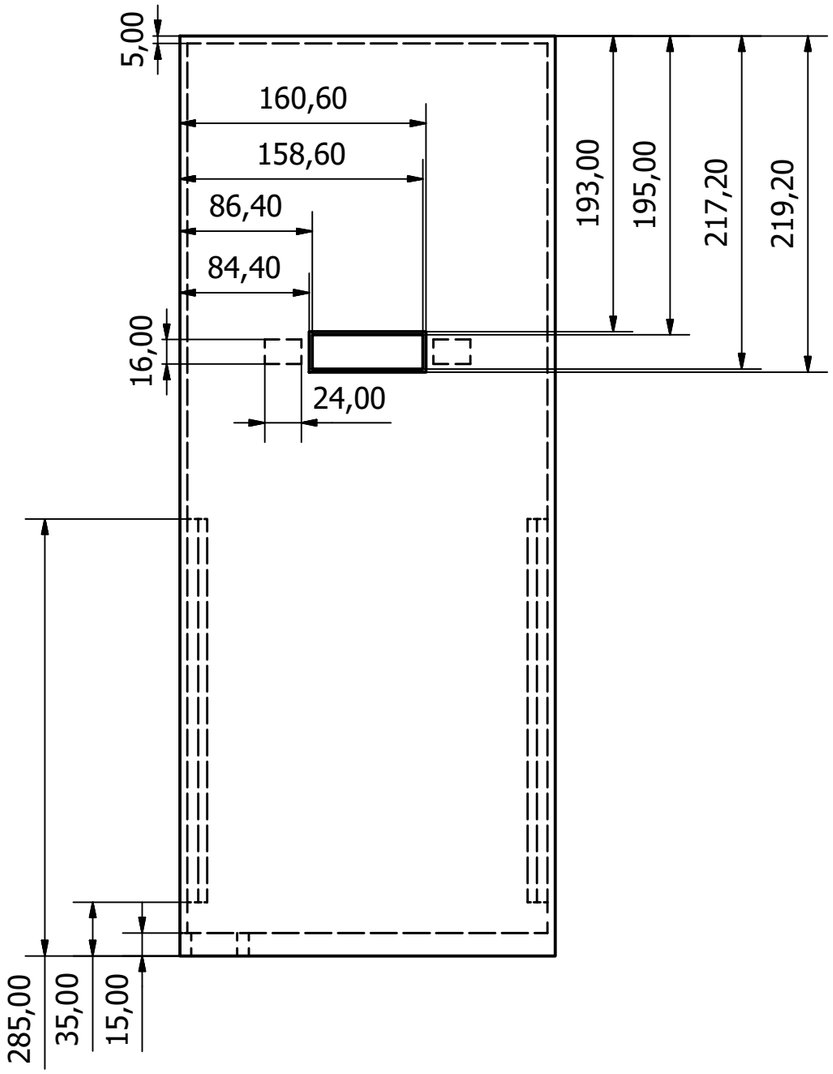

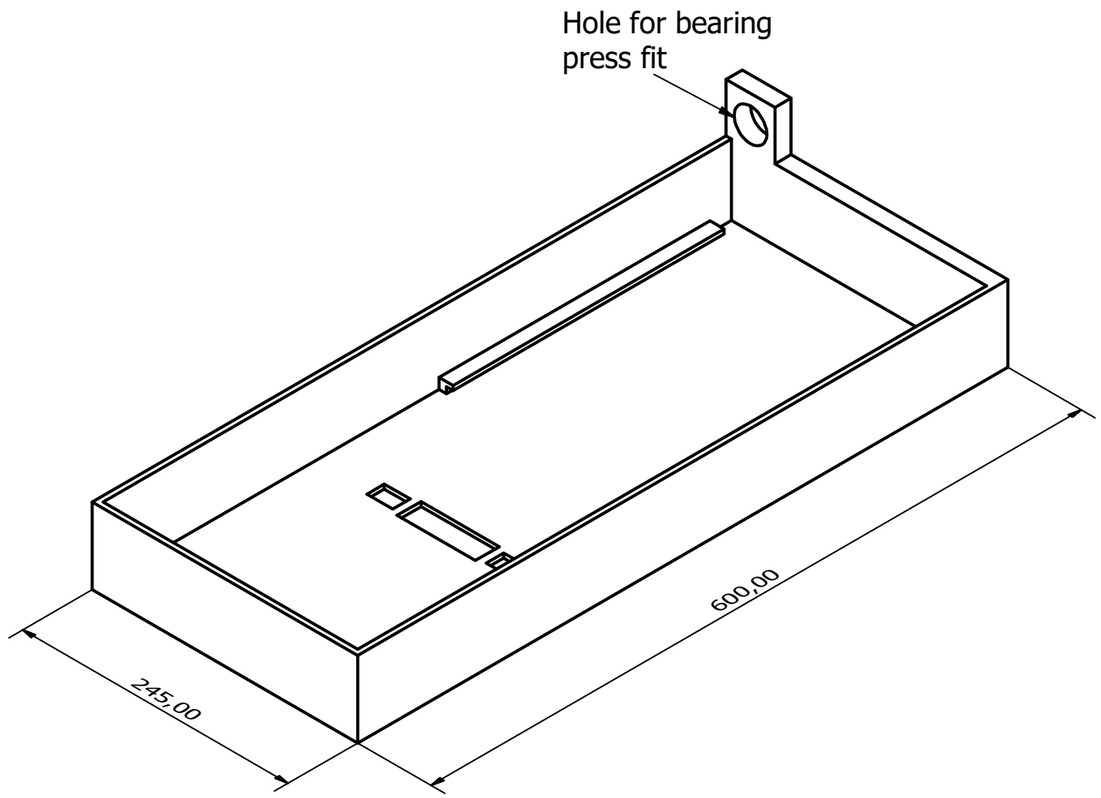

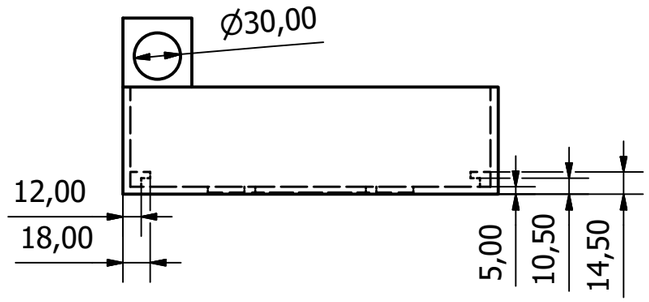

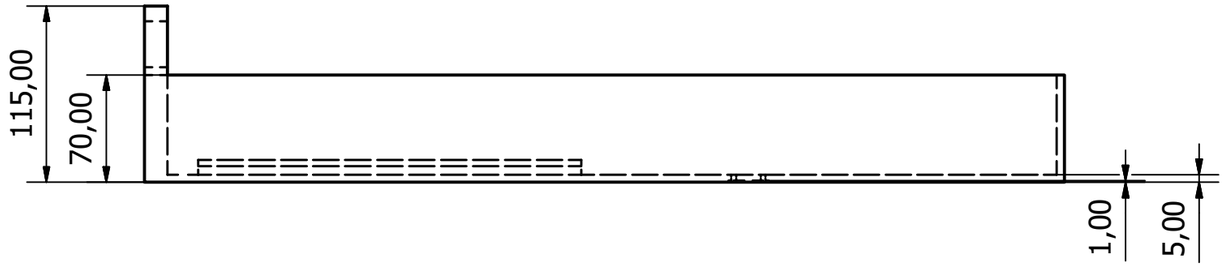

Designed by	Checked by	Approved by	Date		Date	
Charl Smalberger					2018/11/02	

University of the Witwatersrand	Container		
		Edition	Sheet 1 / 1

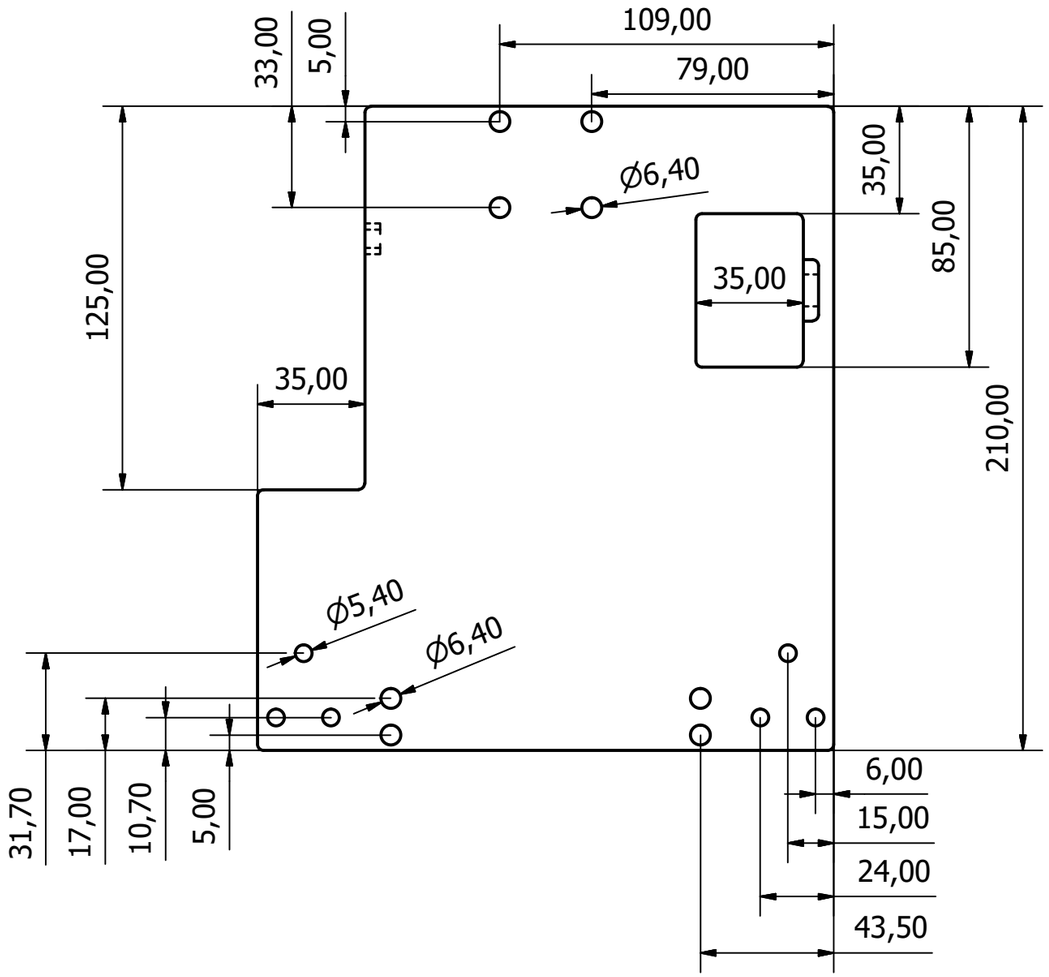

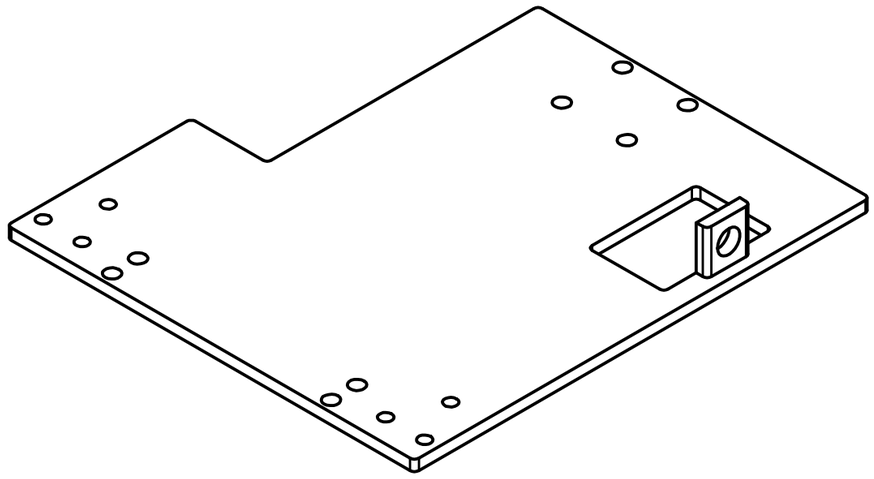

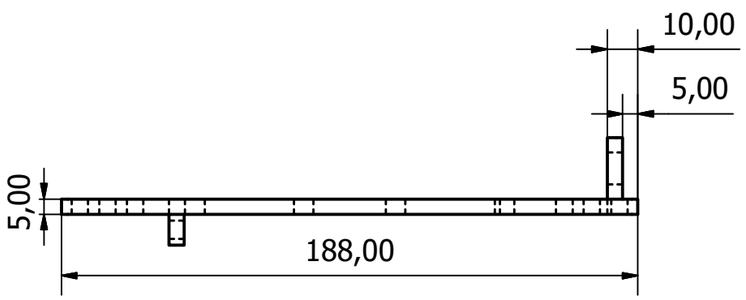

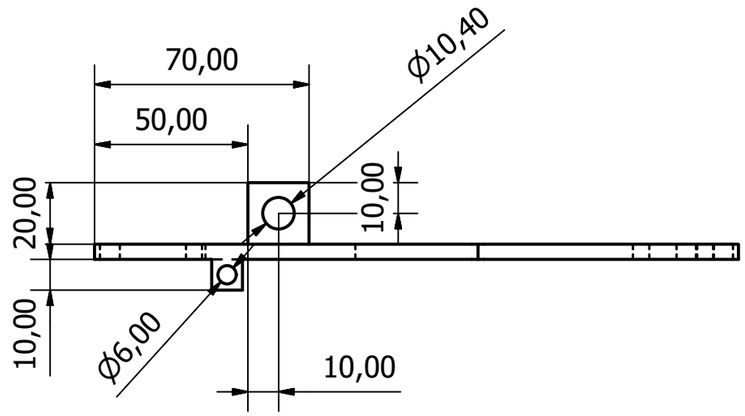

Designed by	Checked by	Approved by	Date		Date	
Charl Smalberger					2018/10/23	

University of the Witwatersrand	Top Plate		
		Edition	Sheet 1 / 1

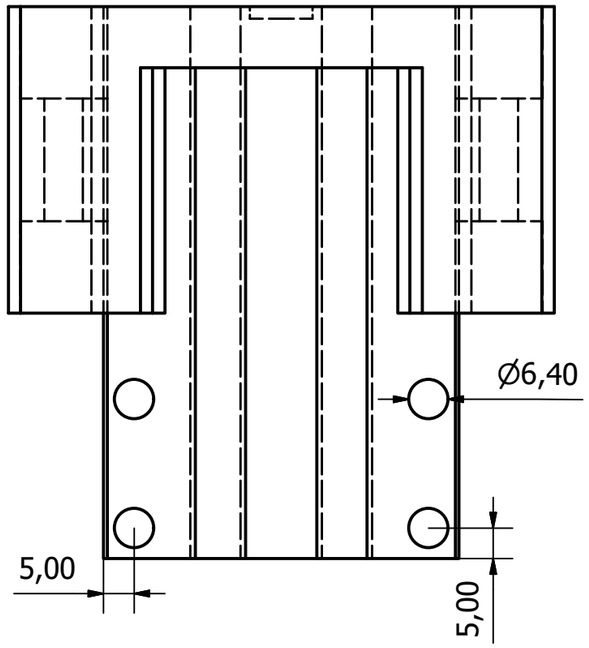

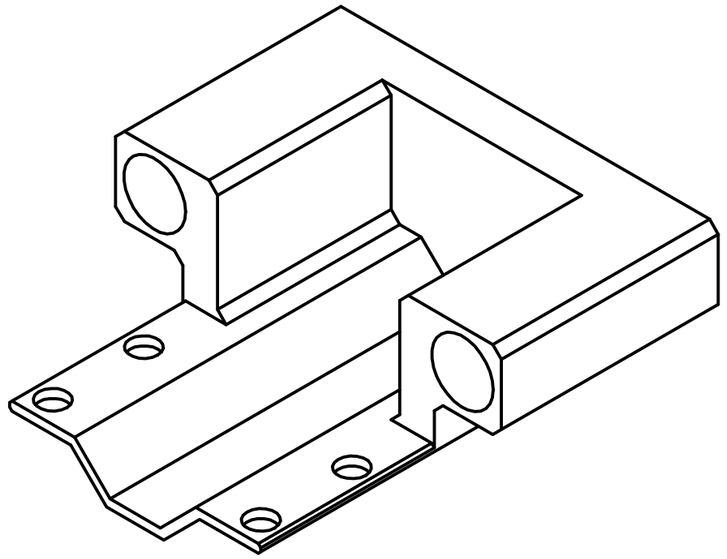

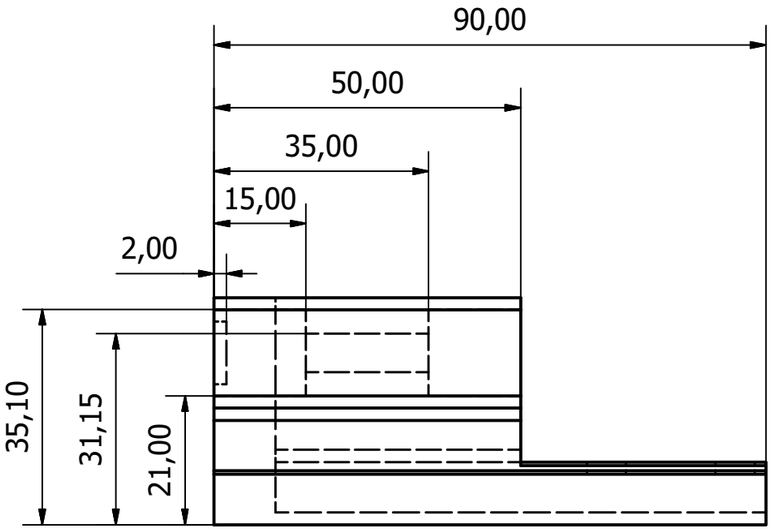

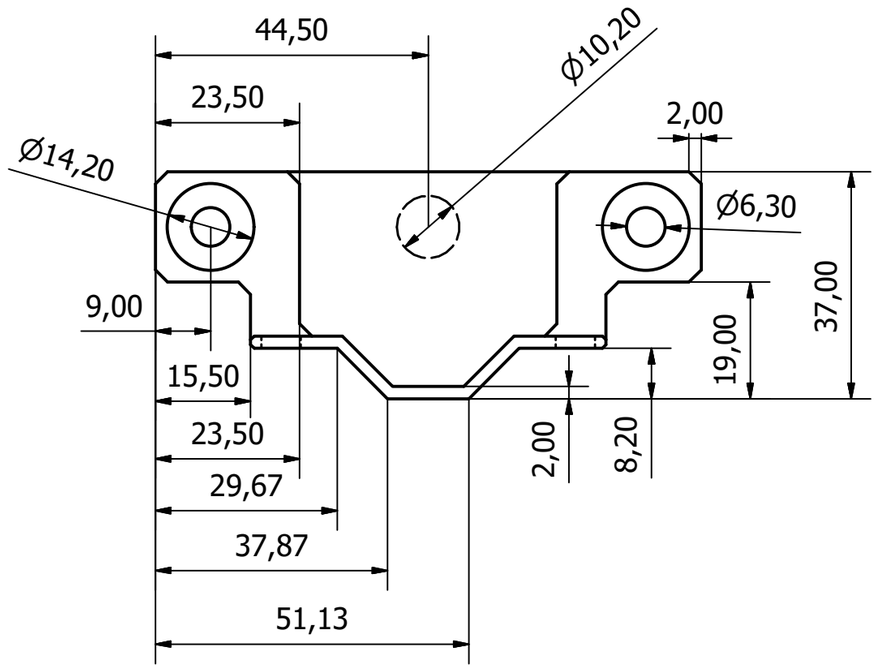

Designed by Charl Smalberger	Checked by	Approved by	Date	Date 2019/12/11	
University of the Witwatersrand		Transducer Bracket			
		Triangle Bracket 3	Edition	Sheet 1 / 1	

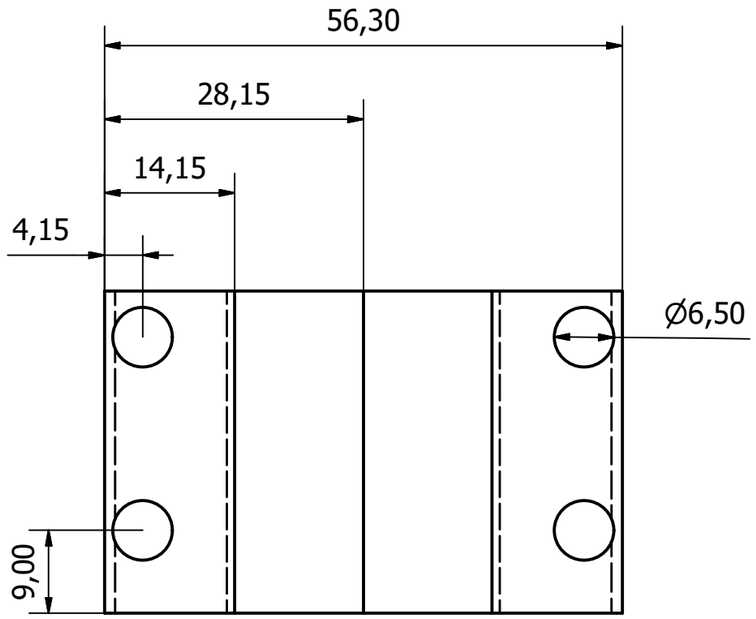

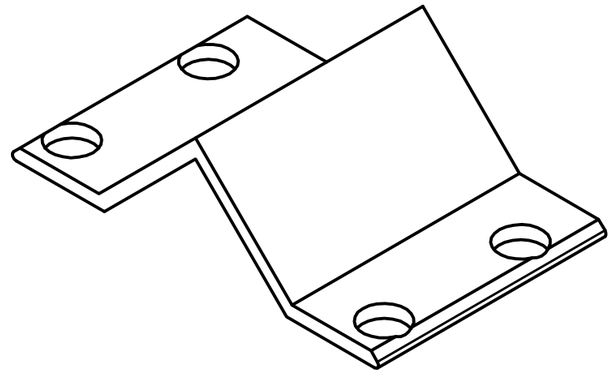

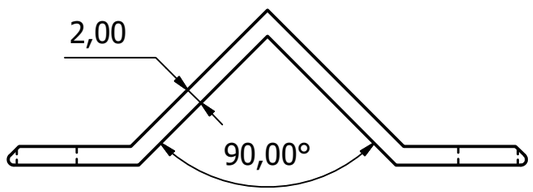

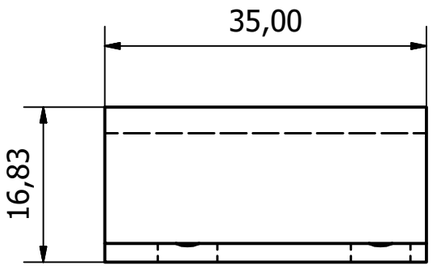

Designed by	Checked by	Approved by	Date		Date	
Charl Smalberger					2018/08/07	

University of the Witwatersrand	Transducer Bracket Hat		
		Edition	Sheet 1 / 1

.2 Appendix B-Hydrophone Datasheets

592 E. Weddell Drive, Suite 7
Sunnyvale, CA 94089
Phone (408) 745-0383 Fax (408) 745-0956
www.ondacorp.com

I. Methodology for Onda's Hydrophone Calibrations

Calibration is obtained by comparison techniques to reference hydrophones calibrated by the National Physical Laboratory (NPL) in the UK. For calibration below 20 MHz, the stepped single frequency comparison technique is used, and for calibration above 20 MHz, the harmonic comparison technique is employed. The procedures are as follows:

Stepped single frequency comparison technique:

1) The reference hydrophone is placed at the focus of a broadband source [1], which is driven by a sinusoidal tone burst. The reference hydrophone is aligned by maximizing the hydrophone signal with the source driven at the maximum end of its frequency range (20 MHz for a 1-20 MHz calibration, 5 MHz for a 0.25-1 MHz calibration). The voltage driving the source is then swept in across the frequency range (i.e., 1 to 20 MHz, or 0.25 to 1 MHz). At each frequency, the output of the reference hydrophone is measured and digitally filtered to separate the primary frequency component from any harmonics that may be present in the signal. The reference hydrophone has previously been calibrated by NPL, so that the voltage it detects can be translated into a pressure value, hence calibrating the pressure output of the source as a function of frequency, at the source's focal position.

2) The reference hydrophone is then replaced by the hydrophone to be calibrated, and re-aligned. The voltage driving the source is again swept across the same frequency settings, and the output of the hydrophone at the fundamental of the driving signal is determined and recorded. This voltage is then divided by the pressure amplitude (measured in step 1) to determine the output of the hydrophone in Volts per Pascal (V/Pa).

Harmonic comparison technique:

1) The reference hydrophone is placed at a position in the non-linear acoustic field produced by a plane circular source transducer driven by a 2.25MHz sinusoidal tone-burst signal. The position was chosen where many strong harmonics of the fundamental frequency are generated in the distorted pressure waveform due to non-linear propagation. Using a 50 MHz high-pass filter, the reference hydrophone is aligned by maximizing the hydrophone's high frequency components in the plane at that position to an optimal orientation. The pressure waveform at that position is recorded after the high-pass filter was removed. An

FFT of the waveform is calculated, and the voltage amplitude at each harmonic is determined. The reference hydrophone has previously been calibrated by NPL, so that the voltage it detects can be translated into a pressure value, hence calibrating the pressure output of the source at each harmonic.

2) The reference hydrophone is replaced by the hydrophone to be calibrated, which is then aligned the same way at the same position as the reference hydrophone. The pressure waveform is recorded with the absence of the high-pass filter. An FFT of the pressure waveform is then calculated, and the voltage at each harmonic is determined. This voltage is then divided by the pressure amplitude (measured in step 1) to determine the output of the hydrophone in Volts per Pascal (V/Pa).

II. Calibration Uncertainty

The uncertainties in the calibration are predominantly systematic in origin, the random error is negligible in comparison. The dominant source of uncertainty is the uncertainty in the calibration of the reference hydrophone (as provided by NPL). The other sources of uncertainty are temperature variation (± 1 °C, resulting in calibration variations of ± 1%) source stability (± 2%) digitizer error (± 2%) and positional repeatability (this effect varies with frequency, from ± 2.5% at 1 Mhz to ± 5% at 20 MHz). The combined effect of these error sources is calculated according to [2-3], with a coverage factor of k = 2 to calculate the uncertainty with a 95% confidence level. This yields uncertainties that are typically within ± 1.5 dB from 0.5 to 1 MHz, ± 1 dB from 1 to 15 MHz, ± 1.5 dB from 15 to 20 MHz, ± 2.2 dB from 20 to 40 MHz and ± 3 dB from 40 to 60 MHz.

III. Important Considerations Regarding Electrical Loading Conditions

HMA and HMB hydrophones are sold with a standard 1-20 MHz calibration into a 50-ohm load. HGL, HNP (formerly HNV), HNC (formerly HNZ), and HNR hydrophones are modular—i.e., they allow the user to choose different amplifiers or no amplifier at all. Because a hydrophone's sensitivity depends on the electrical impedance of the detector or amplifier it is attached to, modular hydrophones are sold with an open-circuit calibration, called formally the "End-of-cable Open Circuit Sensitivity", or EOC sensitivity for short, and designated as $M_c(f)$ [4-5]. $M_c(f)$ is determined by measuring the sensitivity of the hydrophone with a laboratory amplifier, and then subtracting the effect of that amplifier's gain, as well as that of its finite (i.e., non-infinite load). Note that the HGL, HNP, and HNC hydrophones may be connected directly to an amplifier without any cable, so the EOC sensitivity is defined as the sensitivity that would be measured at the hydrophone's connector into an infinite load.

Of course, actual hydrophone usage is made with the customer's choice of amplifier and/or other form of detector. In such cases, the customer may calculate the effect of the amplifier/detector configuration on the hydrophone sensitivity, by mathematically combining hydrophone calibration data and amplifier data, as described below:

Obtaining amplifier-loaded sensitivity from EOC data

The sensitivity of the hydrophone/preamp combination ($M_L(f)$) can be determined using the following formula [4]:

$$M_L(f) = G(f)M_c(f)\left[\frac{\mathrm{Re}(Z_A)^2 + \mathrm{Im}(Z_A)^2}{\{\mathrm{Re}(Z_A) + \mathrm{Re}(Z_H)\}^2 + \{\mathrm{Im}(Z_A) + \mathrm{Im}(Z_H)\}^2}\right]^{1/2} \qquad (1)$$

where

$G(f)$ = amplifier gain (as a function of frequency)
Z_A = input impedance of amplifier
Z_H = impedance of hydrophone
Re(Z) indicates the real part of a complex number Z
Im(Z) indicates the imaginary part of a complex number Z

If the hydrophone and amplifier impedances are primarily capacitive (as is the case with all Onda hydrophones and amplifiers), Eq. (1) can be approximated:

$$M_L(f) = G(f)\, M_c(f)\, \frac{C_H}{C_H + C_A} \qquad (2a)$$

where C_A and C_H and are the capacitance of the amplifier and hydrophone , respectively. C_H is provided with the EOC calibration data shipped with each modular hydrophone. Onda provides C_A with the calibration sheets for all AH2010 and AH2020 amplifiers, and can be purchased for an additional price for other Onda amplifiers.

Note that in some cases, adaptors or short cables may be used between the hydrophone connector and the amplifier. This additional connection length may have an effect which can be approximated by a connection capacitance, designated C_C, which can be accounted for by the following modification to Eq. (2):

$$M_L(f) = G(f)\, M_c(f)\, \frac{C_H}{C_H + C_C + C_A} \qquad (2b)$$

A common example of such a connector is the right angle SMA connector (Onda part number AR-AMAF) which is used to connect an Onda HGL hydrophone to an AH2010 or AH2020 in a right-angle configuration; C_C = 1.6 pF for this case.

Note: Customers are advised to perform their own assessment of the accuracy of Eqs. (2a-b) for their configuration. In particular, customers should be aware that extension cables connecting the hydrophone to the preamplifier or detector may not be accurately modeled as purely capacitive at higher frequencies; in such cases, customers are advised to consider purchasing a separate calibration which includes the use of their extension cables.

IV. Other Common Calibration Units

$M_L(f)$ is in units of voltage divided by pressure and is typically expressed in V/Pa. Alternatively, it can be expressed in units of dB re 1V/μPa using Eq. (3):

$$dB_{re\,1V/\mu Pa}[M_L(f)] = 20 * \log_{10}[M_L(f)] - 120 \qquad (3)$$

It is also common to express the calibration in terms of acoustic intensity. Strictly speaking, a simple calibration factor exists only under conditions of a sinusoidal signal and under the assumption that intensity is equal to the time-averaged value of the pressure squared divided by the acoustic impedance of the medium. Under these conditions the following relation applies:

$$I = V_{RMS}{}^2 / K \qquad (4)$$

where I is the acoustic intensity, and V_{RMS} is the root-mean-square voltage of the sinusoidal signal. The calibration factor K is given by

$$K = z_a[M_L(f)]^2 \qquad (5)$$

where z_a is the acoustic impedance of the medium (1.5 MRayls for water). Because it is common to express I in units of W/cm^2,

$$K\{volts^2 cm^2 / Watt\} = 1.5x10^{10}[M_L(f)\{volts/Pa\}]^2 \quad \textbf{\textit{for water}} \qquad (6)$$

V. Examples

Example I. An HNV-0400 is supplied by Onda with an EOC calibration:

$M_c(f)$ = 50 nV/Pa at 5 MHz, and C_H = 80 pF

We now wish to determine the sensitivity for this hydrophone connected to an AH-2010 preamplifier.

As determined from the datasheet for the AH-2010, the amplifier impedance is capacitive with C_A = 7 pF, and the gain is 20 dB ($G(f)$ = 10). Application of Eqs. (2a) and 3 shows that $M_L(5MHz)$ = 460 nV/Pa, or –246.7. dB re 1V/μPa. Application of Eq. (6) yields K (5 MHz) = 3.17 x 10^{-3} V^2 cm^2/W.

Example II. An HGL-0200 is supplied by Onda with an EOC calibration:

$M_c(f)$ = 45 nV/Pa at 5 MHz, and C_H = 13 pF

We now wish to determine the sensitivity for this hydrophone connected to an AH-2010 preamplifier through an AR-AMAF connector:

As determined from the datasheet for the AH-2010, the amplifier impedance is capacitive with C_A = 7 pF, and the gain is 20 dB ($G(f)$ = 10). Application of Eqs. (2b) and 3 shows that $M_L(5MHz) = 271$ nV/Pa, or –251.3dB re 1V/μPa. Application of Eq. (6) yields K (5 MHz) = 1.10 x 10^{-3} V^2 cm^2/W.

References

[1] A. Selfridge and P.A. Lewin, "Wideband Spherically Focused PVDF Acoustic Source for Calibration of Ultrasound Hydrophone Probes," IEEE Trans. UFFC, 47(6) 1372-1376, 2000.

[2] R. C. Preston, D.R. Bacon, and R. A. Smith, "Calibration of Medical Ultrasound Equipment: Procedures and Accuracy Assessment," IEEE Transactions on Ultrasonics, ferroelectrics, and Frequency Control, Vo. UFFC-25(2), pp. 110-121, 1988.

[3] M. C. Ziskin, "Measurement Uncertainty in Ultrasonic Exposimetry," in Ultrasonic Exposimetry, M.Ziskin and P. Lewin, eds. (CRC Press), Chapter 14, 1993.

[4] ALUM/NEMA: Acoustic Output Measurement Standard for Diagnostic Ultrasound Equipment. American Institute of Ultrasound in Medicine, 14750 Sweitzer Lane, Suite 100, Laurel MD 20707-5906; National Electrical Manufacturers Association, 1300 North 17thStreet, Suite 1847, Rosslyn VA 22209, 1998.

[5] IEC 61102 Measurement and characterisation of ultrasonic fields using hydrophones in the frequency range 0,5 MHz to 15 MHz.

ONDA

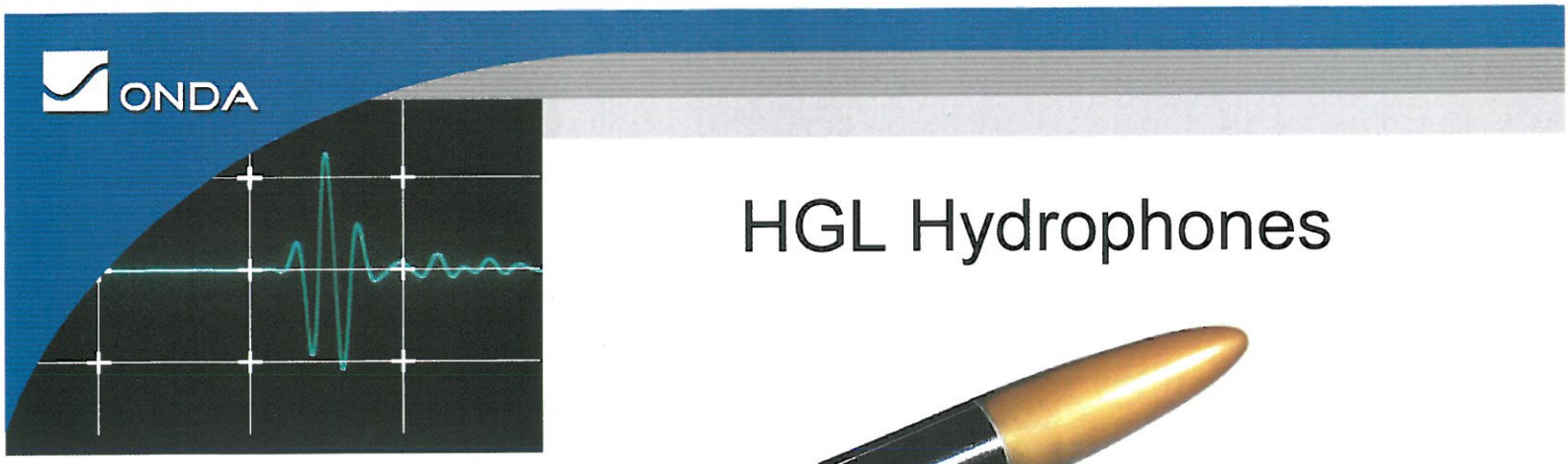

HGL Hydrophones

The HGL Series hydrophones were designed to meet or exceed recommendations of section 3.3.2 of the AIUM Acoustic Output Measurement Standard (May 1998). They have an exceptionally flat sensitivity in a small and sturdy package. These hydrophones are excellent in-house standards for ultrasonic acoustic intensity measurements, and for general purpose field mapping.

HGL hydrophone with AH-2000 series amplifier

Features

* High Sensitivity
* Small effective aperture
* Broadband
* Solid construction
* Flawless integration with AH preamplifiers
* Flat (+/-3dB) 250 KHz to >> 20 MHz

Technical Specifications

	HGL-0085	HGL-0200	HGL-0400	HGL-1000
Frequency range (±3dB)	0.25 to 40 MHz		0.25 to 20 MHz	
Electrode aperture	85μm	200μm	0.4mm	1.0mm
*** EOC Nominal Sensitivity [nV/Pa]**	8	45	160	510
Acceptance angle (-6dB at 5 MHz)	>150°	100°	30°	20°
Capacitance	30 pF			
Max. Operating Temperature	50 °C			

*EOC ("end of cable") is the open-circuit output sensitivity of the hydrophone. Calibration with an amplifier can be determined from the gain and input impedance of the amplifier.

Provided with traceable calibration 1-20 MHz at 50 KHz intervals. Other calibrations available, please visit our web site.

This specification is subject to change without notice.

Typical Open-Circuit Sensitivity Plots (before amplification)

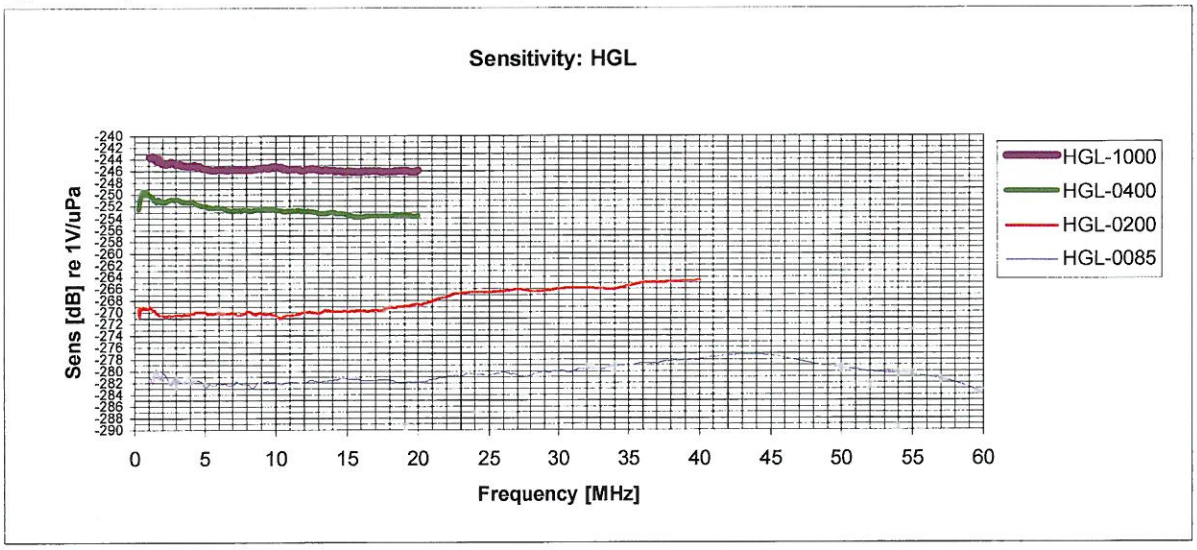

Typical Directivity Plots

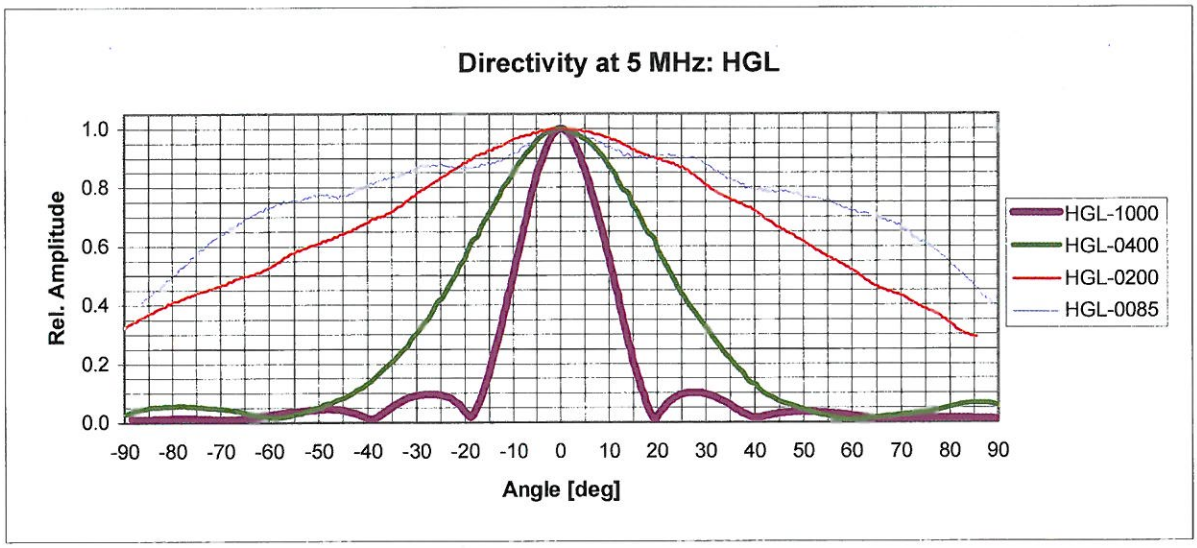

Mechanical specifications

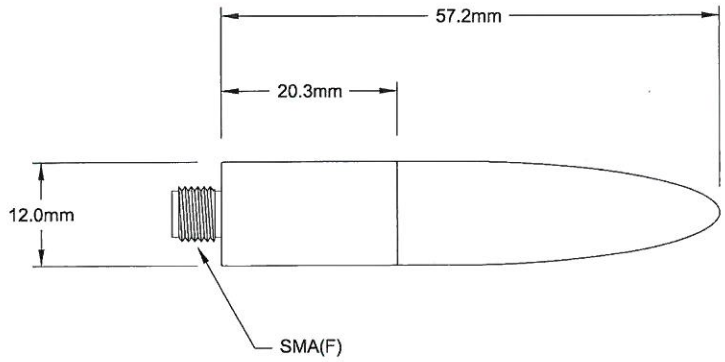

AH-2010 Preamplifier

The AH-2010 Preamplifier is a great combination of performance and features. Designed as an electronic and mechanical match for Onda hydrophones, the AH-2010 has only one coaxial cable going to the oscilloscope. It has a superb frequency response, low noise and high stability, which make it ideal for ultrasonic acoustic intensity measurements.

AH-2010 with HGL hydrophone

Features

* Flat frequency response
* Low noise - up to 78 dB dynamic range
* Fully immersible
* Only one cable in the tank
* Waterproof mating to Onda hydrophones
* Compatible with any hydrophone

Available in two different bandwidths:

AH-2010 -025	50 KHz - 25 MHz
AH-2010 -100	50 Khz - 100 MHz

Performance Specifications

Voltage Gain: 20 dB*
Input Impedance: 1 MΩ in parallel with 7 pF*
Output Impedance: 50 Ω
Max Output into 50 Ω:
4 Vpp below 50 MHz
1 Vpp above 50 MHz
Power Usage: Preamp 0.6 W, Total 2 W

A Precision Gain and Input Capacitance calibration certificate is provided with each device.

Amplifier is supplied in a kit with Universal Power Supply, DC Block, 1m coaxial cable and calibration certificate.

This specification is subject to change without notice

Typical Gain Plots

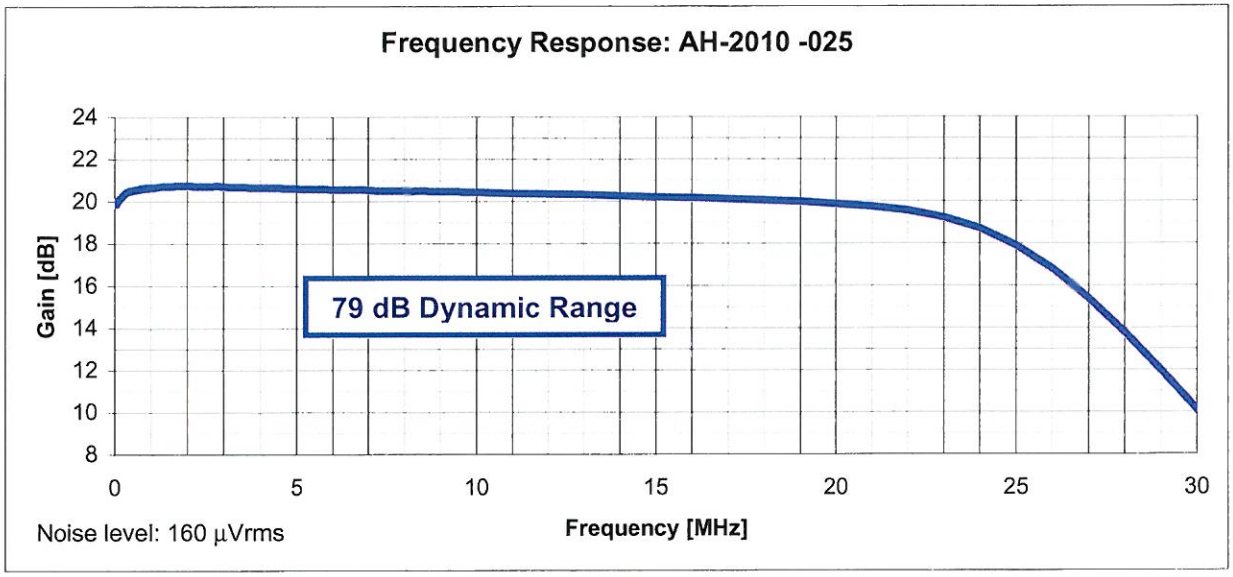

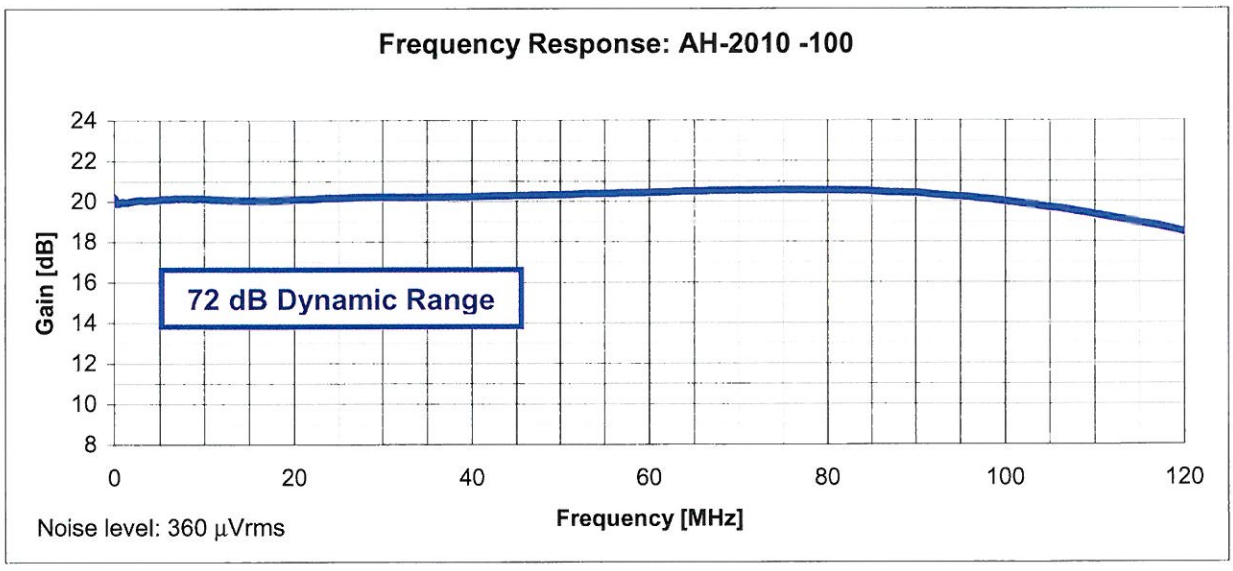

Mechanical Specifications

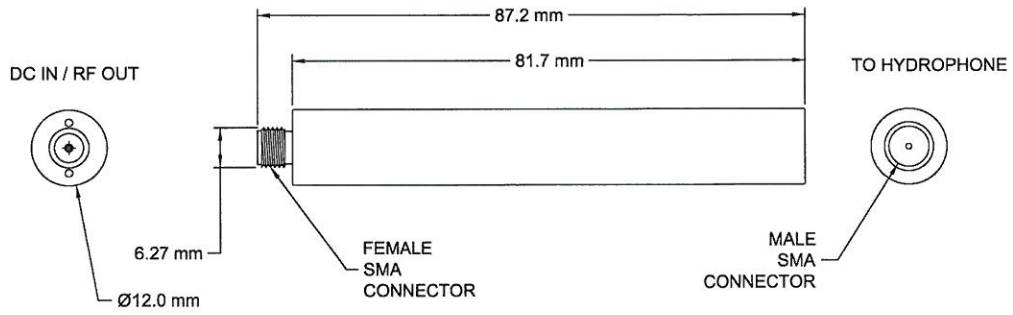

Weight: 36 g
Material: Hermetically sealed stainless steel body.

Important Notes on the Proper Care of ONDA Hydrophones

We are pleased that you have chosen an Onda Corporation acoustic measurement device. To help extend the life of your hydrophone, please take a moment to read the following precautions and maintenance tips.

+ **Never physically touch the tip of your hydrophone.** The thin coating on the tip of the hydrophone can be damaged, leading to corrosion or degradation of the active element. Dropping or bumping the tip of the hydrophone on a hard surface will generally result in some damage to the coating, the active element, or both. Use a squeeze bulb or a 1 atm. pressure stream of clean air or other gas to remove liquids or particles.

+ **Do not insert the tip of the hydrophone into a test fixture.** Doing so may cause inadvertent contact between the tip and the fixture, and is one of the most common ways of destroying hydrophones. You may use a side mount clamp to hold it instead.

+ **Limit the amount of time that the hydrophone is immersed in liquid**. During a break or at the end of a test session, it is best to remove the hydrophone from the liquid (water or other). This will help extend the life of the hydrophone.

+ **Use clean de-ionized and degassed water for high intensity measurements.** De-ionized water is best to avoid electrical coupling in strong conducting fields, and degassed water improves the accuracy of the readings. Onda Corporation offers water treatment devices for de-ionizing and degassing water to meet your requirements in this area.

+ **Use only the supplied box to store your hydrophone.** Our hydrophone box is designed to ensure that the tip is safe from all contact while in storage.

For additional information or questions on Onda Corporation hydrophones, please consult our website at www.ondacorp.com or give us a call at (408) 745-0383.

Certificate of Pre-Amplifier Calibration

Model Number:	AH-2010	**Gain:**	20 dB (nominal)
Serial Number:	1242	**Bandwidth:**	25 MHz (nominal)
Calibration Date:	30-Jul-2009	**Input Capacitance:**	6.5 pF (nominal)
Data File Names:		**Output Impedance:**	50 Ohms (nominal)
AH-2010-20-025-1242_090730.txt		**Gain Uncertainty:**	0.03 dB
AH-2010-20-025-1242_1-20c_090730.txt		**Capacitance Uncertainty:**	2.5 %
AH-2010-20-025-1242_1-20t_090730.txt			

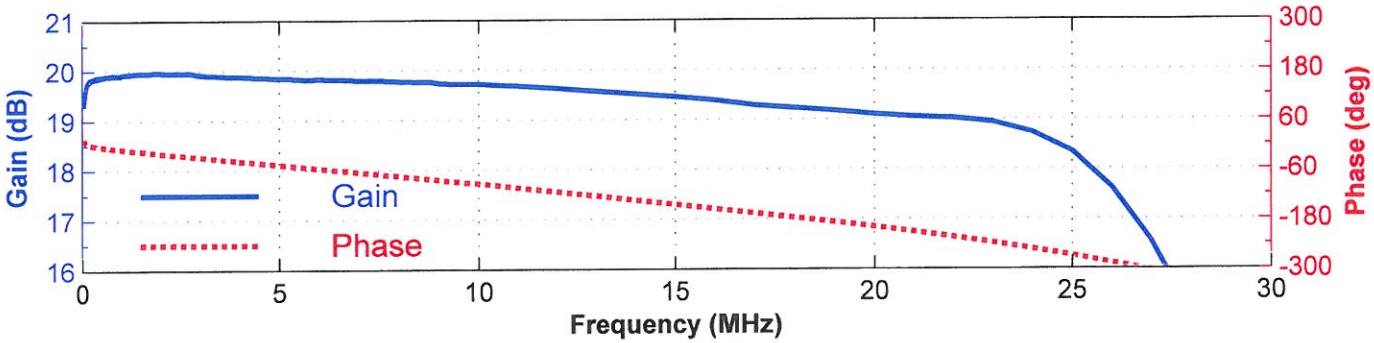

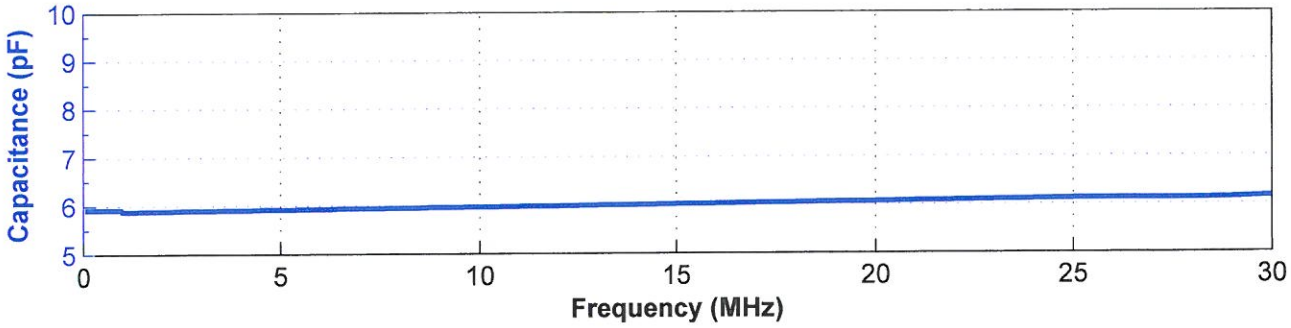

Signature: _____ Date: 7/30/09

592 E. Weddell Drive, Suite 7, Sunnyvale, CA 94089 T:(408)745-0383 F:(408)745-0956

www.ondacorp.com

Certificate of Hydrophone Calibration

Hydrophone:	Onda HGL-0200 S/N: 1269
Cable/Adaptor:	NONE
External Amplifier:	NONE
Electrical Loading:	OpenCircuit
Temperature:	23.2 deg C
Calibration Completed:	29-Jul-2009
Data File Name:	HGL0200-1269_xxxxxx-xxxx-xx_xx_20090729.txt

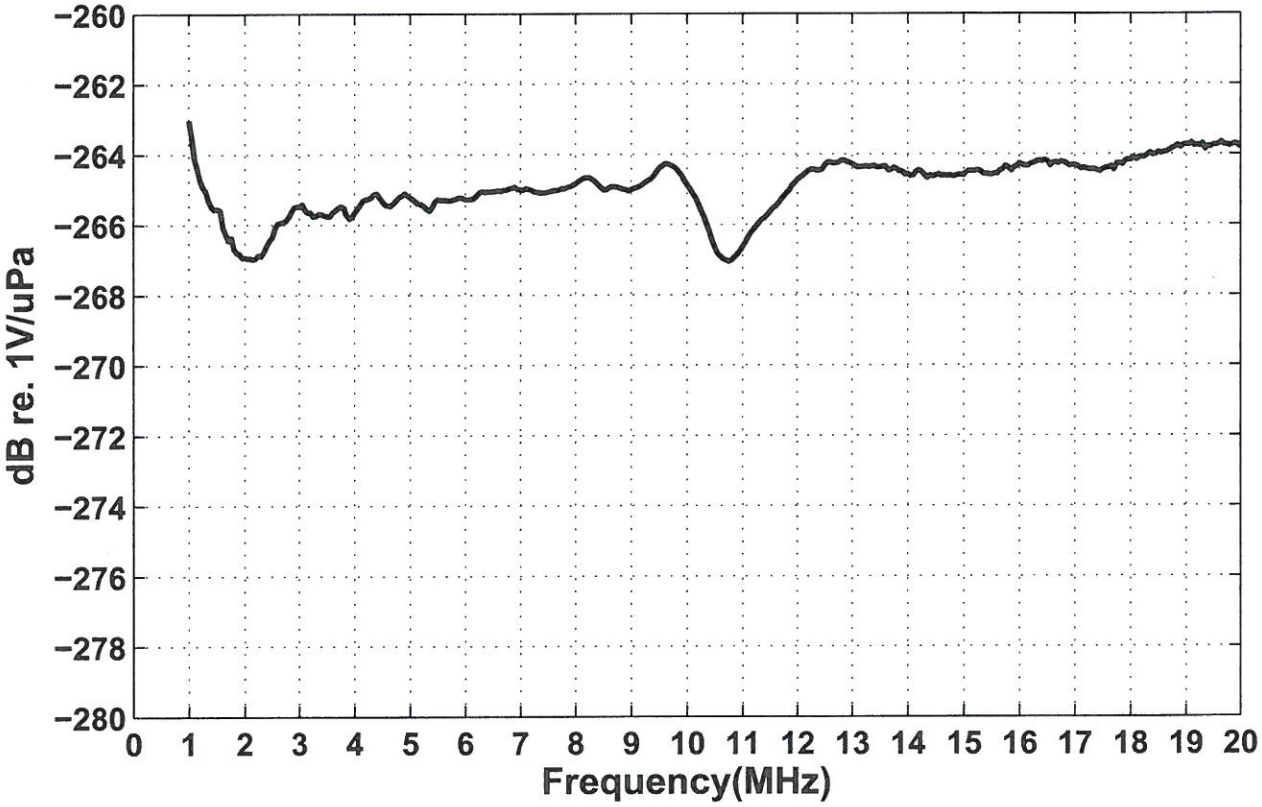

Calibration Method: Stepped single frequency comparison to Reference Standard

Measurement Uncertainty: 1-15 MHz: 1 dB; 15-20 MHz: 1.5 dB

Signature: Hugh Date: 7-29-09

592 E. Weddell Drive, Suite 7, Sunnyvale, CA 94089 T: (408) 745-0383 F: (408) 745-0956
www.ondacorp.com

.3 Appendix C-Ethics

UNIVERSITY OF THE WITWATERSRAND JOHANNESBURG

R14/49 Mr Charl Smallberger

HUMAN RESEARCH ETHICS COMMITTEE (MEDICAL)

CLEARANCE CERTIFICATE NO. M190344

NAME: (Principal Investigator)	Mr Charl Smallberger
DEPARTMENT:	Electrical and Information Engineering Surgery
PROJECT TITLE:	Acoustic properties of red blood cells
DATE CONSIDERED:	29/03/2019
DECISION:	Approved unconditionally
CONDITIONS:	
SUPERVISOR:	Prof M. Postema, D. Rubin and M. Nel
APPROVED BY:	CB Penny Dr CB Penny, Chairperson, HREC (Medical)
DATE OF APPROVAL:	23/07/2019

This clearance certificate is valid for 5 years from date of approval. Extension may be applied for.

DECLARATION OF INVESTIGATORS

To be completed in duplicate and **ONE COPY** returned to the Research Office Secretary on the Third Floor, Faculty of Health Sciences, Phillip Tobias Building, 29 Princess of Wales Terrace, Parktown, 2193, University of the Witwatersrand. I/we fully understand the conditions under which I am/we are authorized to carry out the above-mentioned research and I/we undertake to ensure compliance with these conditions. Should any departure be contemplated, from the research protocol as approved, I/we undertake to resubmit the application to the Committee. **I agree to submit a yearly progress report**. The date for annual re-certification will be one year after the date of convened meeting where the study was initially reviewed. In this case, the study was initially reviewed in **March** and will therefore be due in the month of **March** each year. Unreported changes to the application may invalidate the clearance given by the HREC (Medical).

Principal Investigator Signature

Date 22-07-2019

PLEASE QUOTE THE PROTOCOL NUMBER IN ALL ENQUIRIES

UNIVERSITY OF THE WITWATERSRAND, JOHANNESBURG

Research Office

INSTITUTIONAL BIOSAFETY COMMITTEE (IBC)
(R 14/16)

CLEARANCE CERTIFICATE **PROTOCOL NUMBER: 20190602**

BRIEF DESCRIPTION OF APPLICATION:

Biological cell behaviour in an ultrasound field

APPLICANT: Mr C Smallberger

SUPERVISOR: Prof D Rubin

SCHOOL/DEPARTMENT : Electrical and Information Engineering

DATE CONSIDERED: 05 July 2019

EXPIRY DATE: 05 July 2024

DECISION OF COMMITTEE: Approved unconditionally

1. This clearance certificate expires on 05 July 2024 and may be renewed on application
2. An annual report must be provided on the anniversary date of this certificate, for as long as the project continues
3. Notification of any proposed modifications must be submitted on the attached form
4. Unreported changes to the application may invalidate the clearance given by the IBC

DATE: 05 July 2019

CHAIRPERSON: James F. S. Larkin 2019.07.08 14:29:50 +02'00'

(Professor J Larkin)

DECLARATION OF APPLICANT:

To be completed in duplicate and **one copy** returned to the Research Office, Phillip Tobias Building, Room 301, 3rd Floor, 29 Princess of Wales Terrace, Parktown, Faculty of Health Sciences, University.

1. I have read, understood and accepted the approval conditions above
2. I agree to submit a yearly progress report to the Committee and to submit an interim report on the form provided, in the event of any significant unforeseen event, *e.g.* suspension of a drug trial, temporary closure or relocation of my laboratory, etc
3. I note that the University Safety Officer, or his/her representative, may at any reasonable time inspect my laboratory or trial site to ensure compliance with current Health and Safety legislation. I undertake to offer my full co-operation in any such inspection.
4. I have read, understood and will comply with the *recommended standard operating procedures for the handling of biohazardous materials* posted at http://web.wits.ac.za/Academic/Research/Biosafety.htm
5. I declare (delete as appropriate) that:
    a. I have all the approvals required by statute or regulation and by the funding agencies supporting this work, or
    b. that I will not begin work until such approvals are obtained

Signed: _____ **Date:** 11/07/2019

PLEASE QUOTE THE PROTOCOL NUMBER IN ALL ENQUIRIES

Head Office or Zone
1 Constantia Boulevard
Constantia Kloof Ext 22, 1709

Postal Address: Private Bag X14, Weltevreden Park, 1715
Tel: 011 761 9000 **Fax:** 0866747666
Email: customerservice@sanbs.org.za

NPO Number: 049066NPO
NPC Registration No. 2000/026390/08

SOUTH AFRICAN NATIONAL BLOOD SERVICE NPC
Human Research Ethics Committee

OHRP Number : IORG0006278
FWA Registration Number : IRB00007553
SA NHREC Registration Number : REC-270606-013

Secretariat: Tel: 011 761 9096 | Valencia.Simmadari@sanbs.org.za

To : Prof. David Rubin
Email : david.rubin@wits.ac.za

Dear, Prof. Rubin

DATE OF COMMITTEE MEETING : **11th June 2019**
PROJECT TITLE : **THE IN-VITRO BEHAVIOR OF BLOOD CELLS AND PLATELETS UNDER THE INFLUENCE OF ULTRASOUND**
DECISION OF THE COMMITTEE : **Approved**
CLEARNACE CERTIFICATE NO. : **2019/0468**

1. Execution of the study must be compliant with applicable guidelines and policies.
2. Any amendment, extension or any other modifications to the protocol must be submitted to this Ethics Committee for approval prior to implementation.
3. The Committee must be informed of any serious adverse event, planned and unplanned termination of the study.
4. A progress report should be submitted yearly for studies longer than a year and a final report at completion of the study for both short term and long term studies.
5. Kindly refer to the SANBS HREC clearance certificate number on all future correspondence on this study to the HREC secretariat.
6. This approval is valid for 5 years from the date stated above.

COMMITTEE GUIDANCE DOCUMENTS:

- International Conference on Harmonization (ICH) Good Clinical Practices (GCP) Guideline (ICH, 1996), Ethics in Health Research: Principles, Structures and Procedures (SA Department of Health, 2015); Guidelines for Good Practice in the Conduct of Clinical Trials in Human Participants in South Africa (SA Department of Health, 2006); Ethical Principles for Medical Research Involving Human: Declaration of Helsinki (World Medical Association, 2013); Reviewing Clinical trials: A Guide For Ethics Committees (Karlberg and Speers, 2010).

CHAIRPERSON: Prof J.N. Mahlangu

05 August 2019
DATE

.4 Appendix D-Matlab Code

```
%x-displacement vs time and position plots
%Parameters
frame = 161;
time = 266.66;
cal = 0.4124;
%pop = 0;
legStr = ["WBC" "RBC" "RBC" "RBC" "RBC" "RBC" "RBC" "RBC" "RBC" "RBC"];
%--------------------------------------------------------------------------
%Import Data
opts = delimitedTextImportOptions("NumVariables", 7);

% Specify range and delimiter
opts.DataLines = [2, Inf];
opts.Delimiter = ",";

% Specify column names and types
opts.VariableNames = ["Trackn", "Slicen", "X", "Y", "Distance", "Velocity",
"PixelValue"];
opts.VariableTypes = ["double", "double", "double", "double", "double",
"double", "double"];
opts.ExtraColumnsRule = "ignore";
opts.EmptyLineRule = "read";

% Import the data
data = readtable("C:\Users\Charl Smalberger\Documents\Photron\Photron FASTCAM
Viewer 3\10-
16\5_FreshBlood_1.5mlTS_26.2ulvacutainer_NULL_C001H001S0001\Data\data.csv",
opts);
clear opts
%--------------------------------------------------------------------------

%Setup matrix to process
filename = data;
raw = [filename.Trackn filename.Slicen filename.X filename.Y];

track = raw(1,1);
count = 1;

%find amount of columns
for i = 1:length(raw)
    if raw(i,1)~= track
     count = count + 1;
    track = raw(i,1);
    end
end

%Matrix dimentions
dim = [frame count];

%Setup matrix x and y
x = NaN(dim(1),dim(2));
y = NaN(dim(1),dim(2));

track = raw(1,1);
row = 1;
```

```
col = 1;
for i = 1:length(raw)

    if raw(i,1) == track
        x(raw(i,2),col) = raw(i,3);
        y(raw(i,2),col) = raw(i,4);
        track = raw(i,1);
        row = row + 1;
    else
        track = raw(i,1);
        col = col + 1;
        row = 1;
        x(raw(i,2),col) = raw(i,3);
        y(raw(i,2),col) = raw(i,4);
        row = row + 1;
    end
end

%Setup matrices and vectors for displacemnt and time data
d = zeros(dim(1),dim(2));
acD = zeros(dim(1),dim(2));
t = ((time/frame):(time/frame):time)';
%Y-axis fix
y = abs(y - 512);

%Data processing - calculating displacements
 for j = 1:dim(2)
    for i = 1:(dim(1)-1)
        d(i,j) = (sqrt((x(i+1,j) - x(i,j))^2))*(cal);
         if x(i+1,j) - x(i,j) < 0
             d(i,j) = d(i,j)*(-1);
         end
         d(dim(1),j)=NaN;
    end
 end

  for j = 1:dim(2)
      sum = 0;
    for i = 1:(dim(1))
        if isnan(d(i,j))
            acD(i,j) = NaN;
        else
        sum = d(i,j) + sum;
        acD(i,j) = sum;
        end
    end
  end

%Finding first and last x and y value for o and x
px = (zeros(2,dim(2)))';
py = (zeros(2,dim(2)))';

%to find x and y of first value
for j = 1:dim(2)
    tempX = NaN;
    tempY = NaN;
```

```
   for i = 1:dim(1)
    if isnan(x(i,j))
        tempX = NaN;
        tempY = NaN;
    else
        tempX = x(i,j);
        px(j,1) = tempX;
        tempY = y(i,j);
        py(j,1) = tempY;
        break;
    end
   end
end

%to find x and y of last value
for j = 1:dim(2)
    tempX = NaN;
    tempY = NaN;
   for i = dim(1):-1:1
    if isnan(x(i,j))
        tempX = NaN;
        tempY = NaN;
    else
        tempX = x(i,j);
        px(j,2) = tempX;
        tempY = y(i,j);
        py(j,2) = tempY;
        break;
    end
   end
end

%convert px and py to um before plotting
px = px*cal;
py = py*cal;

%Extract displacement data final values
delete Export.xlsx
exportRow = zeros(dim(2),1);
for j = 1:dim(2)
    tempacD = NaN;
   for i = dim(1):-1:1
    if isnan(acD(i,j))
        tempacD = NaN;
    else
        tempacD = acD(i,j);
        exportRow(j) = tempacD;
        break;
    end
   end
end

WBCCount = 0;
for i = 1:length(legStr)
    if strcmp(legStr(i), 'WBC')
        WBCCount = WBCCount + 1;
```

```
    end
end

WBCexport = zeros(WBCCount,1);
RBCexport = zeros(length(exportRow) - WBCCount,1);
z = 1;
for i = 1:length(exportRow)
    if i <= WBCCount
       WBCexport(i) = exportRow(i);
    else
        RBCexport(z) = exportRow(i);
        z = z + 1;
    end
end

writematrix(WBCexport,'Export.xlsx','Sheet',1);
writematrix(RBCexport,'Export.xlsx','Sheet',2);


%Plotting
%Fixed colour matrix
col = {[0 0 1],[1 0.4 0.6],[0 1 1],[1 0 0],[0 1 0],[1 0 1],[0 0.5 0],[0.5 0.5
0.5],[0.7 0.3 0],[1 1 0]};
%x-displacement plot
txt = '{\it x}-displacement (\mum)';
subplot(1,2,1)
a = plot(t,acD);
axis([0, 280, -150, 150]);
set(a,{'Color'},col')

xlabel('time (s)', 'Interpreter', 'none','FontSize',18);
ylabel(txt,'FontSize',18);
title('{\it x}-displacement vs time','FontSize',18);
legend(legStr, 'Location', 'SouthWest','FontSize',8,'NumColumns',2);

figLab1 = '(a)';
text(7,138,figLab1,'FontSize',18);

%WBC pop and ultrasound on code
%hold on;
%p = plot(t(pop),acD(pop),'rx');

%for i =1:dim(2)
 %   plot(t(usFr),acD(usFr,i),'ko');
%end

%Initial and final positions of cells plot
subplot(1,2,2)
txt1 = '{\it x} (\mum)';
txt2 = '{\it y} (\mum)';
hold on;

for j = 1:size((px),2)
    for i = 1:size((px),1)
        if j == 1
```

```
            scatter(px(i,j),py(i,j),'MarkerEdgeColor',col{(i)});
        else
            scatter(px(i,j),py(i,j),'x','MarkerEdgeColor',col{(i)});
        end
    end
end
axis([0, 211, 0, 211]);
xlabel(txt1,'FontSize',18);
ylabel(txt2,'FontSize',18);
title('postion','FontSize',18);
%setup legend for this plot
custLeg = zeros(2,1);
custLeg(1) = plot(NaN,NaN,'ok');
custLeg(2) = plot(NaN,NaN,'xk');
legend(custLeg,'initial position','final position','Location',
'SouthWest','FontSize',8);

hold off;
figLab2 = '(b)';
text(7,203,figLab2,'FontSize',18);


%x-displacement at various mechanical indices

% Import data from spreadsheet
% Script for importing data from the following spreadsheet:
%
%    Workbook: C:\Users\Charl Smalberger\Documents\Photron\Data General\Super
Figure.xlsx
%    Worksheet: Combimed
%
% Auto-generated by MATLAB on 03-Dec-2019 08:51:00

% Setup the Import Options
opts = spreadsheetImportOptions("NumVariables", 14);

% Specify sheet and range
opts.Sheet = "Combimed";
opts.DataRange = "A3:N98";

% Specify column names and types
opts.VariableNames = ["WBC0", "RBC0", "VarName3", "WBC2", "RBC2", "VarName6",
"WBC25", "RBC25", "VarName9", "WBC3", "RBC3", "VarName12", "WBC4", "RBC4"];
opts.SelectedVariableNames = ["WBC0", "RBC0", "VarName3", "WBC2", "RBC2",
"VarName6", "WBC25", "RBC25", "VarName9", "WBC3", "RBC3", "VarName12",
"WBC4", "RBC4"];
opts.VariableTypes = ["double", "double", "string", "double", "double",
"string", "double", "double", "string", "double", "double", "string",
"double", "double"];
opts = setvaropts(opts, [3, 6, 9, 12], "WhitespaceRule", "preserve");
opts = setvaropts(opts, [3, 6, 9, 12], "EmptyFieldRule", "auto");

% Import the data
SuperFigure = readtable("C:\Users\Charl Smalberger\Documents\Photron\Data
General\Super Figure.xlsx", opts, "UseExcel", false);
```

```
% Clear temporary variables
clear opts
%-------------------------------------------------------------------------
---------------------------------
%assign vector variables
MI = [0 0.2 0.3 0.35 0.4];
WBC0 = SuperFigure.WBC0;
RBC0 = SuperFigure.RBC0;

WBC2 = SuperFigure.WBC2;
RBC2 = SuperFigure.RBC2;

WBC25 = SuperFigure.WBC25;
RBC25 = SuperFigure.RBC25;

WBC3 = SuperFigure.WBC3;
RBC3 = SuperFigure.RBC3;

WBC4 = SuperFigure.WBC4;
RBC4 = SuperFigure.RBC4;

place = NaN(96,1);

hold on
boxplot([WBC0,RBC0,place,WBC2,RBC2,place,WBC25,RBC25,place,WBC3,RBC3,place,WB
C4,RBC4],'color','krw');

set(gca,'xtick',1.5:3:50)
set(gca,'xticklabel',{'MI = 0','MI = 0.2','MI = 0.25','MI = 0.3','MI = 0.4'})
txt = '{\it x}-displacement (\mum)';
%axis([0 0 -100, 100]);
xlabel('mechanical index');
ylabel(txt);
title('box and whisker plot of {\it x}-displacement at mechanical index');

custLeg = zeros(3,1);
custLeg(1) = plot(NaN,NaN,'sk');
custLeg(2) = plot(NaN,NaN,'sr');
custLeg(3) = plot(NaN,NaN,'+r');
legend(custLeg,'WBCs','RBCs','outliers','Location',
'SouthWest','FontSize',8);

hold off

%-------------------------------------------------------------------------
-----------------------------------------------

%absolute %x-displacement at various mechanical indices

% Import data from spreadsheet
% Script for importing data from the following spreadsheet:
%
```

```
%    Workbook: C:\Users\Charl Smalberger\Documents\Photron\Data General\Super
Figure.xlsx
%    Worksheet: Combimed
%
% Auto-generated by MATLAB on 03-Dec-2019 08:51:00

% Setup the Import Options
opts = spreadsheetImportOptions("NumVariables", 14);

% Specify sheet and range
opts.Sheet = "Combimed";
opts.DataRange = "A3:N98";

% Specify column names and types
opts.VariableNames = ["WBC0", "RBC0", "VarName3", "WBC2", "RBC2", "VarName6",
"WBC25", "RBC25", "VarName9", "WBC3", "RBC3", "VarName12", "WBC4", "RBC4"];
opts.SelectedVariableNames = ["WBC0", "RBC0", "VarName3", "WBC2", "RBC2",
"VarName6", "WBC25", "RBC25", "VarName9", "WBC3", "RBC3", "VarName12",
"WBC4", "RBC4"];
opts.VariableTypes = ["double", "double", "string", "double", "double",
"string", "double", "double", "string", "double", "double", "string",
"double", "double"];
opts = setvaropts(opts, [3, 6, 9, 12], "WhitespaceRule", "preserve");
opts = setvaropts(opts, [3, 6, 9, 12], "EmptyFieldRule", "auto");

% Import the data
SuperFigure = readtable("C:\Users\Charl Smalberger\Documents\Photron\Data
General\Super Figure.xlsx", opts, "UseExcel", false);


% Clear temporary variables
clear opts
%-------------------------------------------------------------------------------
---------------------------------
%assign vector variables
MI = [0 0.2 0.3 0.35 0.4];
WBC0 = SuperFigure.WBC0;
RBC0 = SuperFigure.RBC0;

WBC2 = SuperFigure.WBC2;
RBC2 = SuperFigure.RBC2;

WBC25 = SuperFigure.WBC25;
RBC25 = SuperFigure.RBC25;

WBC3 = SuperFigure.WBC3;
RBC3 = SuperFigure.RBC3;

WBC4 = SuperFigure.WBC4;
RBC4 = SuperFigure.RBC4;

place = NaN(96,1);

hold on
```

```
boxplot([abs(WBC0),abs(RBC0),place,abs(WBC2),abs(RBC2),place,abs(WBC25),abs(R
BC25),place,abs(WBC3),abs(RBC3),place,abs(WBC4),abs(RBC4)],'color','krw');

set(gca,'xtick',1.5:3:50)
set(gca,'xticklabel',{'MI = 0','MI = 0.2','MI = 0.25','MI = 0.3','MI = 0.4'})
txt = 'absolute {\it x}-displacement (\mum)';
%axis([0 0 -100, 100]);
xlabel('mechanical index');
ylabel(txt);
title('box and whisker plot of absolute{\it x}-displacement at mechanical
index');

custLeg = zeros(3,1);
custLeg(1) = plot(NaN,NaN,'sk');
custLeg(2) = plot(NaN,NaN,'sr');
custLeg(3) = plot(NaN,NaN,'+r');
legend(custLeg,'WBCs','RBCs','outliers','Location',
'SouthWest','FontSize',8);

hold off
```

.5 Appendix E-Results

.5.1 Null-Experiments

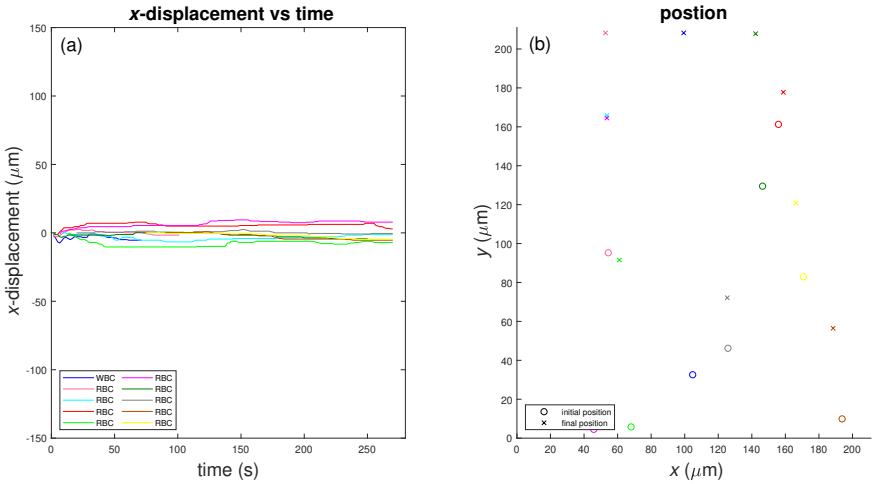

Figure 1: White and red blood cell x-displacement (a) and position (b) during a control experiment where no ultrasound is applied to the sample.

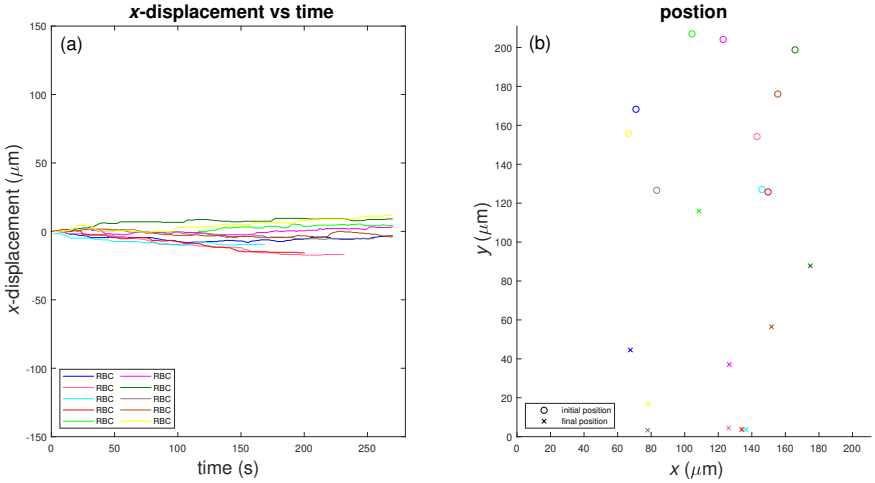

Figure 2: Red blood cell x-displacement (a) and position (b) during a control experiment where no ultrasound is applied to the sample.

.5.2 Ultrasound-experiments

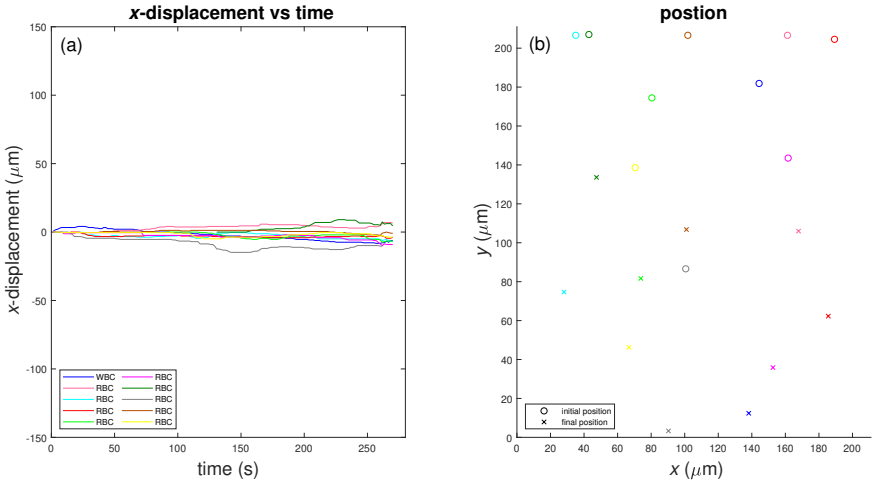

Figure 3: White and red blood cell x-displacement (a) and position (b) during a control experiment where no ultrasound is applied to the sample.

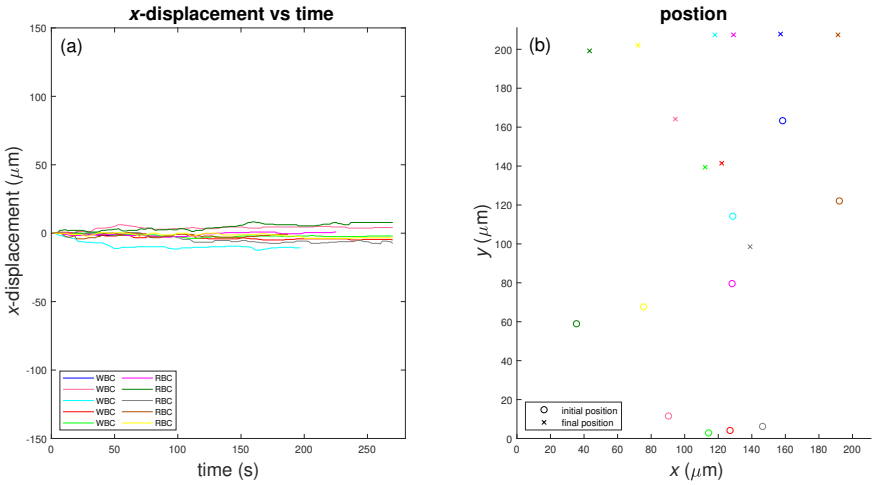

Figure 4: White and red blood cell x-displacement (a) and position (b) during a control experiment where no ultrasound is applied to the sample.

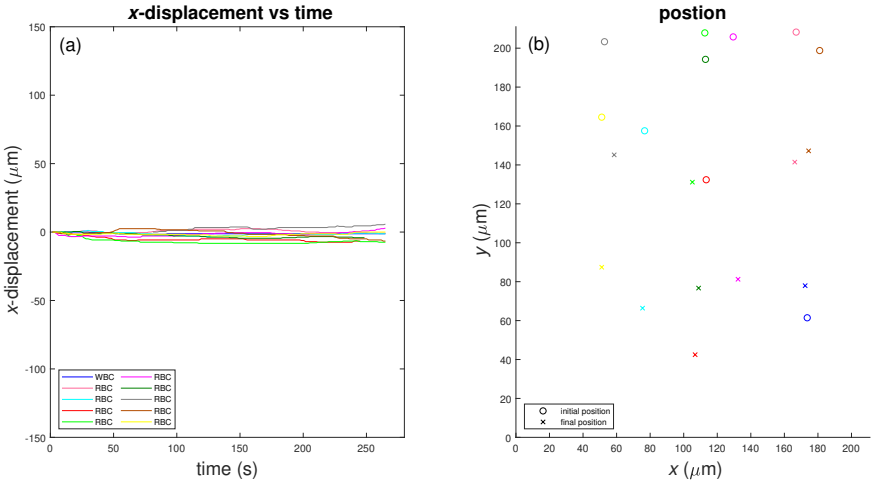

Figure 5: White and red blood cell x-displacement (a) and position (b) during a control experiment where no ultrasound is applied to the sample.

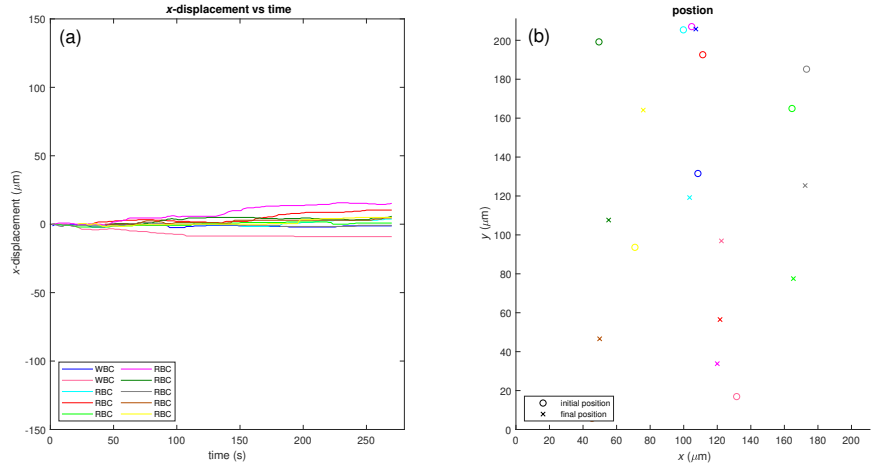

Figure 6: White and red blood cell x-displacement (a) and position (b) during a control experiment where no ultrasound is applied to the sample.

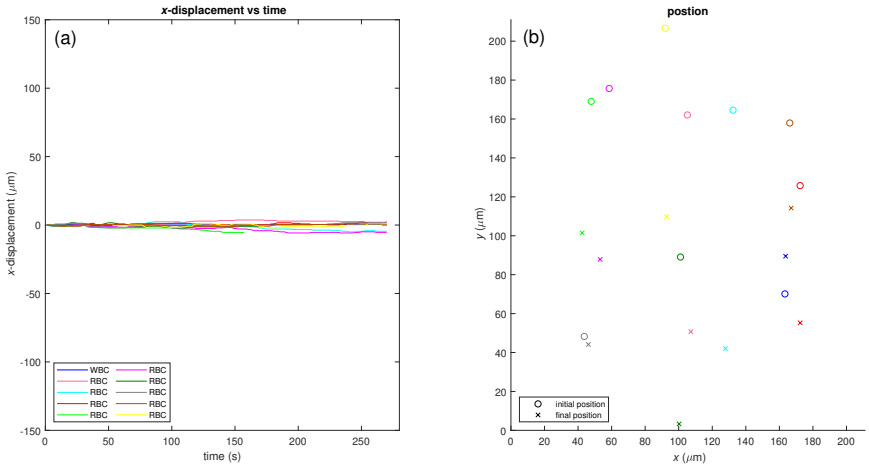

Figure 7: White and red blood cell x-displacement (a) and position (b) during a control experiment where no ultrasound is applied to the sample.

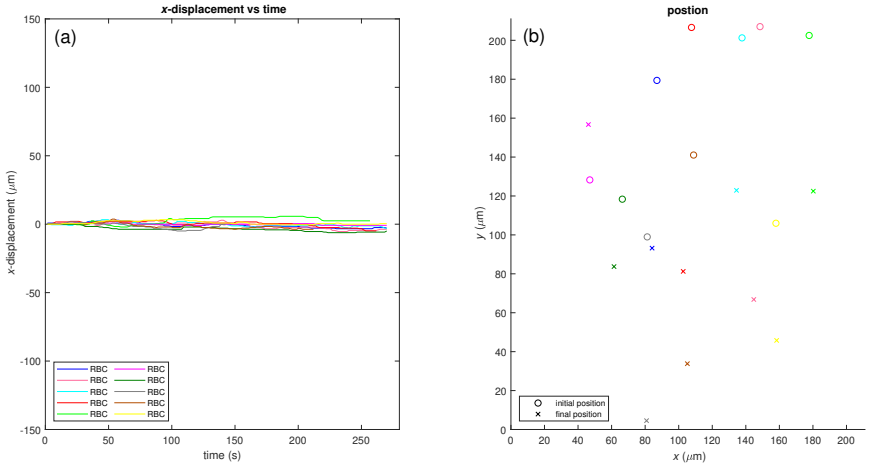

Figure 8: Red blood cell x-displacement (a) and position (b) during a control experiment where no ultrasound is applied to the sample.

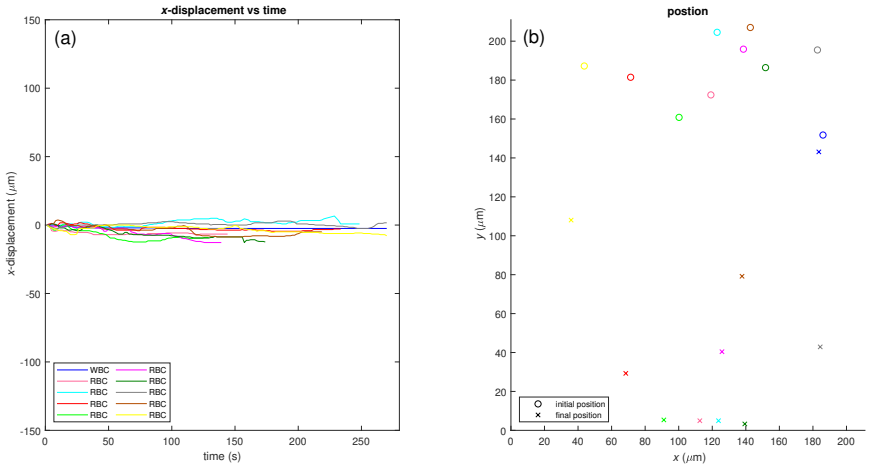

Figure 9: White and red blood cell x-displacement (a) and position (b) during a control experiment where no ultrasound is applied to the sample.

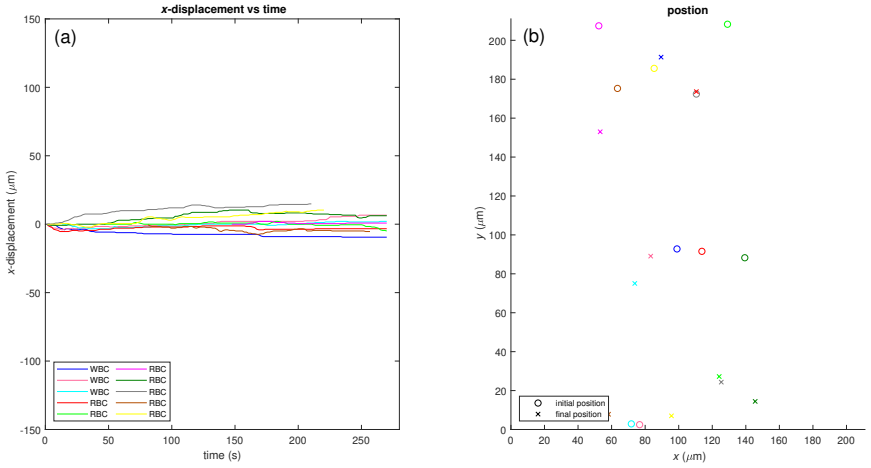

Figure 10: White and red blood cell x-displacement (a) and position (b) during a control experiment where no ultrasound is applied to the sample.

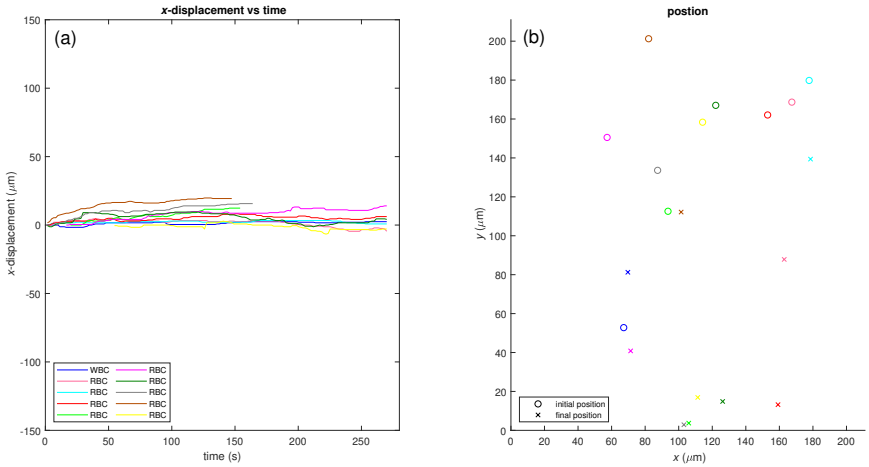

Figure 11: White and red blood cell x-displacement (a) and position (b) during a control experiment where no ultrasound is applied to the sample.

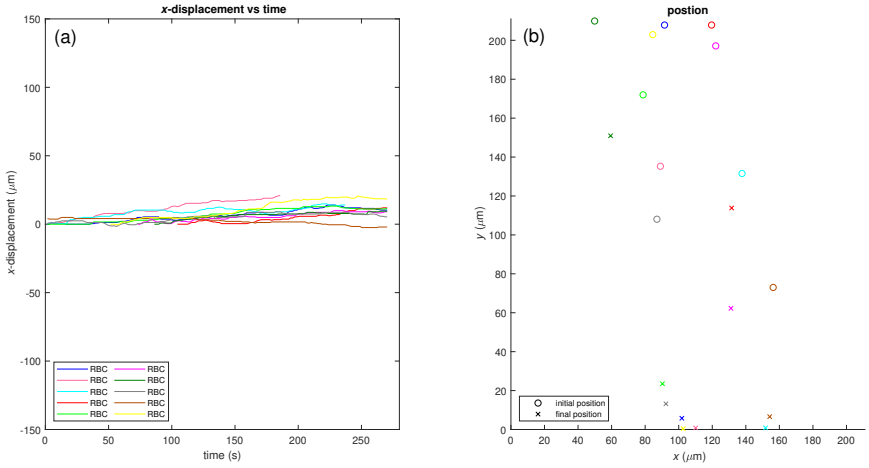

Figure 12: Red blood cell x-displacement (a) and position (b) during a control experiment where no ultrasound is applied to the sample.

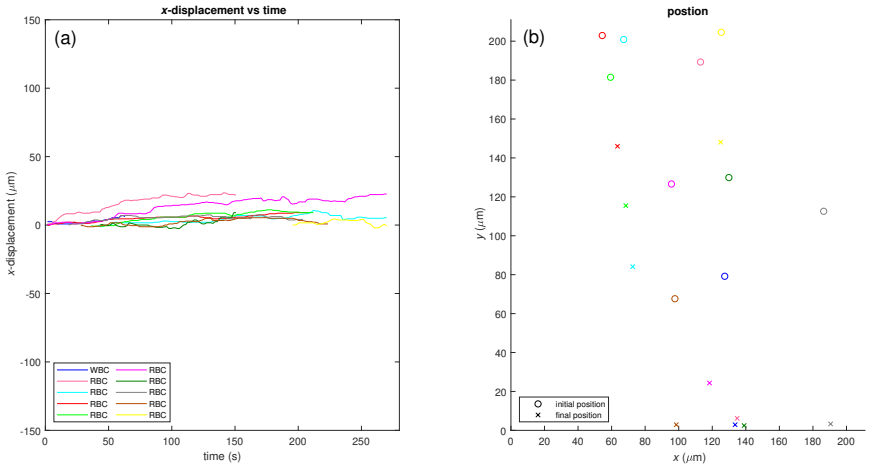

Figure 13: White and red blood cell x-displacement (a) and position (b) during a control experiment where no ultrasound is applied to the sample.

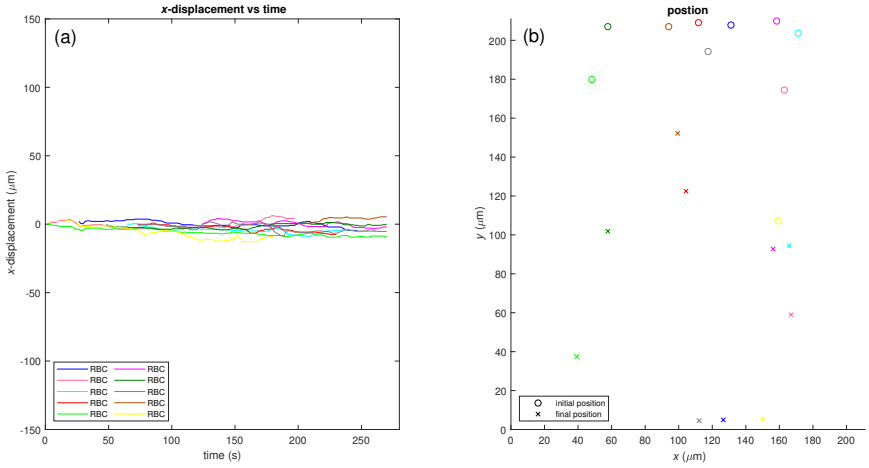

Figure 14: Red blood cell x-displacement (a) and position (b) during a control experiment where no ultrasound is applied to the sample.

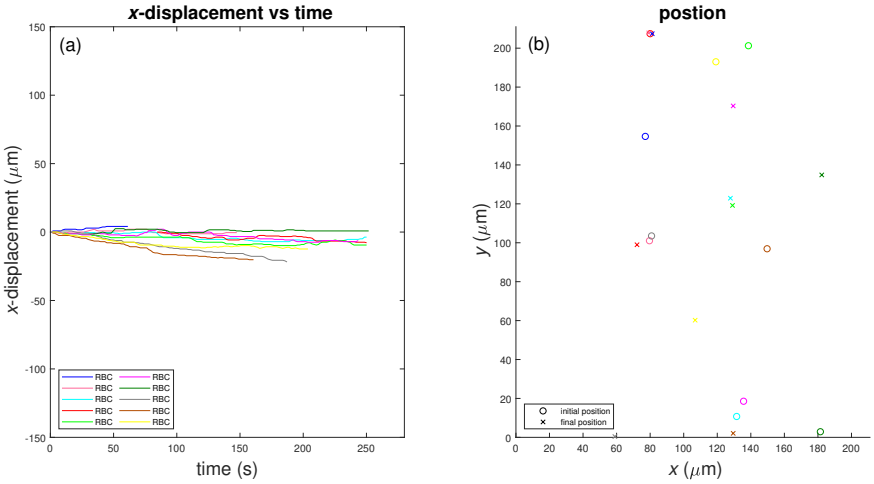

Figure 15: Red blood cell x-displacement (a) and position (b) during a control experiment where no ultrasound is applied to the sample.

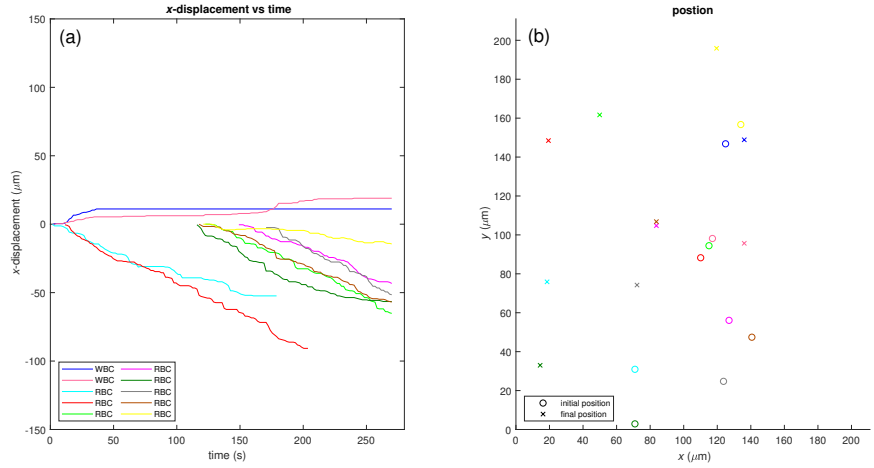

Figure 16: White and red blood cell x-displacement (a) and position (b) during a pulsed 5.8-MHz, 0.5-MPa ultrasound with a 10% duty-cycle.

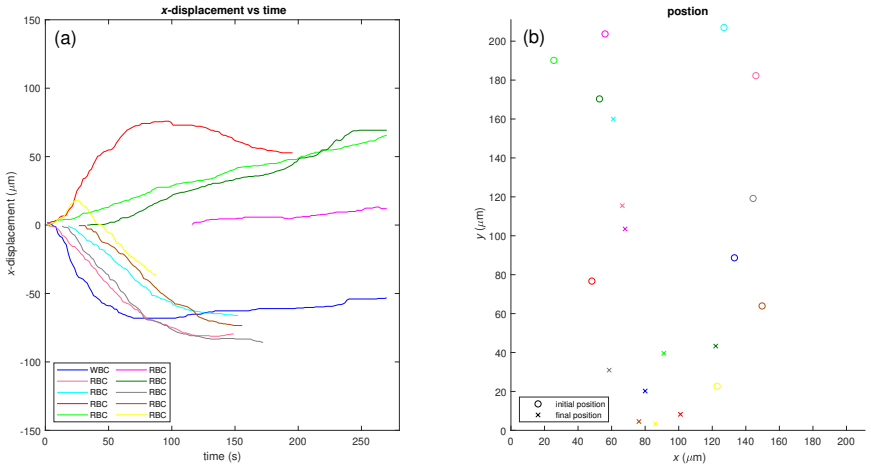

Figure 17: White and red blood cell x-displacement (a) and position (b) during a pulsed 5.8-MHz, 0.7-MPa ultrasound with a 15% duty-cycle.

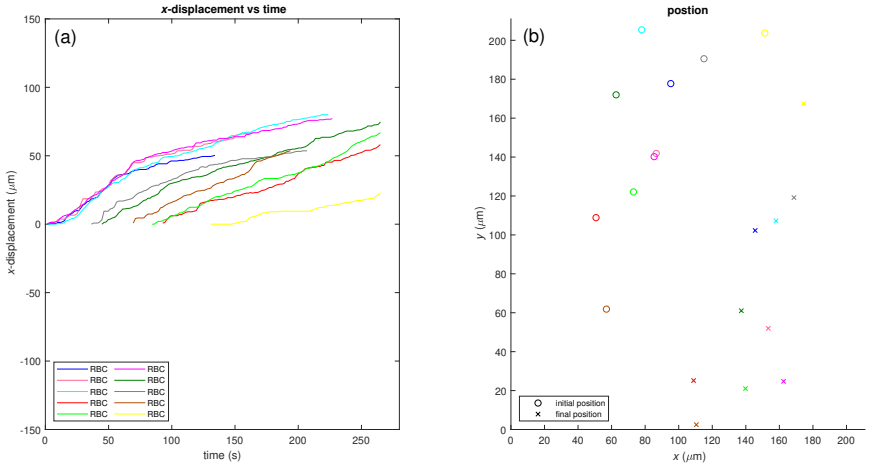

Figure 18: Red blood cell x-displacement (a) and position (b) during a pulsed 5.8-MHz, 0.6-MPa ultrasound with a 35% duty-cycle.

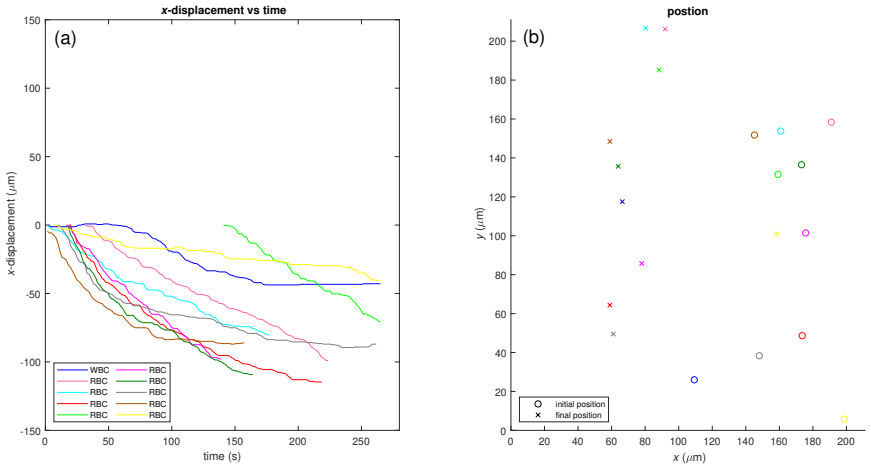

Figure 19: White and red blood cell x-displacement (a) and position (b) during a pulsed 5.8-MHz, 0.6-MPa ultrasound with a 35% duty-cycle.

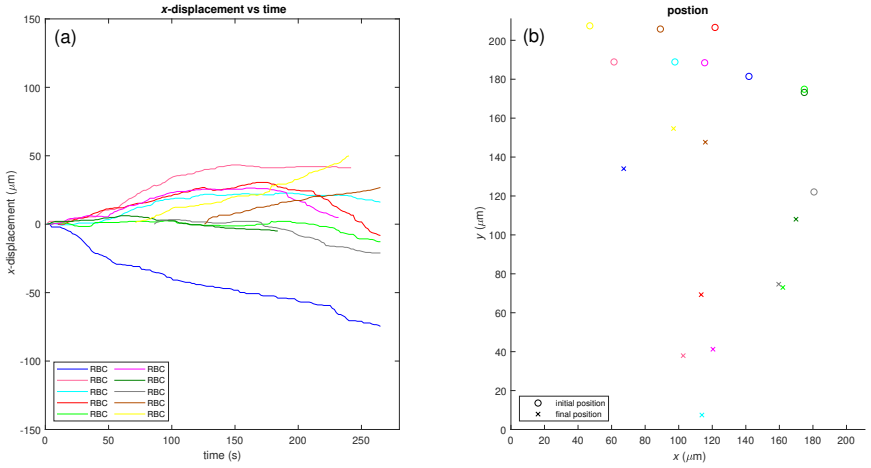

Figure 20: Red blood cell x-displacement (a) and position (b) during a pulsed 5.8-MHz, 0.6-MPa ultrasound with a 35% duty-cycle.

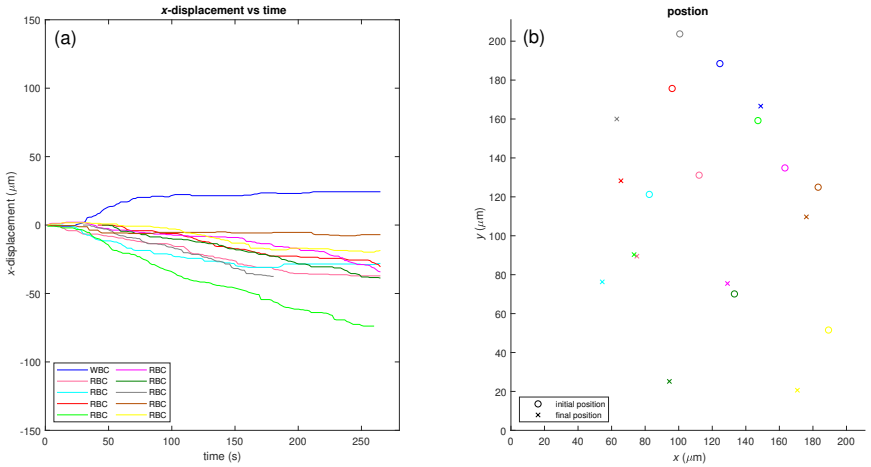

Figure 21: White and red blood cell x-displacement (a) and position (b) during a pulsed 5.8-MHz, 0.6-MPa ultrasound with a 35% duty-cycle.

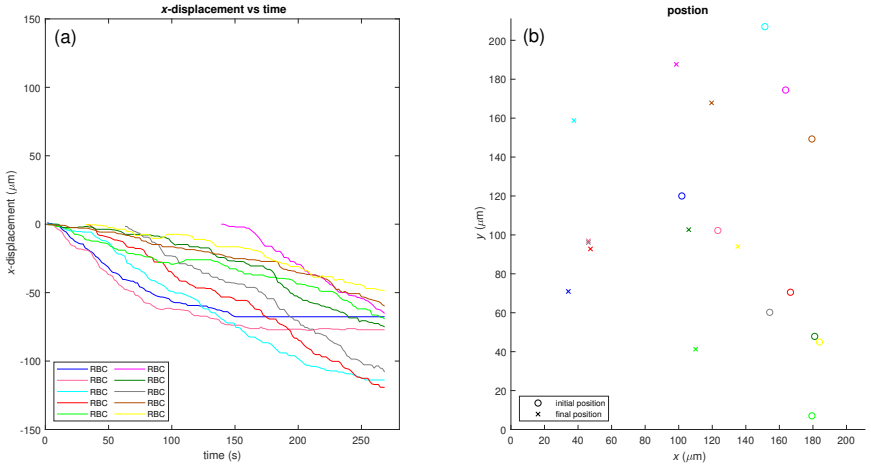

Figure 22: Red blood cell x-displacement (a) and position (b) during a pulsed 5.8-MHz, 0.8-MPa ultrasound with a 35% duty-cycle.

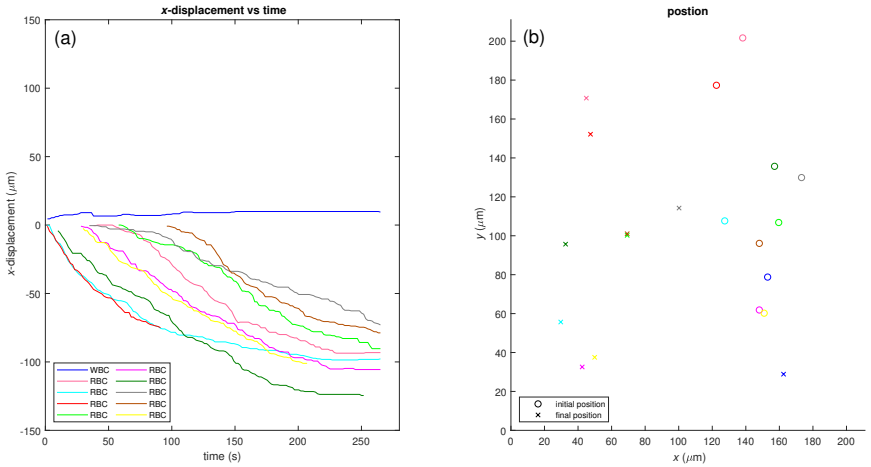

Figure 23: Red blood cell x-displacement (a) and position (b) during a pulsed 5.8-MHz, 0.8-MPa ultrasound with a 35% duty-cycle.

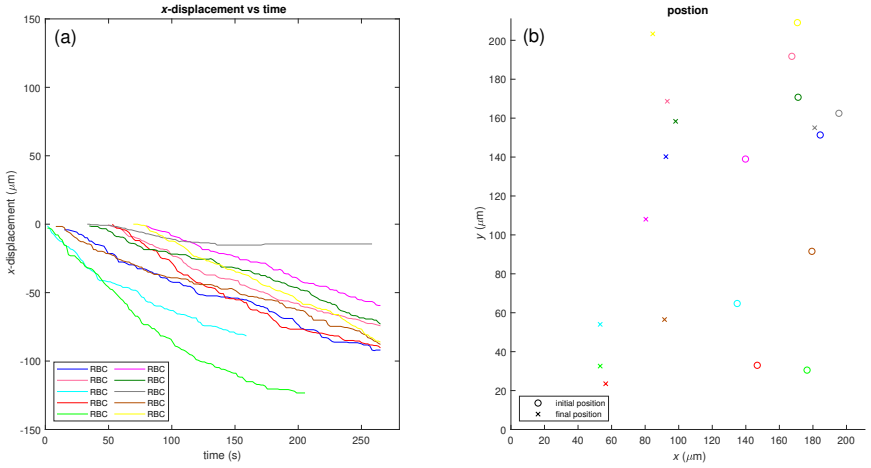

Figure 24: Red blood cell x-displacement (a) and position (b) during a pulsed 5.8-MHz, 0.8-MPa ultrasound with a 35% duty-cycle.

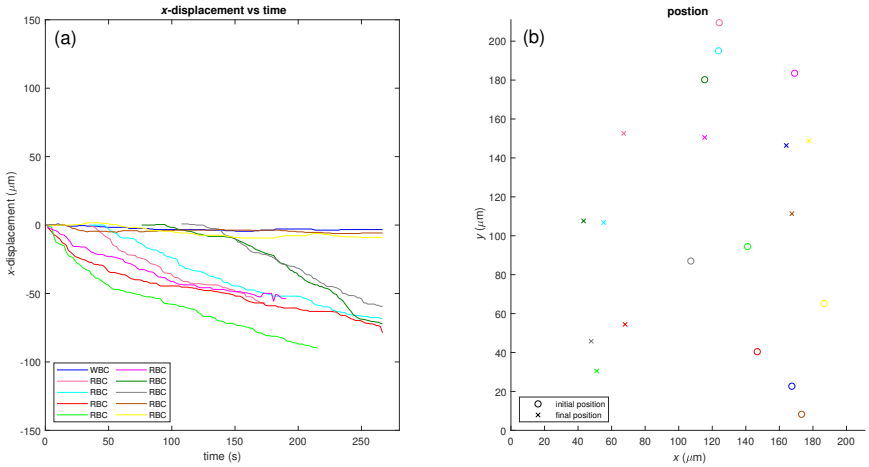

Figure 25: White and red blood cell x-displacement (a) and position (b) during a pulsed 5.8-MHz, 0.8-MPa ultrasound with a 35% duty-cycle.

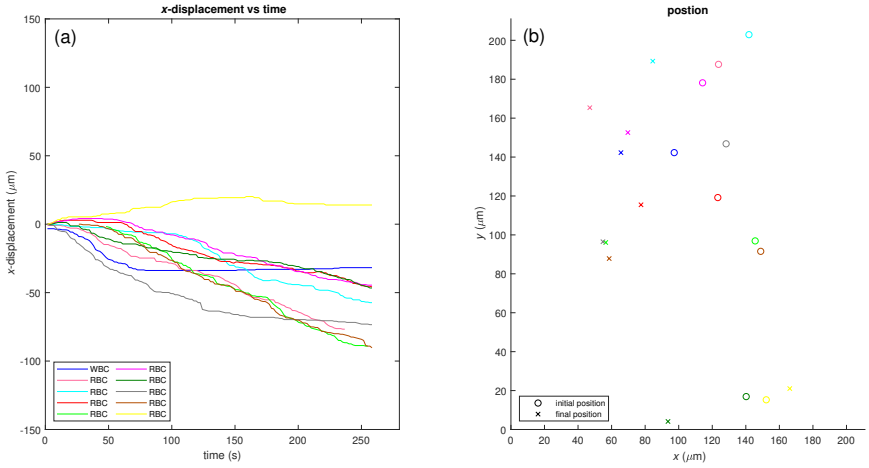

Figure 26: White and red blood cell x-displacement (a) and position (b) during a pulsed 5.8-MHz, 0.8-MPa ultrasound with a 35% duty-cycle.

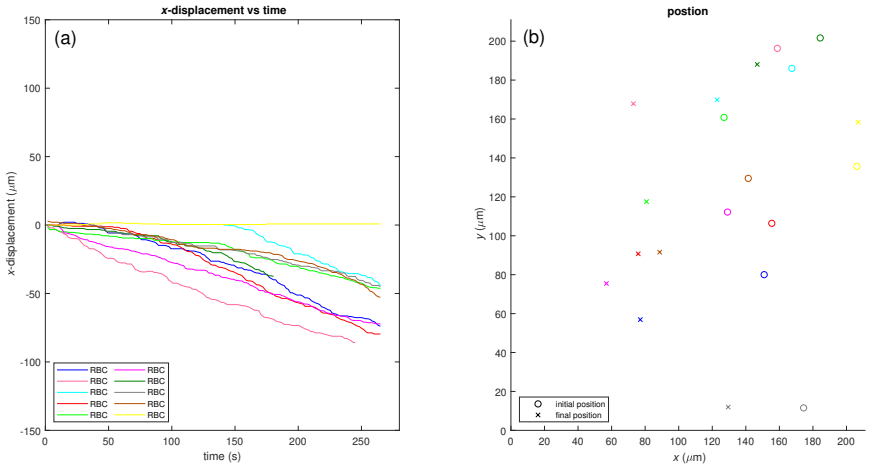

Figure 27: Red blood cell x-displacement (a) and position (b) during a pulsed 5.8-MHz, 0.8-MPa ultrasound with a 35% duty-cycle.

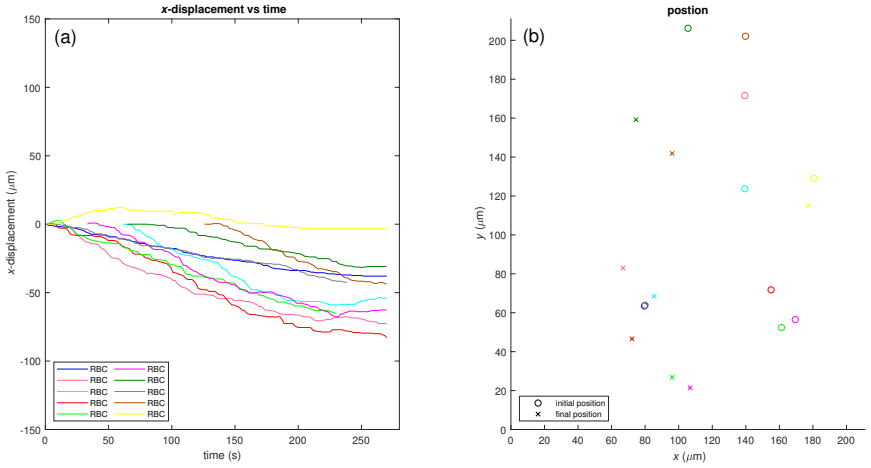

Figure 28: Red blood cell x-displacement (a) and position (b) during a pulsed 5.8-MHz, 0.8-MPa ultrasound with a 35% duty-cycle.

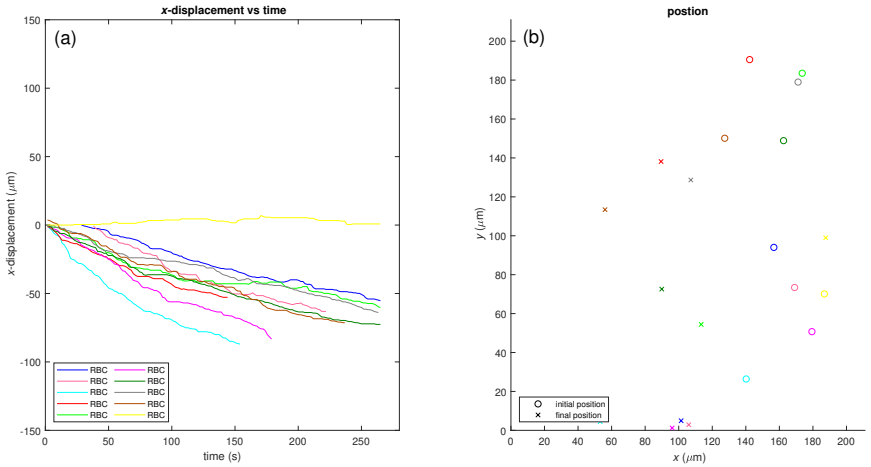

Figure 29: Red blood cell x-displacement (a) and position (b) during a pulsed 5.8-MHz, 0.85-MPa ultrasound with a 35% duty-cycle.

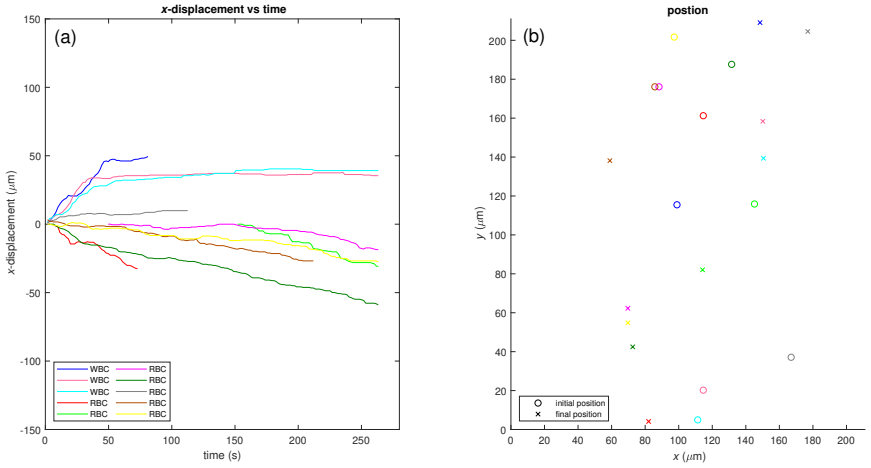

Figure 30: White and red blood cell x-displacement (a) and position (b) during a pulsed 5.8-MHz, 0.85-MPa ultrasound with a 35% duty-cycle.

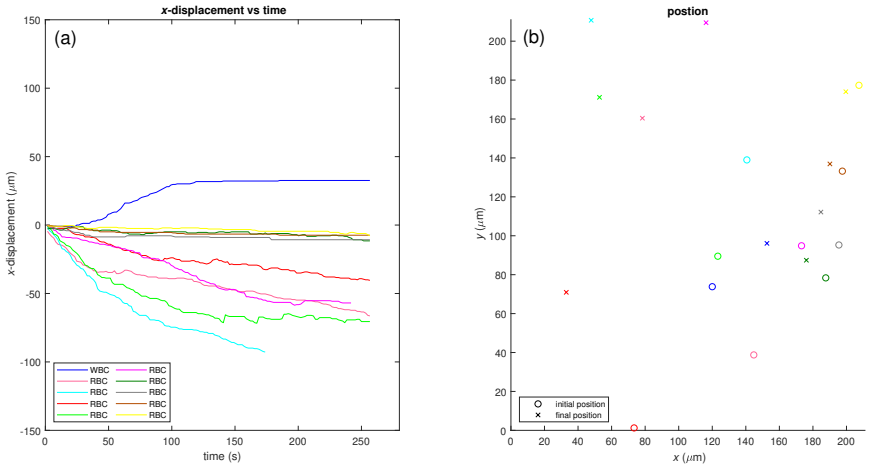

Figure 31: White and red blood cell x-displacement (a) and position (b) during a pulsed 5.8-MHz, 0.85-MPa ultrasound with a 35% duty-cycle.

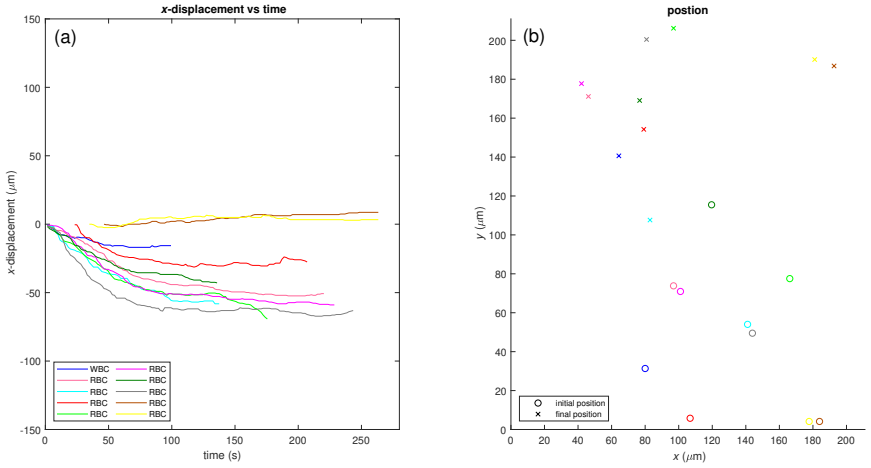

Figure 32: White and red blood cell x-displacement (a) and position (b) during a pulsed 5.8-MHz, 0.85-MPa ultrasound with a 35% duty-cycle.

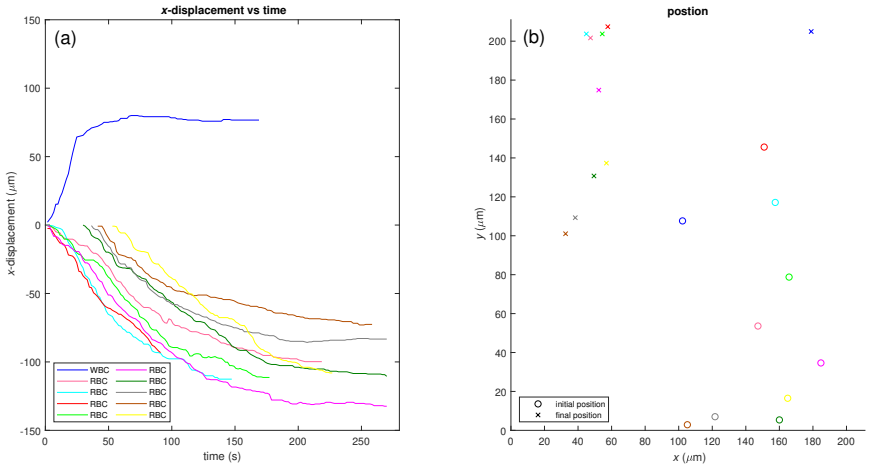

Figure 33: White and red blood cell x-displacement (a) and position (b) during a pulsed 5.8-MHz, 0.85-MPa ultrasound with a 35% duty-cycle.

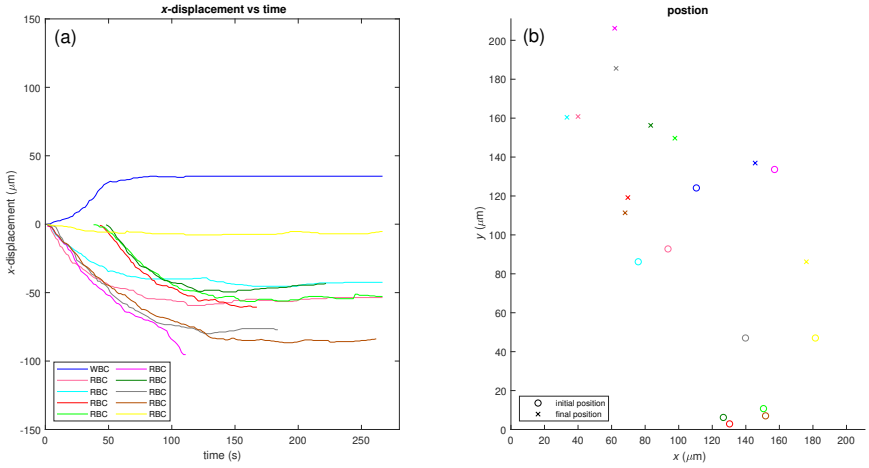

Figure 34: White and red blood cell x-displacement (a) and position (b) during a pulsed 5.8-MHz, 0.85-MPa ultrasound with a 35% duty-cycle.

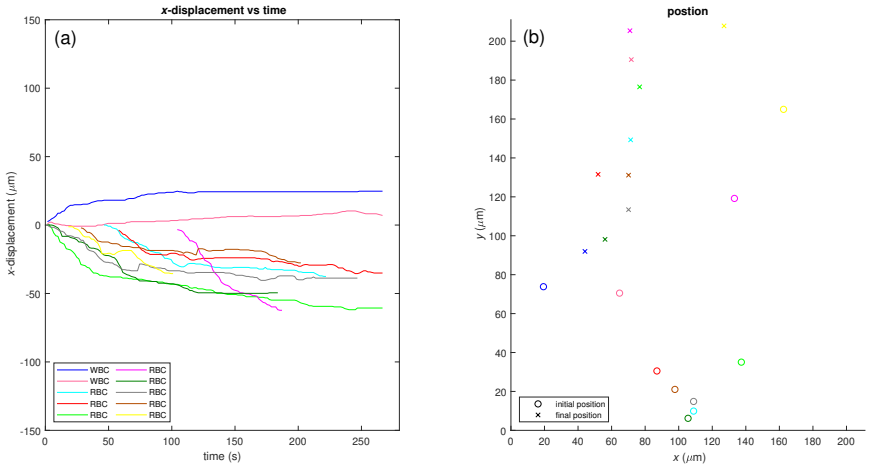

Figure 35: White and red blood cell x-displacement (a) and position (b) during a pulsed 5.8-MHz, 0.85-MPa ultrasound with a 35% duty-cycle.

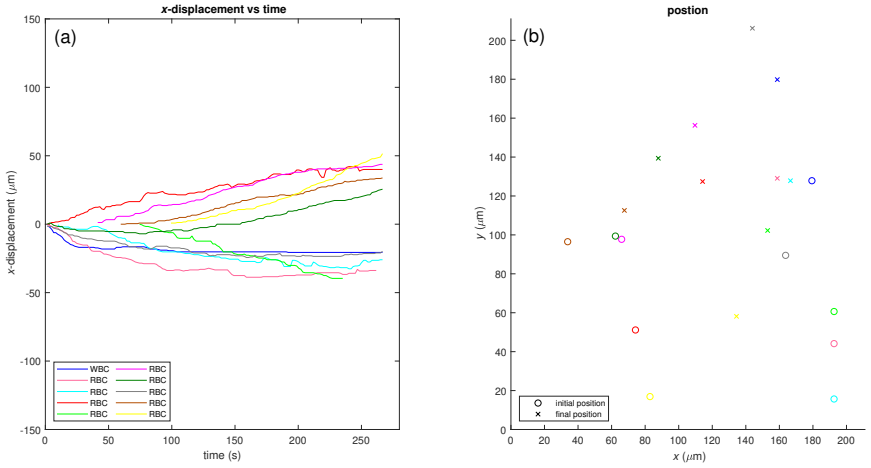

Figure 36: White and red blood cell x-displacement (a) and position (b) during a pulsed 5.8-MHz, 0.85-MPa ultrasound with a 35% duty-cycle.

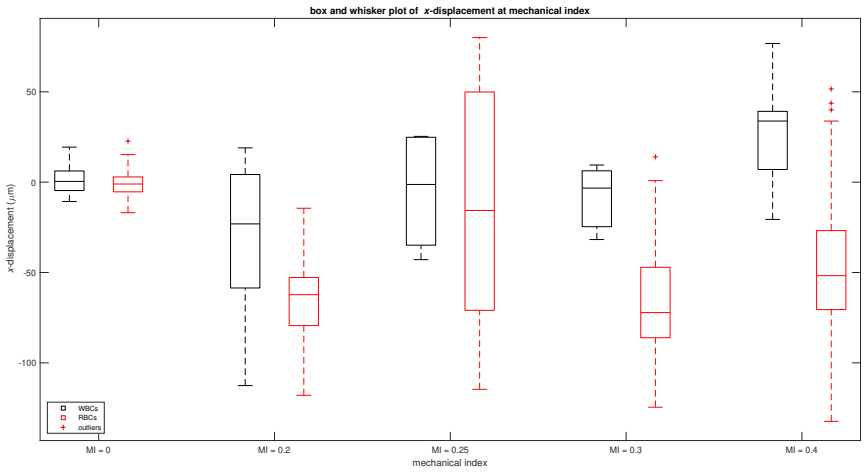

Figure 37: Box and whisker plot showing x-displacement at different mechanical indices. The direction of the sound field is assumed to be positive

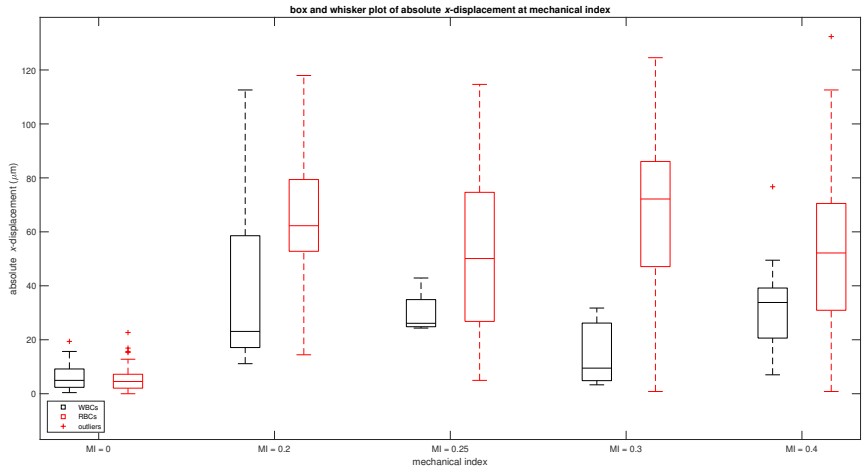

Figure 38: Box and whisker plot showing absolute x-displacement at different mechanical indices.